

BACHELOR

## Validation of Acoustic Boundary Conditions in OpenFOAM

**Autor:**  
Ulrich Hartmann

**Matrikel-No:**  
03662110

**Betreuer:**  
Simon van Buren, M. Sc.  
Prof. Wolfgang Polifke, Ph. D.

September 28, 2018



## **Erklärung**

Hiermit versichere ich, die vorliegende Arbeit selbstständig verfasst zu haben. Ich habe keine anderen Quellen und Hilfsmittel als die angegebenen verwendet.

---

Ort, Datum

Ulrich Hartmann

# Abstract

This thesis investigates the implementation of a new acoustic boundary condition in a simulation environment - the Characteristic Based State-Space Boundary Condition (CBSBC).

The new boundary conditions were applied at the inlet and outlet of a 2D channel. The influence of slip and no-slip wall boundary conditions to the reflection coefficient in a laminar flow is validated.

For the slip simulation cases, defined reflection coefficients are proving the behavior of the CBSBC. Possibilities to set a mean-flow in the new boundary conditions are discussed. Resulting  $f$  and  $g$  waves are evaluated for different mean-flows.

For the investigation of the influence of no-slip boundary condition to the reflection coefficient, the outlet was set to be non-reflecting in the CBSBC. A development of the reflection coefficient perpendicular to the flow direction as well as in x-direction is observed. Additionally, the influence of higher frequencies and the effect of different mean-flows to the CBSBC are investigated.

# Contents

<b>Nomenclature</b>	<b>vii</b>
<b>1 Introduction</b>	<b>1</b>
<b>2 Theoretical Background</b>	<b>4</b>
2.1 Calculation of the Wave Equation . . . . .	4
2.2 Solution of the Wave Equation . . . . .	7
2.3 Plane Acoustic Waves . . . . .	8
2.4 Navier-Stokes Characteristic Boundary Conditions (NSCBC) . . . . .	9
2.5 The Local One-Dimensional Inviscid (LODI) Relations . . . . .	12
2.6 NSCBC with Plane Wave Masking (PVW) . . . . .	14
2.7 Characteristic Based State-Space Boundary Conditions (CBSBC) . . . . .	17
2.8 Stokes Boundary Layer . . . . .	19
2.9 OpenFOAM . . . . .	21
<b>3 Simulation Results for Slip Boundary Conditions</b>	<b>23</b>
3.1 Simulation Setup of Slip Case . . . . .	23
3.2 Generation of Results for Slip Case . . . . .	24
3.3 Applying Reflecting CBSBC . . . . .	25
3.4 Applying Non-Reflecting CBSBC . . . . .	28
3.5 Applying a Mean-Flow to the Slip Simulation Case . . . . .	29
3.6 Comparison of $R_c$ for different Mean-Flows . . . . .	31
3.7 Discussion about Slip Boundary Conditions . . . . .	33
<b>4 Simulation Results for No-Slip Boundary Condition</b>	<b>35</b>
4.1 Simulation Setup of No-Slip Case . . . . .	35
4.2 Generation of Results for No-Slip Case . . . . .	37
4.3 Development of $R_c$ in Flow Direction . . . . .	42
4.4 Comparison of $R_c$ for different Frequencies . . . . .	45
4.5 Discussion about $R_c$ Evolution for No Mean-Flow . . . . .	48
4.6 Applying a Mean-Flow to the No-Slip Simulation Case . . . . .	49
4.7 Development of $R_c$ in Flow Direction with Mean-Flow . . . . .	51
4.8 Comparison of $R_c$ for different Mean-Flows . . . . .	52
4.9 Influence of Mean-Flow to $R_c$ . . . . .	55
<b>5 Summary and Conclusion</b>	<b>56</b>

## CONTENTS

---

<b>Appendices</b>	<b>57</b>
<b>A Inlet Pressure</b>	<b>58</b>
A.1 Linearization of the Inlet Pressure . . . . .	58
A.2 CBSBC Implementation in OpenFOAM . . . . .	59
A.2.1 FractionExpression . . . . .	59
A.2.2 ValueExpression . . . . .	59
A.2.3 GradExpression . . . . .	59
<b>B Outlet Pressure</b>	<b>60</b>
B.1 Linearization of the Outlet Pressure . . . . .	60
B.2 CBSBC Implementation in OpenFOAM . . . . .	61
B.2.1 FractionExpression . . . . .	61
B.2.2 ValueExpression . . . . .	61
B.2.3 GradExpression . . . . .	62
<b>C Inlet Temperature</b>	<b>63</b>
C.1 Linearization of the Inlet Temperature . . . . .	63
C.2 CBSBC Implementation in OpenFOAM . . . . .	64
C.2.1 FractionExpression . . . . .	64
C.2.2 ValueExpression . . . . .	64
C.2.3 GradExpression . . . . .	65
<b>D Outlet Temperature</b>	<b>66</b>
D.1 Linearization of the Outlet Temperature . . . . .	66
D.2 CBSBC Implementation in OpenFOAM . . . . .	67
D.2.1 FractionExpression . . . . .	67
D.2.2 ValueExpression . . . . .	67
D.2.3 GradExpression . . . . .	68
<b>E Extract of Velocity Boundary Condition File</b>	<b>69</b>
<b>F Matlab Code</b>	<b>70</b>
<b>G <math>U_x</math> for selected Mean-Flows</b>	<b>72</b>
<b>Bibliography</b>	<b>73</b>

# Nomenclature

## Roman Symbols

$\bar{p}$	Mean value of pressure	[Pa]
$\bar{u}$	Mean value of velocity	$[\frac{m}{s}]$
$\vec{u}$	Velocity vector	$[\frac{m}{s}]$
$\vec{x}$	Position vector	[m]
$c_0$	Speed of sound	$[\frac{m}{s}]$
$e$	Internal Energy	[J]
$F$	Frequency	[Hz]
$f$	f wave	$[\frac{m}{s}]$
$g$	g wave	$[\frac{m}{s}]$
$p$	Pressure	[Pa]
$p'_A$	Acoustic fluctuation of pressure	[Pa]
$p'_T$	Turbulent fluctuation of pressure	[Pa]
$Pr$	Prandtl number	[-]
$q_i$	Heat flux	$[\frac{W}{m^2}]$
$R_c$	Reflection coefficient	[-]
$R_s$	Specific gas constant	$\left[ \frac{J}{kg \cdot K} \right]$
$T$	Temperature	[K]
$t$	Time	[s]
$u'_A$	Acoustic fluctuation of velocity	$[\frac{m}{s}]$

## CONTENTS

---

$u'_T$  Turbulent fluctuation of velocity  $\left[ \frac{m}{s} \right]$

### Greek Symbols

$\delta$	Stokes boundary layer thickness	[m]
$\kappa$	Thermal conductivity	$\left[ \frac{W}{m \cdot K} \right]$
$\lambda_i$	Characteristic wave amplitude	$\left[ \frac{m}{s} \right]$
$\mu$	Dynamic viscosity	$\left[ \frac{kg}{m \cdot s} \right]$
$\nu$	Kinematic viscosity	$\left[ \frac{m^2}{s} \right]$
$\omega$	Angular frequency	[rad]
$\rho$	Density	$\left[ \frac{kg}{m^3} \right]$

### Acronyms

CBSBC Characteristic Based State Space Boundary Condition

CFD Computational Fluid Dynamics

LODI Local One-Dimensional Inviscid

NSCBC Navier-Stokes Characteristic Boundary Condition

PVM Plane Wave Masking

# 1 Introduction

When constructing a rocket combustion chamber, the extremely thermal and mechanic pressure has to be calculated. The process of burning hydrogen creates acoustic noise, which can be reflected off combustion walls. These reflections can be unstable and can cause mechanical failures within the chamber, resulting in unsuccessful take-offs. Therefore, a reliable design for a rocket's combustion chamber is crucial to avoid any problems.

A resonator acts as an acoustic dampener, which would help to reduce the reflection. However, due to the big dimension of the combustion chamber, a detailed numerical investigation of the acoustic influence can not be performed. Instead, the simulation must concentrate on the immediate surroundings of the resonator to gain accurate readings. Hence, in order to obtain the full acoustic behavior within the combustion chamber, the environment above and below the resonator is modeled using a state-space model. The pairing of numerical and state-space data is achieved using the acoustic CBSBC - the Characteristic Based State-Space Boundary Condition, see figure 1.1.

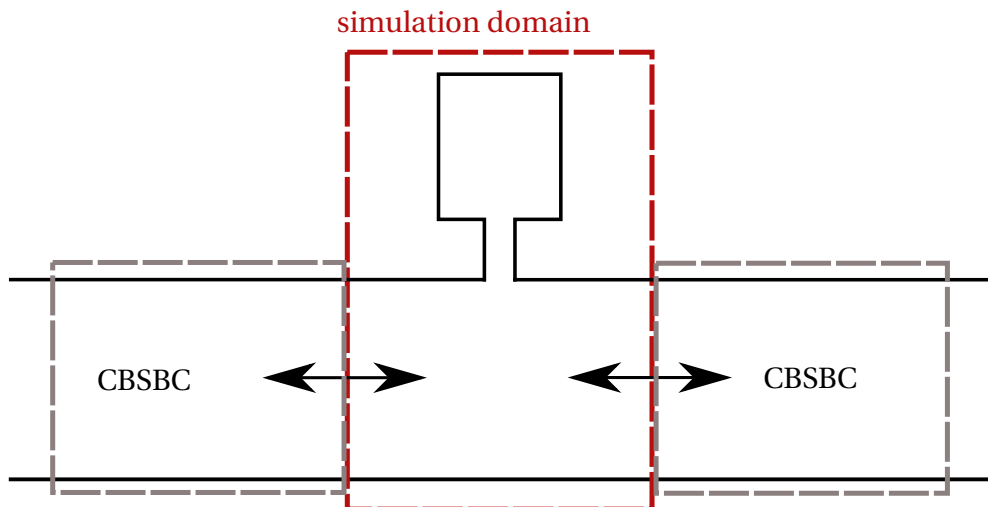


**Figure 1.1:** Model of coupling between the CBSBC and the simulation domain with resonator.

The CBSBC boundary conditions are already implemented in the CFD software OpenFOAM, but not fully validated. This thesis concentrates on the verification of the boundary condition for a channel flow without a resonator, see figure 1.2.

The thesis is structured as follows. In chapter 2, the theoretical background of the acoustic involved formula and the related equations concerning the new introduced boundary con-

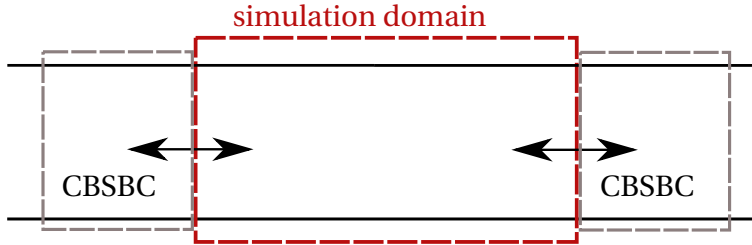


**Figure 1.2:** Model of coupling between the CBSBC and the simulation domain without resonator.

dition are explained. As acoustic waves are investigated, the wave equation and its solution are introduced in the beginning. After that, the development to obtain the CBSBC boundary condition is reproduced shortly. Figure 1.3 is showing the steps in a diagram. An assumption is made by considering plane waves. Then Navier-Stokes Characteristic Boundary Conditions (NSCBC) are explained, to model the behavior of the acoustic at the boundaries and to obtain a physical correct reflection. After applying the NSCBC for a two-dimensional case (LODI Relations), the plane wave masking is shown, which is a modification for reflecting boundary conditions. Finally, the Characteristic Based State Space Boundary Condition (CBSBC) is introduced, which contains the related equations for the investigated simulations. The description of the used simulation software and the implementation of the CBSBC boundary condition in OpenFOAM is done in the section 2.9.

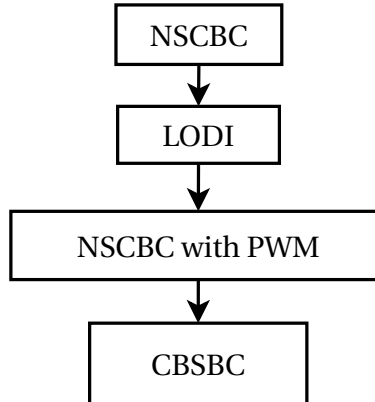


**Figure 1.3:** Derivation of CBSBC displayed in a diagram.

Chapter 3 is dealing with the simulations for slip boundary conditions. In the beginning, the general behavior of the CBSBC condition for slip wall boundary conditions is introduced. Simulations with reflecting and non-reflecting boundary conditions are shown. Furthermore, few options to set a mean-flow to the simulation are investigated. The chapter ends with a discussion about the resulting reflection coefficient graphs for different mean-flows.

Simulations for no-slip wall boundary conditions are investigated in chapter 4. The reflection coefficient is set to zero in the CBSBC. Nevertheless, the wall has an high influence to the

---

reflection coefficient perpendicular to the flow direction. In the beginning of the chapter, the procedure to calculate the reflection coefficient is demonstrated for five selected cells along the y-axis. Figures of velocity and pressure for the selected cells are displayed. Furthermore, the calculated  $f$  and  $g$  waves are presented to help understanding the resulting reflection coefficient graph. Additionally, the development of the reflection coefficient in flow direction was investigated. After, different frequencies were applied to the setup, to investigate the influence of frequency to the reflection behavior of the CBSBC. Finally a mean-flow was applied for the no-slip part. Again, figures of pressure and velocity for selected cells are demonstrated. It ends with a discussion about the development of the reflection coefficient along the x-axis for different mean-flow setups.

## 2 Theoretical Background

The related equations for the propagation of acoustic waves are introduced in this chapter. Furthermore, the development to obtain the CBSBC is reproduced here shortly. This chapter is closing with basic information about OpenFOAM and the implementation of the CBSBC in OpenFOAM.

### 2.1 Calculation of the Wave Equation

This thesis contains the propagation of acoustic waves and their reflection behavior for a new introduced boundary condition type. For this reason, the wave equation is introduced here. Starting point are the base equations of fluid mechanics, the Navier-Stokes Equations. They are considering Newtonian, compressible fluid and consists of the continuity, the momentum and the energy equation. The continuity (2.1) and the momentum (2.2) equations are written in Einstein notation with the relation between the density  $\rho$  and the velocity of the fluid  $u_i$  in space  $x_i$  and in time  $t$ .

- continuity

$$\frac{D\rho}{Dt} + \rho \frac{Du_i}{Dx_i} = 0, \quad (2.1)$$

- momentum

$$\rho \frac{Du_i}{Dt} = -\frac{\partial p}{\partial x_i} + \frac{\partial}{\partial x_j} \left( 2\mu S_{ij} - \frac{2}{3}\mu \frac{\partial u_k}{\partial x_k} \delta_{ij} \right), \quad (2.2)$$

- energy

$$\rho \frac{De}{Dt} = -p \frac{\partial u_i}{\partial x_i} + 2\mu S_{ij} S_{ij} - \frac{2}{3}\mu S_{kk} S_{ii} + \frac{\partial}{\partial x_i} \left( \kappa \frac{\partial T}{\partial x_i} \right), \quad (2.3)$$

where

$$S_{ij} = \frac{1}{2} \left( \frac{\partial u_i}{\partial x_j} + \frac{\partial u_j}{\partial x_i} \right).$$

Here,  $\frac{D \cdot}{Dt} = \frac{\partial \cdot}{\partial t} + u_i \frac{\partial \cdot}{\partial x_i}$  is defined as the material derivative. For the transport equation for the internal energy  $e$  (2.3), the variables  $T$  and  $\kappa$  are defined as the temperature and the thermal conductivity.

In addition to the partial different equations (PDEs) above, two other equations are introduced to obtain a complete description of the problem. The first equation treats the ideal gas law, which is defined as

$$p = \rho R_s T, \quad (2.4)$$

where  $R_s$  is the specific gas constant. As we assume an ideal gas, the internal energy  $e$  and the temperature  $T$  are linked by the relation

$$e = \int c_v dT = \int c_p dT - \frac{p}{\rho}. \quad (2.5)$$

Here,  $c_v$  and  $c_p$  denote the heat capacities at constant specific volume and at constant pressure. In the following, the viscous stress and the bulk viscosity are neglected for simplification reasons. This results in the so called Euler equation for equation (2.2), which describes the conservation of momentum for a friction-less fluid without volume forces to

$$\rho \frac{Du_i}{Dt} + \frac{\partial p}{\partial x_i} = 0. \quad (2.6)$$

As we are interested in the acoustic behavior, isotropic disturbances of flow variables are considered. Ehrenfried [2] proposed to linearize and decompose the equations (2.1) and (2.6) into its mean and fluctuation parts as

$$p = p_0 + p', \quad (2.7)$$

$$\rho = \rho_0 + \rho', \quad (2.8)$$

$$\vec{u} = \vec{u}_0 + \vec{u}' \equiv \vec{u}'. \quad (2.9)$$

Following, every term with higher order in the fluctuation part is neglect. For (2.9), the assume that the fluid is situated in a state of rest  $\vec{u}_0 = 0$  and every movement is only caused by its fluctuation [2].

Insert the linearization into the continuity equation (2.1) and assuming that  $\rho' \ll \rho$ , the linear continuity equation gets to

$$\frac{\partial \rho'}{\partial t} + \rho_0 \frac{\partial u'_i}{\partial x_i} = 0. \quad (2.10)$$

Consequently, the Euler equation transforms to

$$\rho_0 \frac{\partial \vec{u}'}{\partial t} + \frac{\partial p'}{\partial x_i} = 0, \quad (2.11)$$

where  $\frac{\partial}{\partial t}$  describes the material derivative  $\frac{D}{Dt} = \frac{\partial}{\partial t} + u_i \frac{\partial}{\partial x_i}$  for a mean-flow  $\vec{u}_0 = 0$ . Furthermore the time derivation for  $\rho_0$  and  $p_0$  are zero, as the density and the pressure are a constant value. For an isotropic compression, the relation between pressure and force is obtained to

$$p = p(\rho). \quad (2.12)$$

## Theoretical Background

---

As the definition of pressure force relation (2.12) is a function and therefore can not be separated into mean and fluctuation parts, equation (2.12) is developed with the Taylor series as

$$p(\rho) = p(\rho_0) + (\rho - \rho_0) \frac{dp}{d\rho}(\rho_0) + \dots \quad (2.13)$$

Applying (2.13) into (2.12) and neglecting higher order terms, we get

$$p' = \rho' \frac{dp}{d\rho}(\rho_0). \quad (2.14)$$

The derivation above is shortened with

$$\frac{dp}{d\rho}(\rho_0) = c_0^2. \quad (2.15)$$

Finally, the linearized pressure-force relation is

$$p' = c_0^2 \rho', \quad (2.16)$$

where

$$c_0^2 = \left( \frac{\partial p}{\partial \rho} \right)_s. \quad (2.17)$$

The variable  $c_0$  is defined as *speed of sound*, where the index  $s$  indicates the isentropic relation. As it can be seen in the gaining wave equation, the acoustic perturbations propagate in space with the speed of sound. For an ideal gas, the speed of sound can be calculated using this formula

$$c_0 = \sqrt{\gamma R_s T}. \quad (2.18)$$

It is to mention here that the linearized equations (2.11), (2.10) and (2.16) are only valid, if the amplitudes of the disturbance are small in comparison to the mean part

$$|p'| \ll p_0 \quad \text{and} \quad |\rho'_0| \ll \rho_0.$$

To obtain the wave equation for the sound pressure, the linearized continuity equation (2.10) is derived by time. After interchanging the time derivative with the divergence, the following equation is produced as

$$\frac{\partial^2 \rho'}{\partial t^2} + \rho_0 \frac{\partial}{\partial x_i} \left( \frac{\partial \vec{v}'}{\partial t} \right) = 0 \quad (2.19)$$

For the linearized Euler equation (2.11), its divergence will be calculated to

$$\frac{\partial}{\partial x_i} \left( \frac{\partial \vec{v}}{\partial t} \right) + \frac{\partial}{\partial x_i} \frac{\partial p'}{\partial x_i} = 0. \quad (2.20)$$

After subtracting equation (2.20) from (2.19), the terms with  $\vec{v}'$  vanish and the equation below is generated

$$\frac{\partial^2 \rho'}{\partial t^2} + \frac{\partial^2 p'}{\partial x_i^2} = 0. \quad (2.21)$$

After all, the fluctuation density  $\rho'$  can be replaced by  $p'$  using the linearized force-pressure relation (2.16). The wave equation for the sound pressure is finally calculated appearing

$$\frac{\partial^2 p'}{\partial t^2} - c_0^2 \frac{\partial^2 p'}{\partial x_i \partial x_i} = 0. \quad (2.22)$$

The second order partial differential wave equation as seen in (2.22) describes the propagation of small disturbances, if the medium is at rest.

## 2.2 Solution of the Wave Equation

For a 1-D problem, the wave equation (2.22) can be factorized as follows, if the speed of sound  $c_0$  is constant

$$\left( \frac{\partial}{\partial t} + c_0 \frac{\partial}{\partial x} \right) \left( \frac{\partial}{\partial t} - c_0 \frac{\partial}{\partial x} \right) p' = 0. \quad (2.23)$$

According to Ehrenfried [2], an easy solution of the wave equation is the one dimensional wave development. It is assumed that the wave is only travelling in x-direction. This leads to

$$p'(x, t) = f(x - ct) + g(x + ct). \quad (2.24)$$

The solution of the one-dimensional wave equation are sums of two waves. One right traveling function  $f$  and one left traveling function  $g$ , both travelling with speed of sound  $c_0$  relative to the mean fluid motion. These two characteristic waves, also known as *Riemann invariants*, can be defined as [3]

$$f = \frac{1}{2} \left( \frac{p'}{\rho c} + u' \right) \quad \text{and} \quad g = \frac{1}{2} \left( \frac{p'}{\rho c} - u' \right). \quad (2.25)$$

Characteristic wave amplitudes  $f, g$  and acoustic fluctuations of pressure  $p'$  and velocity  $u'$  are related to each other as follows

$$\frac{p'}{\rho c} = f + g \quad \text{and} \quad u' = f - g. \quad (2.26)$$

A model of the  $f$  and  $g$  wave in a 2D channel can be seen in figure 2.1. The  $f$  wave is travelling in x-direction, while the  $g$  wave is propagating in negative flow direction.

To avoid any further uncertainties between the common acronym for frequency and the here introduced  $f$  wave, the shortcut for the frequency in this thesis is  $F$ .

The reflection coefficient  $R_c$  is a possibility to characterize acoustically the ratio of the oncoming wave ( $g$ ) to the expatiate wave ( $f$ ). It is defined as

$$R_c = \frac{\hat{g}}{\hat{f}}. \quad (2.27)$$

Here, the variables are denoted in the frequency domain  $\hat{\cdot}$ . The reflection coefficient is a good value to qualify the reflection behavior of a boundary.

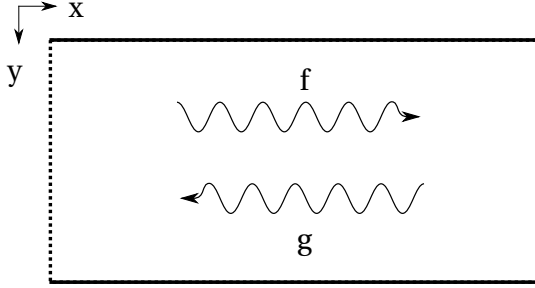


**Figure 2.1:** Model of  $f$  and  $g$  wave in a channel.

## 2.3 Plane Acoustic Waves

For simplification reason and assuming that the frequency is lower than the cut-off frequency of the first order, the waves are behaving in a plane characteristic way [6]. The assumption allows an easy and fast separation of the acoustic fluctuation from the mean-flow. The flow variables,  $p$  and  $u$ , can be separated as

$$p(t, x, y, z) = \bar{p}(t, x, y, z) + p'_T(t, x, y, z) + p'_A(t, x), \quad (2.28)$$

$$u(t, x, y, z) = \bar{u}(t, x, y, z) + u'_T(t, x, y, z) + u'_A(t, x). \quad (2.29)$$

The temporal averaged fields denotes the bar ( $\bar{\cdot}$ ), while the turbulent and acoustic fluctuations are marked by the indexes 'T' and 'A'. Pressure and velocity are propagating in time  $t$  and in the spatial coordinates  $x, y, z$ . As plane waves are assumed, the acoustic fluctuation only depends on time and on the x-direction.

Considering the perturbation amplitudes are small enough, acoustic signal components can be described in terms of the linearized characteristic wave amplitudes  $f$  and  $g$  as

$$f = f(x - (\bar{u} + \bar{c})), \quad (2.30)$$

$$g = g(x - (\bar{u} - \bar{c})), \quad (2.31)$$

travelling in the positive and negative x-direction (see figure 2.1). Plane acoustic waves can now be described by the characteristic wave amplitudes  $f$  and  $g$ , in which acoustic fluctuations of pressure  $p'_A$  and velocity  $u'_A$  are related to each other as

$$f = \frac{1}{2} \left( \frac{p'_A}{\bar{\rho} \bar{c}} + u'_A \right), \quad (2.32)$$

$$g = \frac{1}{2} \left( \frac{p'_A}{\bar{\rho} \bar{c}} - u'_A \right). \quad (2.33)$$

Here,  $\rho$  and  $c$  are the density and the speed of sound, respectively.  $f$  corresponds to the wave traveling in downstream direction and  $g$  is travelling in upstream direction. The characteristic wave amplitudes  $f$  and  $g$  are related to each other as

$$\frac{p'_A}{\bar{\rho} \bar{c}} = f + g, \quad (2.34)$$

$$u'_A = f - g. \quad (2.35)$$

To identify the acoustic signal components  $f$  and  $g$  from the flow variables  $u$  and  $p$ , the acoustic fluctuation  $p'_A$  and  $u'_A$  has to be separated from the flow field. According to Polifke [9], "an area average over sampling planes perpendicular to the duct axis" is applied to the turbulent fluctuation. As the spatial correlation length of the turbulent fluctuation is very small, the turbulent eddies vanish  $\langle p'_T \rangle = 0$  and  $\langle u'_T \rangle = 0$  [9]. This leads to the correlation of the acoustic fluctuation as

$$p'_A = \langle p - \bar{p} \rangle, \quad (2.36)$$

$$u'_A = \langle u - \bar{u} \rangle. \quad (2.37)$$

Here,  $\langle \cdot \rangle$  represents a spatial average of a plane perpendicular to the traveling direction of the acoustic waves. Applying this new correlation to the general equations of  $f$  (2.32) and  $g$  (2.33) results in

$$f = \frac{1}{2} \left( \frac{\langle p - \bar{p} \rangle}{\bar{\rho} \bar{c}} + \langle u - \bar{u} \rangle \right) \quad (2.38)$$

$$g = \frac{1}{2} \left( \frac{\langle p - \bar{p} \rangle}{\bar{\rho} \bar{c}} - \langle u - \bar{u} \rangle \right) \quad (2.39)$$

The new correlation can now be used to calculate the  $f$  and  $g$  waves, especially when a mean-flow is applied, this formula helps to separate the acoustic fluctuation part from its mean part.

## 2.4 Navier-Stokes Characteristic Boundary Conditions (NSCBC)

As explained in the section 2.2, the solution of the wave equation consist of two waves,  $f$  and  $g$ . The computational domain is considered with a determined sizes, where the boundary conditions interact with the environment. An accurate determination of these boundary condition is necessary for a good simulation result. Figure 2.2 is showing the  $f$  and  $g$  waves leaving the simulation domain at the outlet ( $x = L$ ).

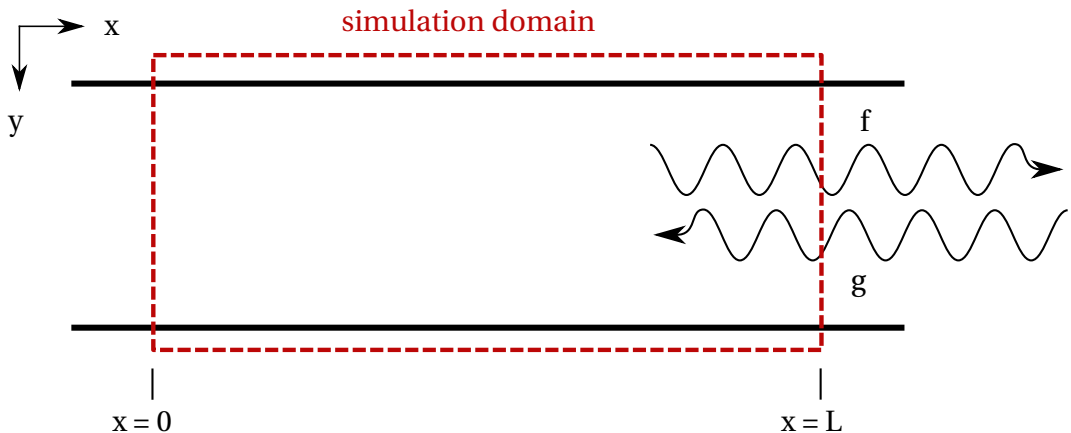


**Figure 2.2:** Model of  $f$  and  $g$  wave at the outlet ( $x = L$ ).

## Theoretical Background

---

In this thesis, the NSCBC approach by Poinsot and Lele [8] is used to determine the boundary conditions. The method is explained as an "appealing technique for specifying boundary conditions for hyperbolic systems [...] to use relations based on characteristic lines" [8] and is summarized here shortly. A detailed description of the mathematical background of boundary conditions based on characteristic lines can be seen in the papers of Kreiss [7] or Engquist and Majda [5].

To obtain the NSCBC, the Navier-Stokes Equations for a compressible flow in Cartesian coordinates are shown [12]:

$$\frac{\partial \rho}{\partial t} + \frac{\partial}{\partial x_i} (m_i) = 0, \quad (2.40)$$

$$\frac{\partial \rho E}{\partial t} + \frac{\partial}{\partial x_i} [(\rho E + p) u_i] = \frac{\partial}{\partial u_j \tau_{ij}} - \frac{\partial q_i}{\partial x_i}, \quad (2.41)$$

$$\frac{\partial m_i}{\partial t} + \frac{\partial}{\partial x_j} (m_i u_j) + \frac{\partial p}{\partial x_i} = \frac{\partial \tau_{au_{ij}}}{\partial x_j}, \quad (2.42)$$

where

$$\rho E = \frac{1}{2} \rho u_k u_k + \frac{p}{\gamma - 1}, \quad (2.43)$$

$$m_i = \rho u_i, \quad (2.44)$$

$$\tau_{ij} = \mu \left( \frac{\partial u_i}{\partial x_j} + \frac{\partial u_j}{\partial x_i} - \frac{2}{3} \delta_{ij} \frac{\partial u_k}{\partial x_k} \right). \quad (2.45)$$

The thermodynamic pressure is given by the variable  $p$ , the total energy density (kinetic + thermal) is defined as  $\rho E$ , while  $m_i$  shows the momentum density in the  $x_i$  direction. Additionally, the equations of the heat flux  $q_i$  and of the thermal conductivity  $\lambda$  are

$$q_i = -\lambda \frac{\partial t}{\partial x_i}, \quad (2.46)$$

$$\lambda = \frac{\mu C_p}{P_r}, \quad (2.47)$$

where  $P_r$  is the Prandtl number, and  $\mu$  is the viscosity coefficient.

As explained in the paper of Poinsot and Lele [8], the approach to apply the conservation equations directly on the boundary is used to complement the set of physical boundary conditions. To do so, a boundary located at  $x = L$  is considered and the characteristic analysis

from Thompson [10] is applied at this patch. The equations (2.40) - (2.42) transform to:

$$\frac{\partial \rho}{\partial t} + d_1 + \frac{\partial}{\partial x_2}(m_2) + \frac{\partial}{\partial x_3}(m_3) = 0, \quad (2.48)$$

$$\begin{aligned} \frac{\partial \rho E}{\partial t} + \frac{1}{2}(u_k u_k) d_1 + \frac{d_2}{\gamma - 1} + m_1 d_3 + m_2 d_4 + m_3 d_5 + \\ + \frac{\partial}{\partial x_2}[(\rho E + p) u_2] + \frac{\partial}{\partial x_3}[(\rho E + p)] = \frac{\partial}{\partial x_i}(u_j \tau_{ij}) - \frac{\partial q_i}{\partial x_i}, \end{aligned} \quad (2.49)$$

$$\frac{\partial m_1}{\partial t} + u_1 d_1 + \rho d_3 + \frac{\partial}{\partial x_2}(m_1 u_2) + \frac{\partial}{\partial x_3}(m_1 u_3) = \frac{\partial \tau_{1j}}{\partial x_j}, \quad (2.50)$$

$$\frac{\partial m_2}{\partial t} + u_2 d_1 + \rho d_4 + \frac{\partial}{\partial x_2}(m_2 u_2) + \frac{\partial}{\partial x_3}(m_2 u_3) + \frac{\partial p}{\partial x_2} = \frac{\partial \tau_{2j}}{\partial x_j}, \quad (2.51)$$

$$\frac{\partial m_3}{\partial t} + u_3 d_1 + \rho d_5 + \frac{\partial}{\partial x_2}(m_3 u_2) + \frac{\partial}{\partial x_3}(m_3 u_3) + \frac{\partial p}{\partial x_3} = \frac{\partial \tau_{3j}}{\partial x_j}. \quad (2.52)$$

It can be observed that the equations above contain two types of derivatives. One derivative normal to the  $x_1$  boundary, defined as ( $d_1$  to  $d_6$ ), and derivatives parallel to the  $x_1$  boundary like  $(\partial/\partial x_2)(m_2 u_2)$  and local viscous terms.

The vector  $\mathbf{d}$  is given by characteristic analysis (Thompson [10]) and can be expressed as

$$\mathbf{d} = \begin{pmatrix} d_1 \\ d_2 \\ d_3 \\ d_4 \\ d_5 \end{pmatrix} = \begin{pmatrix} \frac{1}{2}[L_2 + \frac{1}{2}(L_5 + L_1)] \\ \frac{1}{2}(L_5 + L_1) \\ \frac{1}{2\rho c}(L_5 - L_1) \\ L_3 \\ L_4 \end{pmatrix} = \begin{pmatrix} \frac{\partial m_1}{\partial x_1} \\ \frac{\partial(c^2 m_1)}{\partial x_1} + (1 - \gamma)\mu \frac{\partial p}{\partial x_1} \\ u_1 \frac{\partial u_1}{\partial x_1} + \frac{1}{\rho} \frac{\partial p}{\partial x_1} \\ u_1 \frac{\partial u_2}{\partial x_1} \\ \frac{\partial u_3}{\partial x_1} \end{pmatrix}. \quad (2.53)$$

According to Poinsot and Lele, the  $L'_i$ 's are the amplitudes of characteristic waves associated with each characteristic velocity  $\lambda_i$  [8]. Each characteristic velocity is related to the flow velocity  $u_i$  and to the speed of sound  $c$  as [10]

$$\lambda_1 = u_1 - c, \quad (2.54)$$

$$\lambda_2 = \lambda_2 = \lambda_4 = u_1, \quad (2.55)$$

$$\lambda_5 = u_1 + c, \quad (2.56)$$

where  $c$  is defined as

$$c^2 = \frac{\gamma p}{\rho}. \quad (2.57)$$

While  $\lambda_1$  is the velocity of wave propagating in the negative  $x$ -direction,  $\lambda_5$  is moving in positive direction, respectively. The convection velocity is related to  $\lambda_2$ , and  $\lambda_3$  and  $\lambda_4$  are the advection velocity for  $u_2$  and  $u_3$  into the  $x_1$  direction. The  $L_i$ 's are related to the characteristic

waves  $\lambda_i$  as

$$L_1 = \lambda_1 \left( \frac{\partial p}{\partial x_1} - \rho c \frac{\partial u_1}{\partial x_1} \right), \quad (2.58)$$

$$L_2 = \lambda_2 \left( c^2 \frac{\partial \rho}{\partial x_1} - \frac{\partial p}{\partial x_1} \right), \quad (2.59)$$

$$L_3 = \lambda_3 \frac{\partial u_2}{\partial x_1}, \quad (2.60)$$

$$L_4 = \lambda_4 \frac{\partial u_3}{\partial x_1}, \quad (2.61)$$

$$L_5 = \lambda_5 \left( \frac{\partial p}{\partial x_1} + \rho c \frac{\partial u_1}{\partial x_1} \right). \quad (2.62)$$

## 2.5 The Local One-Dimensional Inviscid (LODI) Relations

For one-dimensional Euler equations, it is possible to specify the values of  $L'_i$ 's for the waves, crossing the boundary. A LODI [8] system can be generated from equations (2.48) to (2.52) by neglecting viscous and transverse terms. As shown in figure 2.3, the procedure is done here for the outlet, located at  $x = L$ . Considering a system depending on primitive variables, the

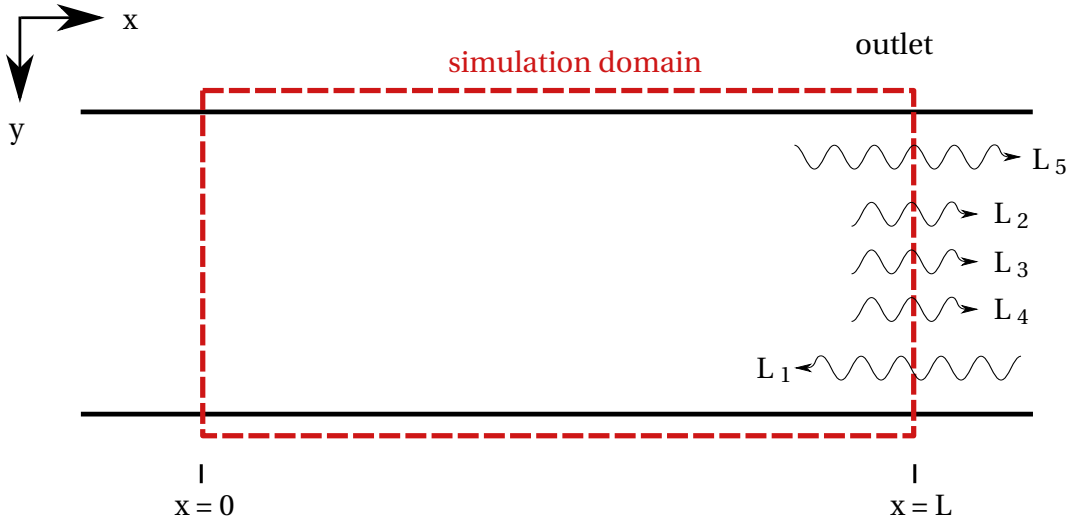


**Figure 2.3:** Model of  $L_i$  waves at the outlet.

equations (2.48) to (2.52) simplify to

$$\frac{\partial \rho}{\partial t} + \frac{1}{c^2} \left[ L_2 + \frac{1}{2} (L_5 + L_1) \right] = 0, \quad (2.63)$$

$$\frac{\partial p}{\partial t} + \frac{1}{2} (L_5 + L_1) = 0, \quad (2.64)$$

$$\frac{\partial u_1}{\partial t} + \frac{1}{2\rho c} (L_5 - L_1) = 0, \quad (2.65)$$

$$\frac{\partial u_2}{\partial t} + L_3 = 0, \quad (2.66)$$

$$\frac{\partial u_3}{\partial t} + L_4 = 0. \quad (2.67)$$

Poinsot [8] explained the gained relation as not of "physical conditions but should be more viewed as a compatibility relations made by the physical boundary conditions and the wave amplitudes crossing the boundary".

The relations above can also be combined to get a system of equation of the temperature  $T$ , the flow rate  $m_1 = \rho u_1$ , the entropy  $s$ , or the stagnation enthalpy  $h$ .

$$\frac{\partial T}{\partial t} + \frac{T}{\rho c^2} \left[ -L_2 + \frac{1}{2} (\gamma - 1) (L_5 + L_1) \right] = 0, \quad (2.68)$$

$$\frac{\partial m_1}{\partial t} + \frac{1}{c} \left[ M L_2 + \frac{1}{2} \{ (M - 1) L_1 + (M + 1) L_5 \} \right] = 0, \quad (2.69)$$

$$\frac{\partial s}{\partial t} - \frac{1}{(\gamma - 1) \rho T} L_2 = 0, \quad (2.70)$$

$$\frac{\partial h}{\partial t} + \frac{1}{(\gamma - 1) \rho} \left[ -L_2 + \frac{\gamma - 1}{2} \{ (1 - M) L_1 + (1 + M) L_5 \} \right] = 0. \quad (2.71)$$

Here, the enthalpy and the entropy are defined as  $h = (\rho E + p)/\rho = \frac{1}{2} u_i^2 + C_p T$  and  $s = C_v \log p / \rho^\gamma + const.$ . Furthermore,  $C_p$  and  $C_v$  are the specific heat capacities at constant pressure and volume, respectively.  $M$  is the local Mach number:  $M = u_1/c$ .

The system above shows the LODI relations in time derivatives. However, it is also possible to set up such a system in terms of gradients. There, all gradient normal to the boundary  $x_1$  can be calculated with

$$\frac{\partial \rho}{\partial x_1} = \frac{1}{c^2} \left[ \frac{L_2}{u_1} + \frac{1}{2} \left( \frac{L_5}{u_1 + c} + \frac{L_1}{u_1 - c} \right) \right], \quad (2.72)$$

$$\frac{\partial p}{\partial x_1} = \frac{1}{2} \left( \frac{L_5}{u_1 + c} + \frac{L_1}{u_1 - c} \right), \quad (2.73)$$

$$\frac{\partial u_1}{\partial x_1} = \frac{1}{2\rho c} \left( \frac{L_5}{u_1 + c} - \frac{L_1}{u_1 - c} \right), \quad (2.74)$$

$$\frac{\partial T}{\partial x_1} = \frac{T}{\rho c^2} \left[ -\frac{L_2}{u_1} + \frac{1}{2} (\gamma - 1) \left( \frac{L_5}{u_1 + c} + \frac{L_1}{u_1 - c} \right) \right]. \quad (2.75)$$

A quick example demonstrates the easy application and usage of the LODI system. Saying, a constant pressure is applied at the inlet. The corresponding LODI relation (2.64) is rewritten here again

$$\frac{\partial p}{\partial t} + \frac{1}{2} (L_5 + L_1) = 0,$$

it can be seen that the wave amplitudes have to be set in relation  $L_5 = -L_1$ , to guarantee the constant pressure assumption.

$$\frac{\partial p}{\partial t} = 0 \quad \rightarrow \quad L_5 = -L_1.$$

## 2.6 NSCBC with Plane Wave Masking (PW)

For a one-dimensional Euler equation system, the LODI relations allow to determine the values of  $L'_I$ 's, as introduced in the previous section 2.5. One advantage of using the NSCBC approach is the identification of the waves crossing the boundary. According to figure 2.3, two wave directions can be observed. At the outlet,  $L_2$  to  $L_5$  are leaving the simulation domain, while  $L_1$  is entering it. For calculating the wave exiting the domain, the points inside the domain can be used to determine its further behavior. For waves, accessing the domain, the behavior has to be specified by some approximations. A method to determine these waves is now introduced.

Rewriting the LODI relations for pressure and velocity, we get

$$\frac{\partial p}{\partial t} + \frac{1}{2} (L_5 + L_1) = 0, \tag{2.76}$$

$$\frac{\partial u}{\partial t} + \frac{1}{2\rho c} (L_5 - L_1) = 0. \tag{2.77}$$

Two types of reflecting boundary conditions are distinguish, a fully reflecting boundary condition and a partially reflecting boundary condition.

### Fully reflecting boundary conditions

Examples for a fully reflecting boundary condition are an open end or a closed end. Imposing an open end at the outlet, the acoustic fluctuation of pressure is defined as  $p_A = f + g = 0$  [9], which leads to a LODI relation (2.76) of  $L_1 + L_5 = 0$ . While for a closed end inflow boundary, the acoustic fluctuation is obtained by the velocity to the formula of  $u_A = f - g = 0$  that results in a LODI relation (2.77) of  $L_1 = L_5$ .

### Partially reflecting boundary conditions

For the partially reflecting boundary condition, some specifications has to be done to use them reasonable. Poinsot [8] constructed a low reflecting outflow boundary condition with the help of a relaxation factor  $\sigma$ . Without the linear relaxation term, Poinsot investigated a

wrong reflection behavior, as the information propagating with the waves are lost, which leads to a ill posed problem.

For an outflow, the leaving wave  $L_5$  is determined with the inner points of the computational domain as

$$L_5 = (u + c) \left( \frac{\partial p}{\partial x} + \rho c \frac{\partial u}{\partial x} \right), \quad (2.78)$$

while  $L_1$  is the reflected wave entering into the domain and is therefore determined as [8]

$$L_1 = \frac{\sigma}{\bar{\rho} \bar{c}} (p - p_\infty). \quad (2.79)$$

Polifke [9] observed that the proposed boundary type from Poinsot (2.79) can not obtain a good reflection behavior for all frequencies. A plane wave masking is added to the NSCBC to minimize the plane acoustic reflection. The idea was to "identify outgoing plane waves at the boundary, and then explicitly eliminate outgoing wave contributions form the linear relaxation term" [9].

For the outflow boundary condition,  $L_5$  is defined as in equation (2.78), while the  $L_1$  wave is calculating with the formula

$$L_1 = \frac{\sigma}{\bar{\rho} \bar{c}} (p - \bar{\rho} \bar{c} (f_d + g_x) - p_\infty) + 2 \frac{\partial g_x}{\partial t}. \quad (2.80)$$

The term  $\bar{\rho} \bar{c} (f + g_x) = p'_A$  express the acoustic part of the pressure fluctuation. This term eliminates any plane wave acoustic fluctuation at the boundary condition. The variables  $g_x$  is the external excitation, where an amplitude of an imposed plane wave entering the domain can be defined.

A non-reflective inflow boundary condition can be constructed, analogously. The wave  $L_1$  exits the computational domain, so it depends on the variables of the internal field. This leads to following formula

$$L_1 = (u - c) \left( \frac{\partial p}{\partial x} - \rho c \frac{\partial u}{\partial x} \right). \quad (2.81)$$

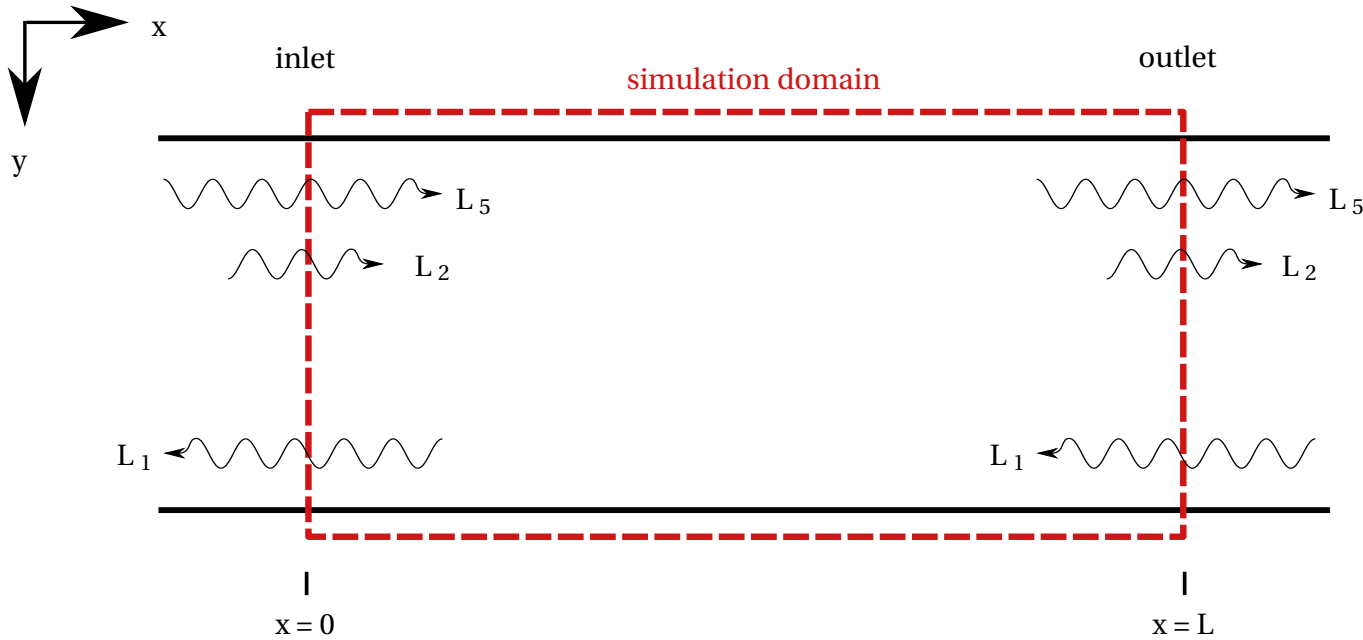
According to PWM [9], the in-going wave  $L_5$  is given as

$$L_5 = \sigma (u - (f_x - g_u) - u_T) + 2 \frac{\partial f_x}{\partial t}. \quad (2.82)$$

Here  $f_x$  is the amplitude of a plane wave imposed at the boundary entering the domain.

In this thesis, the LODI relations for the pressure, velocity and temperature at the inlet and outlet are observed. The boundary conditions are implemented in an OpenFOAM environment. A 2D wave is observed, so the LODI relations for  $L_3$  and  $L_4$  are set to zero, as no advection velocity is assumed ( $\lambda_3 = \lambda_4 = 0$ ). Figure 2.4 is giving a short overview of the waves entering and leaving the simulation domain at the inlet and outlet. Table 2.1 is showing the related formulas. The middle column demonstrates the LODI relations for pressure, velocity and temperature, while the definitions of  $L_1$ ,  $L_2$  and  $L_5$  can be looked up in the first column for the inlet and in the third column for the outlet.

Overview of the related formulas for the implementation of the boundary condition in this thesis:



16

**Figure 2.4:** Model of related  $L_i$  waves for the simulation in this thesis.

Inlet	LODI system	Outlet
$L_1 = (u - c) \left[ \frac{\partial p}{\partial x} - \rho c \frac{\partial u}{\partial x} \right]$ $L_5 = \sigma_5 [u - (f_x - g_u) - u_T] + 2 \frac{\partial f_x}{\partial t}$ $L_2 = \sigma_2 \left[ T - \frac{\gamma-1}{\gamma} (f_d + g_x) - T_t \right]$	$\frac{\partial p}{\partial t} + \frac{1}{2} (L_5 + L_1) = 0$ $\frac{\partial u_1}{\partial t} + \frac{1}{2\rho c} (L_5 - L_1)$ $\frac{\partial T}{\partial t} + \frac{T}{\rho c^2} (-L_2 + \frac{1}{2} (\gamma - 1) (L_5 + L_1))$	$L_1 = \frac{\sigma_1}{\rho c} [p - \rho c (f_d + g_x) - p_\infty] + 2 \frac{\partial g_x}{\partial t}$ $L_5 = (u - c) \left[ \frac{\partial p}{\partial x} + \rho c \frac{\partial u}{\partial x} \right]$ $L_2 = u \left[ c^2 \left( \frac{\partial \rho}{\partial x} - \frac{\partial p}{\partial x} \right) \right]$

**Table 2.1:** LODI relations and the definition of  $L_1$ ,  $L_2$  and  $L_5$  at the inlet and outlet.

## 2.7 Characteristic Based State-Space Boundary Conditions (CBSBC)

The simulation domain is only a small part of the whole combustion chamber. The remaining fluid flow is modeled by one-dimensional state space systems. Therefore, a good coupling between the CFD domain and the state space model is essential. It is realized by the Characteristic Based State Space Boundary condition (CBSBC).

According to Polifke [9], CBSBC is a continuous-time state-space model to describe the frequency dependent reflection of acoustic waves. As linearized Euler and Navier-Stokes equations are used, the state-space model can be determined with a set of linear partial differential equations (PDE). An exhaust duct is used as an example to explain the usage of the CBSBC. Figure (2.5) is showing the model of the CBSBC at the outlet of the simulation domain.

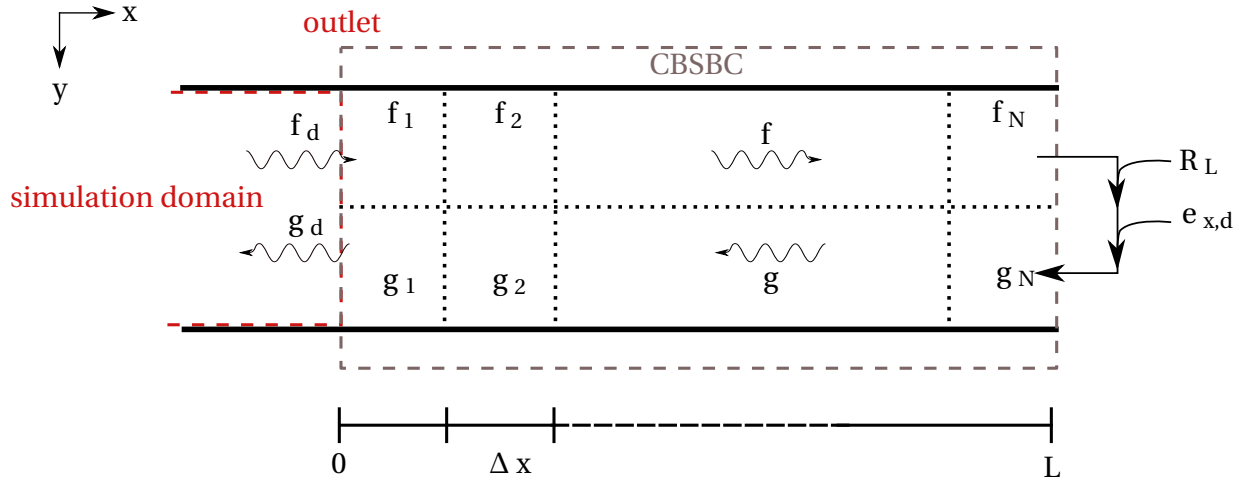


**Figure 2.5:** Model of CBSBC located at the outlet of the simulation domain.

The  $f_d$  wave is leaving the simulation domain and entering into the CBSBC model. It is then propagating through the time-domain model till it reaches the distance  $x = L$ . At this point, the reflection coefficient  $R_L$  is multiplied to wave  $f_n$ , an external source acoustic source  $e_{x,d}$  can be additionally added to obtain  $g_N$ . The  $g$  wave is then propagating back till it leaves the CBSBC domain at  $g_1$  and is reentering the simulation domain via the wave  $g_d$ . The setup for the matrices is showed now:

Considering the one dimensional Euler equation and neglecting mean-flow gradients, the formulas are gained

$$\frac{\partial f}{\partial t} + (\bar{u} - \bar{c}) \frac{\partial f}{\partial x} = 0, \quad (2.83)$$

$$\frac{\partial g}{\partial t} + (\bar{u} - \bar{c}) \frac{\partial g}{\partial x} = 0. \quad (2.84)$$

## Theoretical Background

---

At the positions  $x = 0$  and  $x = L$  of the CBSBC model, the boundaries are defined as

$$f(x = 0, t) = f_1 = f_d, \quad (2.85)$$

$$g(x = L, t) = g_N = R_L f(x = L, t) + e_{x,d}. \quad (2.86)$$

The coupling between the acoustic model and the CFD domain is done via a Dirichlet boundary condition at point  $x = 0$ . The reflection of an acoustic wave at the boundary is done with a scalar reflection coefficient  $R_L$  located at  $x = L$ . An acoustic source  $e_{x,d}$  can be applied, if wanted.

For the spatial discretisation, a linear upwind finite difference scheme is applied. We get

$$\frac{\partial f_i}{\partial t} = -(\bar{u} + \bar{c}) \frac{f_i - f_{i-1}}{\Delta x}, \quad (2.87)$$

$$\frac{\partial g_i}{\partial t} = -(\bar{u} + \bar{c}) \frac{g_i - g_{i-1}}{\Delta x}. \quad (2.88)$$

The boundaries are expressed as

$$\frac{\partial f_2}{\partial t} = -(\bar{u} + \bar{c}) \frac{f_2 - f_d}{\Delta x}, \quad (2.89)$$

$$\frac{\partial g_{N-1}}{\partial t} = -(\bar{u} + \bar{c}) \frac{R_L f_N + e_{x,d} - g_{N-1}}{\Delta x}. \quad (2.90)$$

For the state-space model, the matrix vector form leads to

$$\underbrace{\frac{\partial}{\partial t} \begin{pmatrix} f_2 \\ f_3 \\ \vdots \\ f_N \\ g_1 \\ \vdots \\ g_{N-2} \\ g_{N-1} \end{pmatrix}}_{\dot{\mathbf{x}}} = \underbrace{\begin{bmatrix} -\alpha_+ & 0 \\ \alpha_+ & -\alpha_+ \\ \ddots & \ddots \\ & \alpha_+ & -\alpha_+ \\ & & \alpha_- & -\alpha_- \\ & & \ddots & \ddots \\ & & & \alpha_- & -\alpha_- \\ & & & 0 & \alpha_- \end{bmatrix}}_{\underline{A}} \times \begin{pmatrix} f_2 \\ f_3 \\ \vdots \\ f_N \\ g_1 \\ \vdots \\ g_{N-2} \\ g_{N-1} \end{pmatrix}_{\mathbf{x}} + \underbrace{\begin{bmatrix} \alpha_+ & 0 \\ 0 & 0 \\ \vdots & \vdots \\ 0 & 0 \\ 0 & -\alpha_- \end{bmatrix}}_{\underline{B}} \underbrace{\begin{bmatrix} f_d \\ e_{x,d} \end{bmatrix}}_{\mathbf{u}} \quad (2.91)$$

$$\underbrace{g_d}_{y} = g_1 = \underbrace{\begin{bmatrix} 0 & \cdots & 0 & 1 & 0 & \cdots & 0 \end{bmatrix}}_C \mathbf{x} + \underbrace{\begin{bmatrix} 0 & 0 \end{bmatrix}}_D \mathbf{u} \quad (2.92)$$

with  $\alpha_+ = (\bar{u} + \bar{c}) / \Delta x$  and  $\alpha_- = (\bar{u} - \bar{c}) / \Delta x$ . In this form, the meaning of the parameters of the state space model becomes evident.

The matrices  $\underline{A}$ ,  $\underline{B}$ ,  $\underline{C}$  and  $\underline{D}$  are the state space matrices and  $\mathbf{x}$  is the state vector. The state vector  $\mathbf{x}$  contained the wave values of  $f$  and  $g$  at the knots in the mesh. Matrix  $\underline{A}$  elements are set by the discretisation scheme. The coupling between  $f_n$  and  $g_{N-1}$  is described by the off diagonal element and it also shows the reflection at the outlet of the resonator. Matrix  $\underline{B}$

models, how the input signal  $\mathbf{u}$  affects the temporal derivative of the state vector. As in Matrix  $\underline{\mathbf{A}}$  and  $\underline{\mathbf{B}}$  are set by the discretisation scheme. The feed through is defined as a null vector ( $\underline{\mathbf{D}}$ ). In the matrix  $\underline{\mathbf{C}}$ , the element unlike zero, gives the output  $g_1$  by multiplying the matrix  $\underline{\mathbf{C}}$  with the state vector  $\mathbf{x}$ .  $g_1$  is equal to  $g_d = y$ .

In this thesis, the CBSBC is mainly set to be non-reflecting. Possibilities to generate non-reflection boundary condition is to set the matrices  $\underline{\mathbf{A}}$ ,  $\underline{\mathbf{B}}$  or  $\underline{\mathbf{C}}$  equal to zero. By setting one of the matrices equal to zero, the propagation of the waves through the CBSBC model is interrupted, as the information can not be transported through the whole domain, see (2.91) and 2.92.

## 2.8 Stokes Boundary Layer

Considering an oscillation flow, a boundary layer close to the wall is generated. For a laminar flow, a exact solution of the Navier-Stokes equations can be calculated. The equation is introduced for the case with an oscillating wall and a viscous fluid in rest and will be then extended to the case for oscillating flow and rigid wall. Considering an oscillating plate, the Navier-Stokes equation simplify to [1]

$$\frac{\partial u}{\partial t} = \nu \frac{\partial^2 u}{\partial y^2}, \quad (2.93)$$

describing the viscosity evolution away from the wall. The velocity is assumed to propagate in the x-direction, parallel to the oscillation direction.  $y$  is showing the distance from the wall. Following boundary conditions arise for this problem

$$\begin{aligned} t \leq 0 : \quad y \geq 0 : \quad & u_1(y, t) = 0, \\ t > 0 : \quad y = 0 : \quad & u_1(0, t) = U_0 \cdot \cos(\omega t), \\ y \rightarrow \infty : \quad & u_1(\infty, t) = 0. \end{aligned}$$

For a time  $t \leq 0$  s, the wall is considered in rest. After that, the motion of the wall is  $U_0 \cdot \cos(\omega t)$ . After some transformation, the solution of the flow velocity is gained in the formula (see in [1] for a detailed transformation)

$$u_1(y, t) = U_0 \cdot \exp\left(-\sqrt{\frac{\omega}{2\nu}}y\right) \cdot \cos\left(\omega t \sqrt{\frac{\omega}{2\nu}}y\right) \quad (2.94)$$

where

$$\kappa = \sqrt{\frac{\omega}{2\nu}}, \quad (2.95)$$

can be defined as the wave number in y-direction.  $\omega$  is defined as the *angular frequency of the motion* and can be calculated by using the relation between angular frequency and frequency

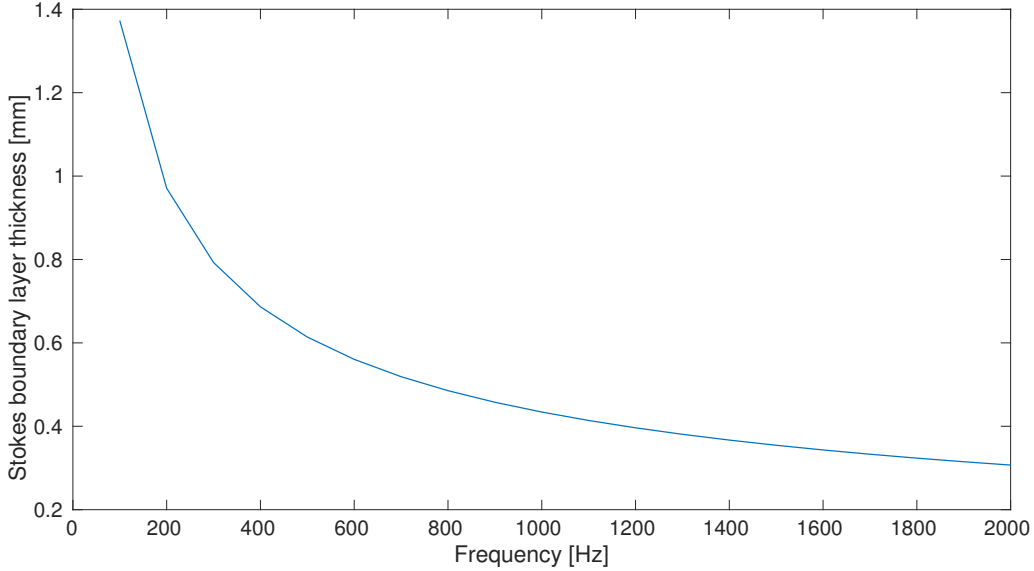


**Figure 2.6:** Stokes Boundary Layer Thickness over frequency.

$\omega = 2\pi F$ , while  $\nu$  is showing the viscosity. Furthermore, a stokes boundary thickness is defined by

$$\delta = \frac{2\pi}{\kappa} = 2\pi \sqrt{\frac{2\nu}{\omega}}. \quad (2.96)$$

The stokes boundary layer thickness was used in this thesis to identify a fully generated boundary layer at the no-slip wall. Figure 2.6 is showing the stokes boundary layer thickness over the frequency.

Considering an oscillating flow near a rigid wall, the solution of the flow velocity changes to

$$u_1(y, t) = U_0 \cdot \left[ \cos(\omega t) \cdot \exp\left(-\sqrt{\frac{\omega}{2 \cdot \nu}} y\right) \cdot \cos\left(\omega t \sqrt{\frac{\omega}{2 \nu}} y\right) \right]. \quad (2.97)$$

## 2.9 OpenFOAM

### Basic

The investigation of the validation of the CBSBC were done using OpenFOAM Version 2.3.1. OpenFOAM is an open source Computational Fluid Dynamic (CFD) software tool. CFD allows to predict and analyze fluid flows by numerical simulation. It plays an important role, as it allows a cheap method to investigate the flow dynamics in early states of a design process. The open code allow to implement and modify models in a huge range, which is very helpful and beneficial for academical research investigations. That's also why the CBSBCs are implemented in this.

The CBSBC were applied as a boundary condition for OpenFOAM and compiled. As a 2D channel were investigated, the geometry and mesh were created using the blockMesh dict. To read out pressure and velocity for the related cells, the swak4Foam [4] toolbox was embed into the software. The rhoPimpleFoam solver was used, as compressible flow is considered. The values from swak4Foam were read into Matlab, from where the  $f$  and  $g$  waves were calculated.

### Implementation of CBSBC in OpenFOAM

The boundary conditions used for the simulations in OpenFOAM were created by the chair "Professur für Thermofluidynamik" of the TUM. It was integrated into the OpenFOAM environment. Following six boundary types were used: CBSBCInletPressure, CBSBCInletTemperature, CBSBCInletVelocity, CBSBCOutletPressure, CBSBCOutletTemperature, CBSBCOutletVelocity.

The implementation in OpenFOAM was done using a Transient Robin Boundary Conditions according to Vilums [11]. In OpenFOAM, the boundary conditions of type Dirichlet and Neumann respectively *fixedValue* and *fixedGradient* are pre-defined. With the help of the *swak4foam* library from B. Gschneider, a mixed boundary condition, called *groovyBC* can be constructed [4]. This boundary condition allows also to define variables and functions on the boundary calculated at every internal iteration. By looking into the source code of *mixed BC* [4], the LODI relations equations has to look like:

$$P_{face}^{n+1} = f \cdot valueExpr + (1 - f) (P_{centre}^{n+1} + gradExpr \cdot \delta). \quad (2.98)$$

Exemplary, the pressure is shown in (2.98). For the temperature, use  $T$  instead of  $P$ . Here,  $f$  is defined as the *fractionExpression* and has to be obtained by user. The distance between the cell centre and cell face is represented by  $\delta$ .

To gain the form of equation as seen in (2.98), the LODI relations has to be linearized. The linearization and the comparison with the implemented values in the .C file are shown in the annex A - D. For the CBSBCInletPressure and CBSBCInletTemperature cases, the different algebraic sign is because the normal patch vector is in the opposite direction than the flow direction.

An extract of the velocity boundary condition, defined in the 0-folder of the simulation, is

## Theoretical Background

---

shown in the annex E and will be described here shortly. For the inlet boundary field, the type of the CBSBC (here CBSBCInletVelocity) and some constant variables are defined in the beginning. The sub-folder of the velocity allows to define a *target value*. Compare with section 2.6, where the formula for the inlet velocity is shown. This value will be changed to set up a mean-flow, but it is considered in more detail in the section 3.5. The text-file of the incoming  $f$  wave is determined in the sub-folder *tableFileCoeffs*. In the text-file *inletf\_700.txt*, a wave with a frequency of  $F = 700$  Hz and a sound pressure level of  $SPL = 75$  dB is selected. For all simulation cases, no changes in  $SPL$  are made. Only the frequency is modified in section 4.4. The *ssFileName* defines the state-space model, named here as "statespace.dat". The state-space model contains two patch numbers of CBSBC. Here, patch -1 is used for the inlet while -2 is used for the outlet. Furthermore, a characteristic acoustic length scale and a initial value can be defined.

The outlet definition has the similar beginning. But for this case, a target value for the pressure is defined. Compare again with 2.6, where the LODI relation and the related formula for the outlet pressure is defined. Furthermore, an excitation signal can be obtained. For the outlet, the *ssPatch* with number -2 is used.

# 3 Simulation Results for Slip Boundary Conditions

Chapter 3 is beginning with the introduction of the geometry and its meshing. The next section displays the general behavior of the CBSBC with a defined reflection coefficient. Figures of velocity, pressure and the waves are demonstrated to get a first impression of the simulation. Then, the CBSBC is set to be non-reflecting, the resulting reflection coefficient is calculated. Furthermore, different options for setting a mean-flow to the simulation are investigated. The chapter slip 3 is closing with investigations for the reflecting coefficient of different mean-flows. If not mentioned explicit, a frequency of  $F = 700\text{Hz}$  is used for all setups.

## 3.1 Simulation Setup of Slip Case

For the slip case, a 2D channel with dimensions of (600 mm x 20 mm x 1 mm) and a meshing of (400 20 1) is used. The mesh of the geometry can be seen in figure 3.1, and a detailed view to see the cell size is done in figure 3.2. This big size of geometry was set because the first simulations does not need this many computational hours and the development of the longitudinal waves (wave crest and wave trough) can be seen (fig. 3.3).

The CBSBC boundary condition is applied at the outlet and inlet patch, while top and bottom wall are set as slip boundary conditions. Waves, with a frequency of  $F = 700\text{Hz}$  and a sound pressure level of  $SPL = 75\text{ dB}$  are propagating through the inlet into the channel and are then interacting with the reflection coefficient at the outlet. As slip boundary conditions are applied, no wall interfaces are expected. So a surface area expression was set in OpenFOAM, to evaluate the values for pressure and velocity. Figure 3.2 is showing a detailed view on the

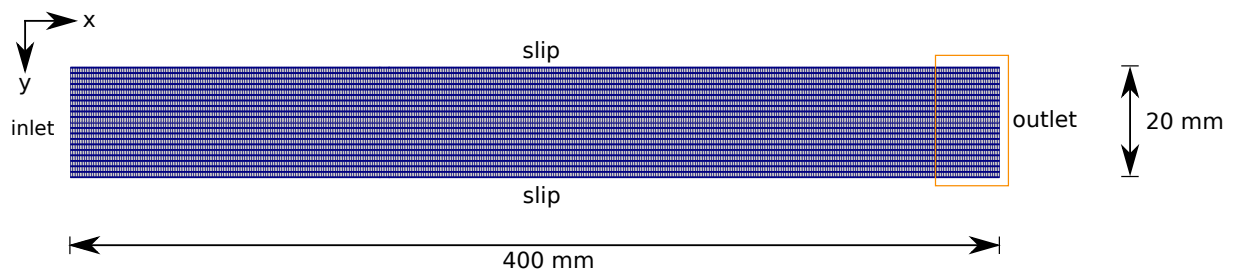


**Figure 3.1:** Mesh of geometry for the slip case.

mesh. The cell size in x-direction is given as  $\Delta x = 1.5\text{ mm}$ , while in y-direction, it is  $\Delta y = 1\text{ mm}$ . The extract is showing 20 cells in y-direction and 12 cells in x-direction.

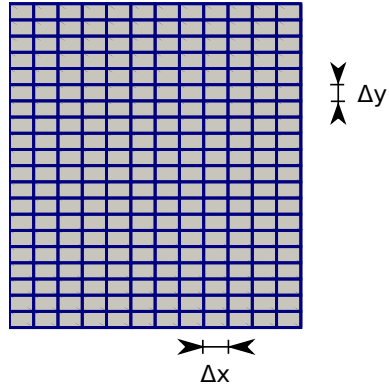


**Figure 3.2:** Detailed view of the mesh for the slip case.

Having a closer look to the velocity distribution for a time  $t = 1.9\text{ ms}$ , displayed in figure 3.3, the longitudinal wave can be detected. As plane waves are treated, the red area is showing the wave crest, while the blue area stands for the wave trough. This figure should manifest the



**Figure 3.3:** Velocity distribution for the time-step  $t = 1.9\text{ ms}$ ; showing wave crest (red) and wave trough (blue).

choice of the selected geometry. A whole wave period can be seen along the x-axis, which was a good help for understanding the results of the first simulations.

## 3.2 Generation of Results for Slip Case

The procedure for calculating the reflection coefficient for the slip case is shown in the diagram below (figure 3.4).

From OpenFOAM, two vectors, one for velocity ( $u_{OF}$ ) and one for pressure ( $p_{OF}$ ), are evaluated for every time step with the help of the *swak4Foam* library. To ensure a good quality of the wave propagation, a time step of  $t = 1 \cdot 10^{-6}\text{ s}$  is used. The velocity and pressure vectors are then written into the MATLAB environment. Applying a mean-flow to the simulation requires an elimination of it. To do so, a mean value over a period time is calculated and then subtracted from the variables. This leads to the acoustic fluctuation of pressure and velocity  $u_A$  and  $p_A$ . Applying no mean-flow does not need to eliminate the mean variable, however it is done to ensure its quality. With the help of  $p_A$  and  $u_A$ , the  $f$  and  $g$  waves can be calculated.

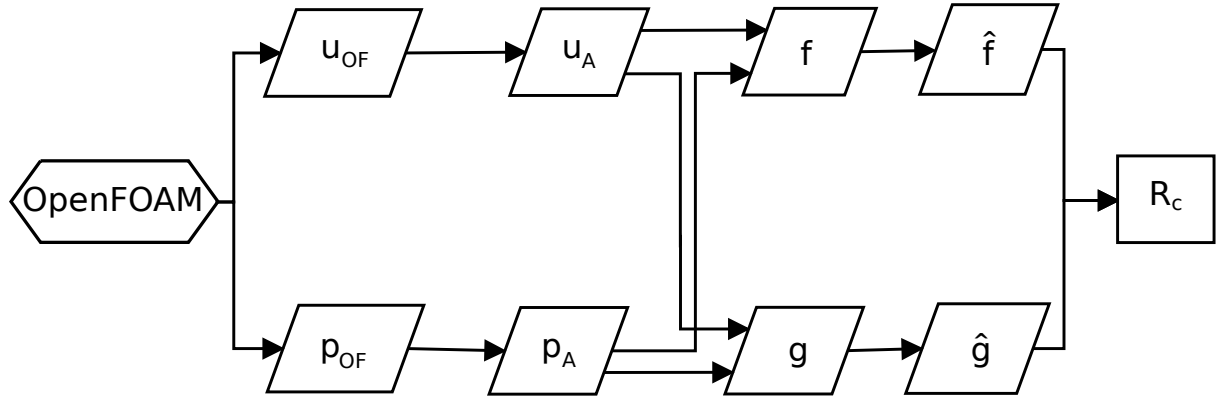


**Figure 3.4:** Diagram for calculating  $R_c$  for the slip case.

The equations are shown here again quickly.

$$f = \frac{1}{2} \left( \frac{p_A}{\bar{\rho} \bar{c}} + u_A \right),$$

$$g = \frac{1}{2} \left( \frac{p_A}{\bar{\rho} \bar{c}} - u_A \right).$$

Applying a Fourier transformation on the  $f$  and  $g$  waves leads to the corresponding amplitudes ( $\hat{f}$  and  $\hat{g}$ ). By setting these in relation, the reflection coefficient  $R_c$  is generated with the formula

$$R_c = \frac{\hat{g}}{\hat{f}}.$$

### 3.3 Applying Reflecting CBSBC

First, the behavior of the CBSBC boundary condition is introduced in a general case. The reflection coefficient is defined as  $R_c = 0.8$  at the outlet and at the inlet. To evaluate the pressure and velocity, surface averages at positions  $x = 0.005\text{ m}$  and  $x = 0.595\text{ m}$  are defined in OpenFOAM. These values were written into the MATLAB environment, to generate the  $f$  and  $g$  waves.

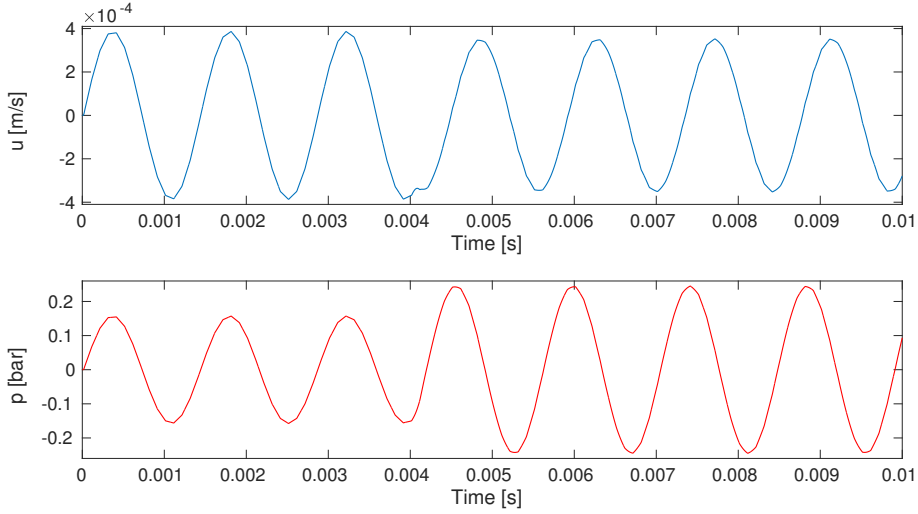
#### Inlet

Figure 3.5 is showing the pressure and velocity evolution over time at the inlet. After a time of  $t = 0.004\text{ s}$ , a little disturbance in the velocity graph can be detected, due to the interaction with the new generated  $g$  wave, compare with figure 3.6. After passing this time, a smaller amplitude of the velocity oscillation can be seen. The pressure graph does not have this disturbance, however, it is changing its amplitude to a higher value after it passes  $t = 0.004\text{ s}$ .

Figure 3.6 is showing the calculated  $f$  and  $g$  wave. The generation of  $g$  wave is beginning at the time  $t = 0.004\text{ s}$ . As explained, this leads to the disturbance seen in the velocity plot

## Simulation Results for Slip Boundary Conditions

---



**Figure 3.5:** Velocity and pressure evolution at the inlet.

of figure 3.5. The  $f$  wave is continuing its behavior without any loss in its amplitude value. Comparing both amplitudes a reflection coefficient of  $R_c = 0.80$  is calculated.

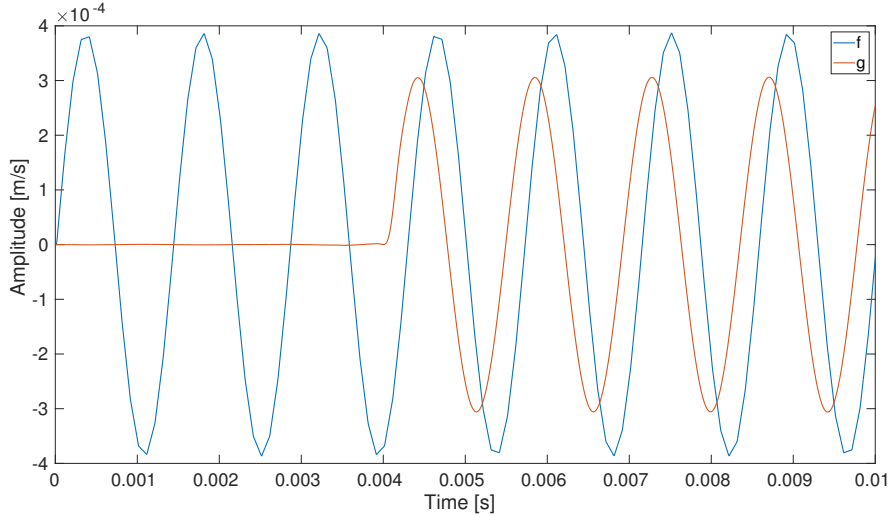


**Figure 3.6:** The  $f$  and  $g$  wave evolution at the inlet.

## Outlet

Having now a look at the outlet, following velocity and pressure evolution is generated, see fig. 3.7. It takes nearly 0.0017 s for the velocity and pressure waves to reach the position of the surface average ( $x = 0.595$  m). After this, it takes one oscillation with a smaller amplitude

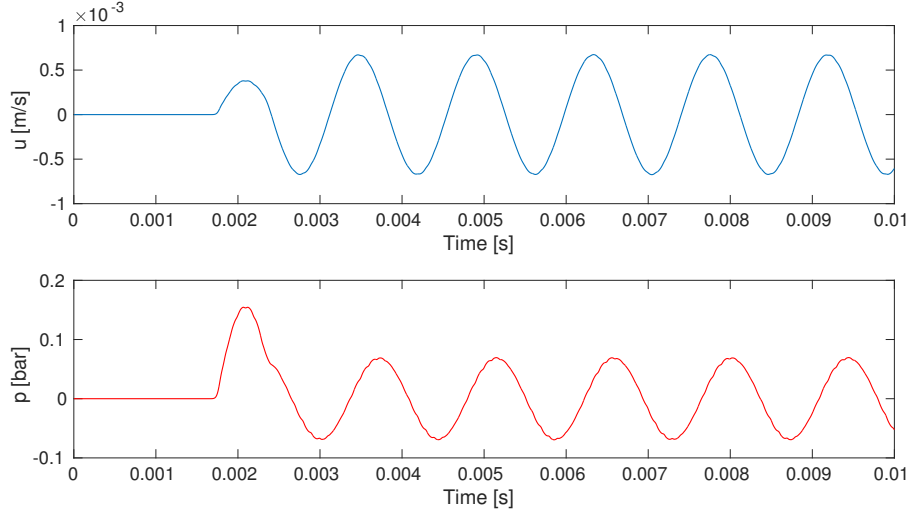


**Figure 3.7:** Velocity and pressure evolution at the outlet.

for the velocity graph to reach its harmonious oscillation behavior. The pressure is raising strongly after the  $f$  wave is reaching the outlet patch, then it has a little kink at the time of  $t = 0.023$  s, and it is then oscillating till the end of simulation time.

The resulting  $f$  and  $g$  wave plots can be seen in figure 3.8. Similar to the velocity and

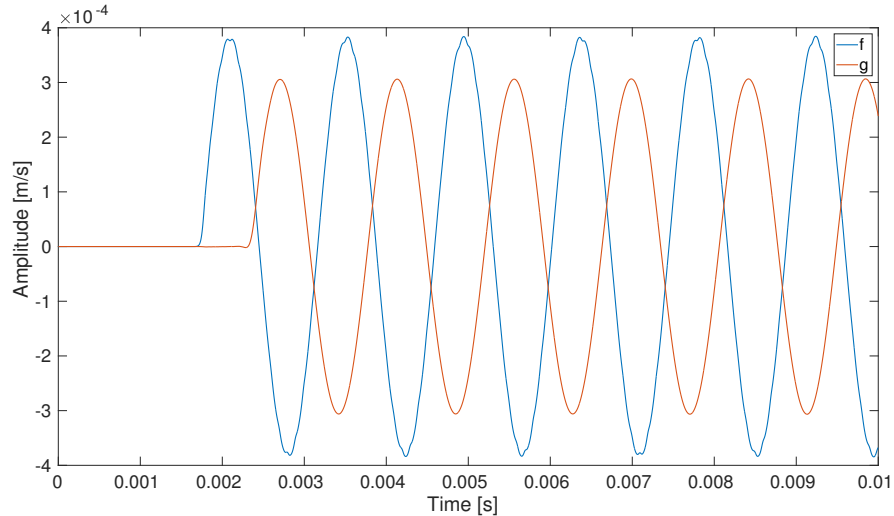


**Figure 3.8:** The  $f$  and  $g$  wave evolution at the outlet.

pressure graphs, it took  $t = 0.0017$  s for the  $f$  wave to reach the outlet. Then it took additionally 0.007 s for the  $f$  wave to cross the state-space model. After 0.025 s the  $g$  wave is generated. The beginning of the  $g$  wave and the kink in the pressure graph (fig. 3.7) are happening at the same time-step, so the pressure kink is due to the generation of the  $g$  wave. Again, a comparison of

the amplitude of  $f$  and  $g$  waves lead to a reflection coefficient of  $R_c = 0.80$ , same as for the inlet observation.

### 3.4 Applying Non-Reflecting CBSBC

After the behavior of the CBSBC boundary condition in a general environment was introduced, a non reflecting boundary condition is now applied at the outlet. As in the declaration of the CBSBC (see sec. 2.7), the matrices  $\underline{A}$ ,  $\underline{B}$  and  $\underline{C}$  can be set to zero to obtain a non reflection. The comparison of all three cases leads to the decision to set the  $\underline{B}$  matrix to zero, as it prevents the reflection the best. In figure 3.9, the reflecting  $g$  wave is almost equal to zero. A

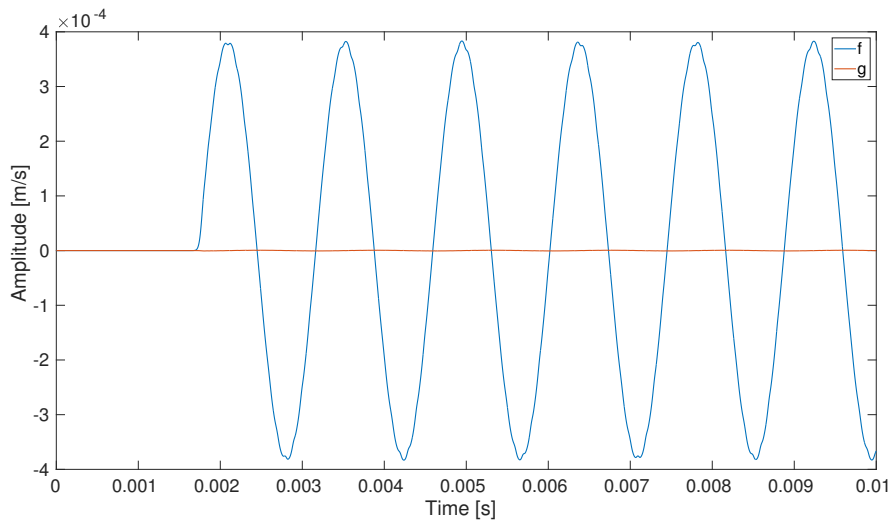


**Figure 3.9:** The  $f$  and  $g$  wave evolution at the outlet for  $\underline{B} = 0$ .

detailed figure of the  $g$  wave (3.10) is showing an anti-cyclical behavior in comparison to the  $f$  wave. The spikes can not be explained in detail. Comparing the amplitudes of  $f$  and  $g$  waves leads to a reflection coefficient of  $R_c = 0.00155$ . This means, the reflecting  $g$  wave has an amplitude smaller than 0.1% in comparison to the  $f$  wave, which leads to the assumptions, that the outlet CBSBC can be suppose to be non-reflective.

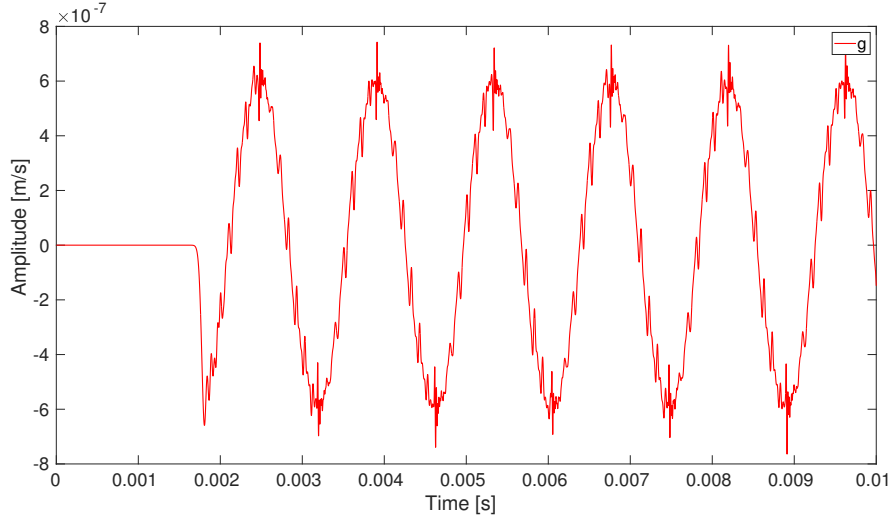


**Figure 3.10:** Detailed view on the  $g$  wave for  $\underline{B} = 0$ .

0-Folder	Sub-item	Option 1	Option 2	Option 3	Option 4
U	uniform	(0 0 0)	(0.001 0 0)	(0 0 0)	(0.001 0 0)
	targetValue	(0.001 0 0)	(0.001 0 0)	(0.001 0 0)	(0.001 0 0)
p	targetValue	(0 0 0)	(0 0 0)	(0.001 0 0)	(0.001 0 0)
T	targetValue	(0 0 0)	(0 0 0)	(0.001 0 0)	(0.001 0 0)

**Table 3.1:** Options to define a mean-flow in the boundary conditions.

## 3.5 Applying a Mean-Flow to the Slip Simulation Case

The previous chapter investigated the behavior of reflection and non-reflection without a mean-flow. Now, a mean-flow is applied to the system. By looking at the CBSBC boundary condition .H file, few options could be detected to generate a mean flow (see appendix E). In the 0-folder, the velocity can be set to an uniform value for the internal field. Also, a target velocity value can be defined at the inlet in the velocity, pressure and temperature file. This section wants to point out the best apply to set a mean-flow. The investigation is done using a mean-flow of  $\bar{u} = 0.001 \text{ m/s}$ , to see its behavior and not wasting much computational power.

Four cases, see table 3.1, are compared for setting a mean-flow to the boundary conditions. Setting the mean-flow only as a *targetValue* for the velocity, leads to mean value not equal to  $\bar{u} = 0.001 \text{ m/s}$ . Adding a uniform velocity to the first setup (Option 2) also does not provide the defined mean-flow. So both Options are not suitable configurations. Option 3 and Option 4 are a good choice to set up mean-flows, as the applied mean-flow is reached after  $t = 0.0075 \text{ s}$ . Option 3 was selected, as a consistent evolution of the velocity and pressure graph could be detected.

For a better understanding, the velocity and pressure evolution and the  $f$  and  $g$  waves for

## Simulation Results for Slip Boundary Conditions

---

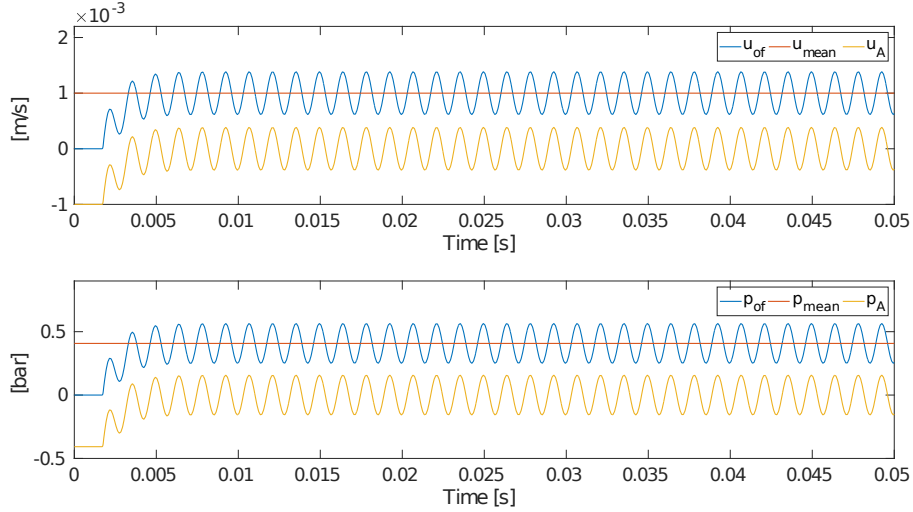


**Figure 3.11:** Velocity and pressure evolution for Option 3.

a mean-flow of  $u = 0.001 \text{ m/s}$  are displayed now for Option 3. Having a look at figure 3.11, it is showing three velocities. The blue graph refers to the velocity evaluated from OpenFOAM ( $u_{OF}$ ). Starting from a value of  $u = 0 \text{ m/s}$ , a mean velocity  $\bar{u} = 0.001 \text{ m/s}$  of the velocity fluctuation is reached after nearly  $t = 0.0075 \text{ s}$ . Variable  $u_{mean}$  is calculated for one time period ( $\Delta T = 1428 \text{ s}$ ) to a value of  $u_{mean} = 0.001 \text{ m/s}$ . For calculating the  $f$  and  $g$  waves, the velocity from OpenFOAM has to be subtracted by the calculated mean velocity. The yellow graph is showing the resulting velocity, the acoustic fluctuation velocity ( $u_A$ ). For the evolution of the three pressure variables, similar behavior is detected. The acoustic fluctuation pressure part  $p_A$  was generated by subtracting  $p_{mean} = 0.4074 \text{ Pa}$  from  $p_{OF}$ . Both yellow graphs ( $u_A$  and  $p_A$ ) are then used to calculate the  $f$  and  $g$  waves, see in fig. 3.12. The blue graph is showing the resulting  $f$  wave, while the  $g$  wave is displayed in red. Due to the generation of the acoustic part of velocity and pressure, the  $f$  wave is starting with a negative value of  $f = -0.001 \text{ m/s}$ . After  $t = 0.01 \text{ s}$ , a stable oscillation around the x-axis can be detected. The maximum amplitude of  $f$  wave is equal to  $\hat{f} = 3.08 \cdot 10^{-4}$ , while  $g$  wave is reaching a maximum value of  $\hat{g} = 6.6 \cdot 10^{-7}$ . Comparing both values leads to a reflection coefficient of  $R_c = 0.00155$ , which is assumed here as non-reflective.

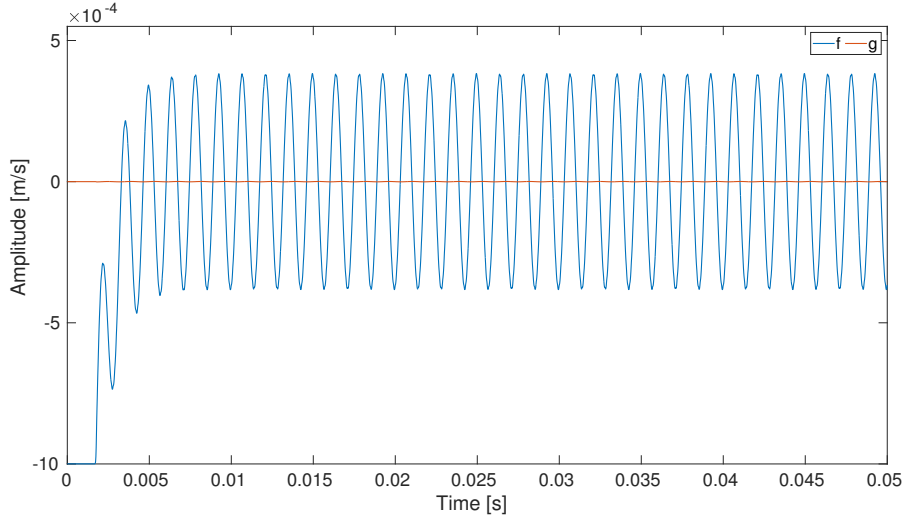


**Figure 3.12:** The  $f$  and  $g$  wave evolution for Option 3.

### 3.6 Comparison of $R_c$ for different Mean-Flows

This section investigates the behavior of the acoustic fluctuation for setups with different mean-flows. Beginning with a mean-flow of  $\bar{u} = 0.001$  m/s the applied mean-flow is increased. Setting a mean-flow leads to some beginning pressure and velocity fluctuations before velocity and pressure oscillate around a mean value. This is sometimes not this easy, as the velocity and pressure are growing small over time. We set a special mean-flow, and therefore a three time period is selected from velocity and pressure graph, where the difference between the set mean-flow and the mean value, the acoustic parts are oscillating, having a small difference. Especially when the mean-flow is raised to a value  $\bar{u} > 1$  m/s, it needs more time to oscillate around the mean value and therefore, more computational time has to be taken. The investigations here are having a mean-flow range starting for a mean-flow of  $\bar{u} = 0.001$  m/s till  $\bar{u} = 1$  m/s with a difference of  $\Delta\bar{u} = 10$ . So four mean-flows are investigated. The mean-flow are applied in behavior as Option 3 as investigated in the previous section (3.5).

First, the  $f$  wave is shown in figure 3.13. Generally, as the global y range of the  $f$  wave is this big, a converged behavior can be seen after a time period of  $t = 0.01$  s for all mean-flow setups. For a higher mean-flow, the beginning of the  $f$  wave is having a lower value. The beginning of each graph is defined by the subtracted mean value and should not be considered in detail. For example, a mean-flow of  $\bar{u} = 1$  m/s is beginning with a value of  $f = -1$  m/s.

Having now a closer look at the  $f$  waves for a selected amplitude range leads to figure 3.14. Comparing all four lines, it is taking longer for a higher mean-flow value to stabilize around the zero value. For the lowest mean-flow  $\bar{u} = 0.001$  m/s, it takes nearly  $t = 0.006$  s to reach a converged state. For the purple graph ( $\bar{u} = 1$  m/s), it nearly takes  $t = 0.013$  s to reach its converged state. Also, the local maximum in the area  $t < 0.01$  s are behaving different for every mean-flow. Small mean-flow are having a big local maximum amplitude, while higher mean-flow only having a little hill till it starts to converge. A Fourier transformation over the

## Simulation Results for Slip Boundary Conditions

---

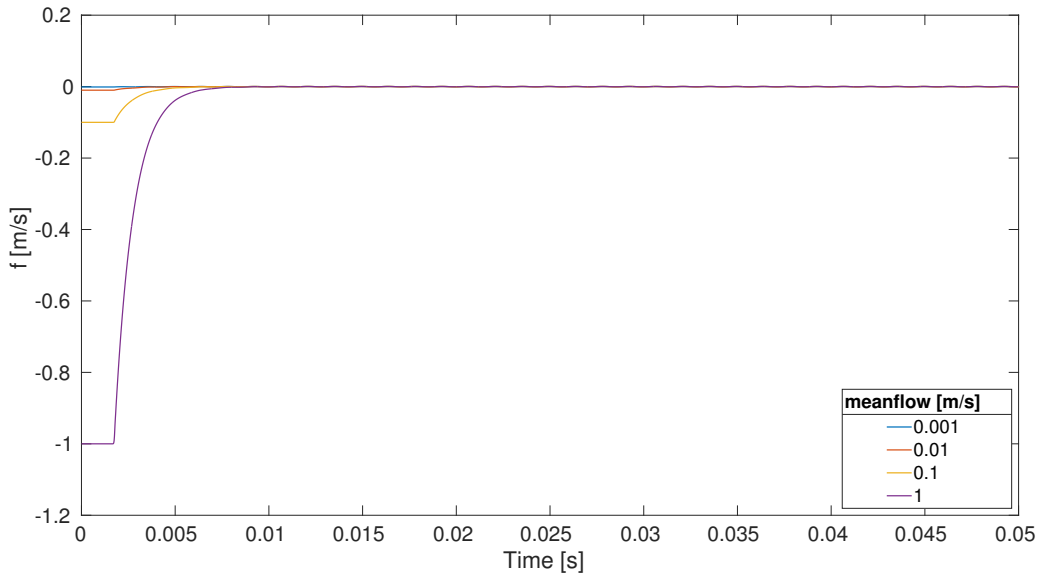


**Figure 3.13:** Comparison of  $f$  waves for different mean-flows in a global range.

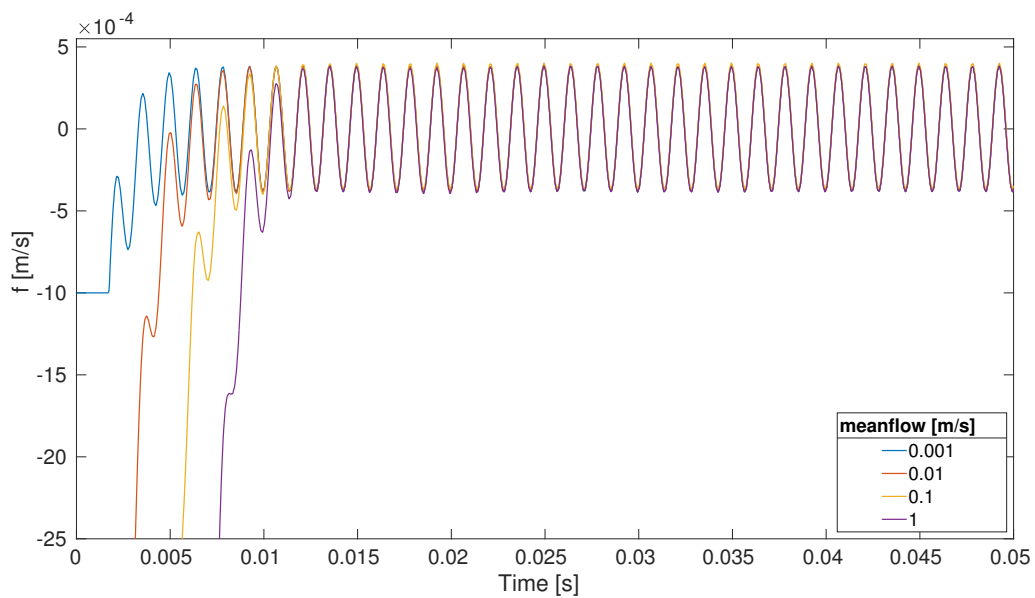


**Figure 3.14:** Comparison of  $f$  waves for different mean-flows for selected amplitude range.

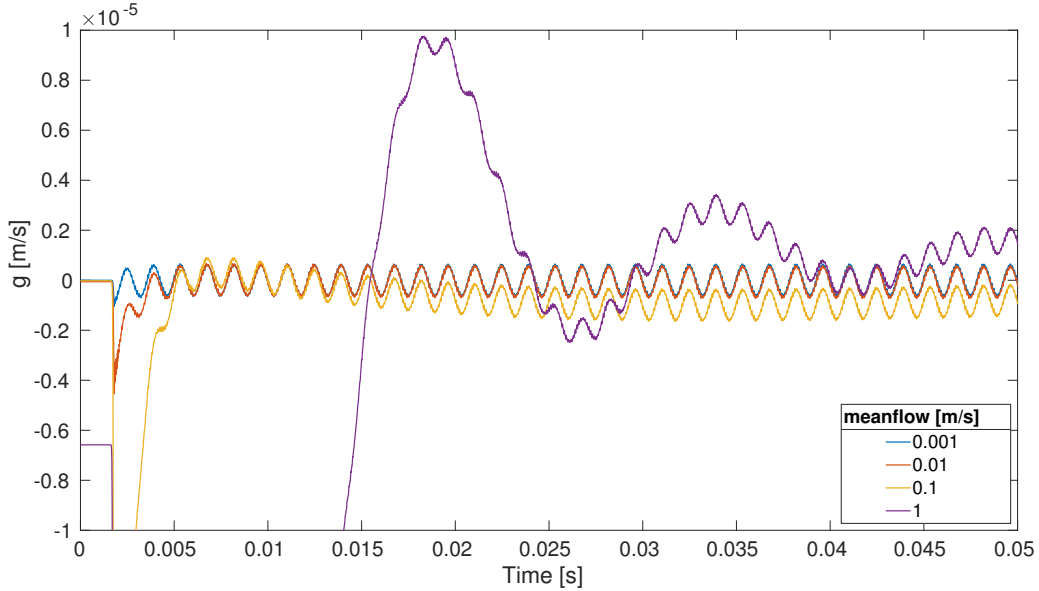


**Figure 3.15:** Comparison of  $g$  waves for different mean-flows for selected amplitude range.

frequency for every line can be seen in table 3.2.

Having now a look at the reflecting  $g$  wave at figure 3.15. For a mean-flow of  $\bar{u} = 0.001 \text{ m/s}$  and  $\bar{u} = 0.01 \text{ m/s}$ , a similar behavior for the  $g$  wave can be observed. Raising the mean value to  $\bar{u} = 0.1 \text{ m/s}$ , a falling behavior for the  $g$  wave can be observed. Raising the mean-flow to a value of  $\bar{u} = 1 \text{ m/s}$  results in no converged status in the investigated time, but a decreasing behavior of the amplitude can be detected. The results of the Fourier transformation of the  $g$  waves can be looked up in table 3.2.

## 3.7 Discussion about Slip Boundary Conditions

In the beginning, the general behavior of the CBSBC was introduced, figures of  $f$  and  $g$  wave demonstrates its behavior at the inlet and outlet. The calculated reflection coefficient was equal to the defined CBSBC one.

Then, the CBSBC was set to be non-reflecting at the outlet, by setting the  $\underline{\mathbf{B}}$  matrix to zero. A reflection coefficient of  $R_c = 0.00155$  was calculated, which is assumed as non-reflecting.

After this, the non-reflection is observed for different mean-flows. Firstly, different options for setting the mean-flow are investigated. Option 3 is showing the best behavior for the investigated mean-flow, it is used for the further observations. Applying a mean-flow does not change the reflection coefficient, as it was also calculated as  $R_c = 0.00155$  for the mean-flow observations.

Closing this chapter with the investigations of  $f$  and  $g$  waves for the mean-flow range of  $\bar{u} = 0.001 \text{ m/s} - \bar{u} = 1 \text{ m/s}$ . The  $f$  wave evolution are behaving the same for different mean-flows. Similar amplitudes around  $\hat{f} = 3.8 \cdot 10^{-4}$  were calculated. However, the  $g$  wave investi-

	mean-flow $\bar{u}$ [m/s]			
	0.001	0.01	0.1	1
$\hat{f} [10^{-4}]$	3.7997	3.7998	3.800	3.800
$\hat{g} [10^{-7}]$	5.9783	5.976	5.9401	5.5241
$R_c [10^{-3}]$	1.5733	1.5727	1.5632	1.4537

**Table 3.2:** Overview of amplitudes for  $f$  and  $g$  waves and the corresponding reflection coefficient for different mean-flows.

gations are leading to different evolution for the investigated mean-flows. A mean-flow lower than  $\bar{u} < 0.01$  m/s generates  $g$  waves with similar oscillations. Increasing the mean-flow occurs different graphs. The highest investigated mean-flow  $\bar{u} = 1$  m/s is generating a  $g$  wave, which is producing a high oscillation in the beginning time, and then having a damped character. For a more detailed investigation, a longer time should be simulated. However, a converged state can be assumed.

The resulting reflection coefficient for the mean-flows, investigated in section 3.6 can be looked up at table 3.2. Here,  $\hat{f}$  corresponds to the calculated amplitude of the Fourier transformation for the  $f$  wave belonging frequency of  $F = 700$  Hz, while  $\hat{g}$  corresponds to the  $g$  wave amplitude. The reflection coefficient is then calculated as  $R_c = \frac{\hat{g}}{\hat{f}}$ . Comparing the reflection coefficient, no big difference can be detected. By increasing the mean velocity, a lower reflection coefficient is calculated. However, the changes are in dimensions of  $10^{-4}$ .

Further investigations for higher mean-flows is proposed. This will probably help to understand more clearly, why the  $g$  wave is having the damping wave character for higher mean-flows, while the  $f$  waves amplitudes are not changing this much.

# 4 Simulation Results for No-Slip Boundary Condition

In this chapter, the influence of a no-slip wall boundary condition to the reflection behavior of the CBSBC is investigated. In all configurations, the reflection coefficient of the CBSBC at the outlet is set to zero (see 3.4). Beginning with the introduction of a new geometry channel, the generation of the reflection coefficient is explained again shortly. Afterwards, the development of  $R_c$  in flow direction is observed, and the influence of higher frequencies is investigated. It ends with a discussion of the reflection coefficient, while a mean-flow is applied.

## 4.1 Simulation Setup of No-Slip Case

The simulated domain is reduced to the dimensions of (30 mm x 5 mm x 1 mm) with a meshing of (200 70 1). The cell size in x-direction is  $\Delta x = 0.15$  mm (fig. 4.1). A higher resolution of cells at the close wall area is necessary, to investigate the influence of the no-slip wall to the flow. Therefore, a grading of 0.01 in negative y-direction is applied in OpenFOAM. This leads to a minimum cell size directly at the wall of  $\Delta y_1 = 3.25 \cdot 10^{-3}$  mm and a cell size of  $\Delta y_{70} = 0.325$  mm at the symmetry patch. The cell-to-cell expansion rate is calculated as  $e = 0.935$ .

The top wall is defined as a no-slip condition. To save computational time, the bottom patch is set as symmetry. The acoustic wave is entering the domain by the inlet, implemented in the CBSBC. If not mentioned explicitly, a frequency of  $F = 700$  Hz with a sound pressure level of  $SPL = 75$  dB is used for the incoming wave. At the outlet, a non-reflection is applied.

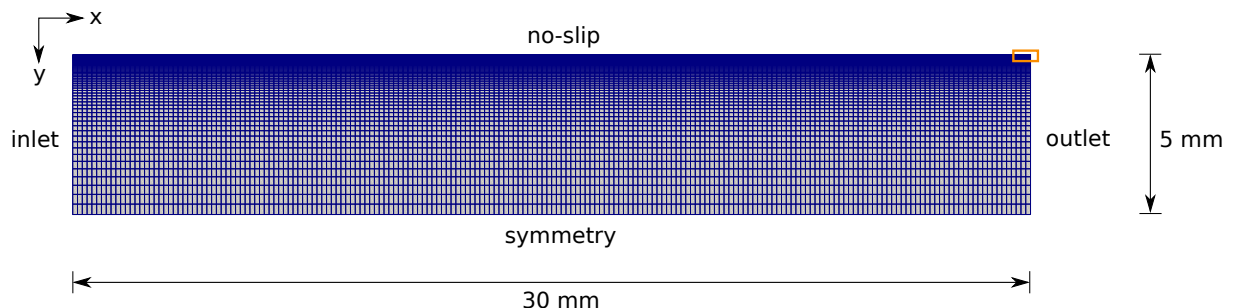


**Figure 4.1:** Mesh of geometry for the no-slip case.

## Simulation Results for No-Slip Boundary Condition

---

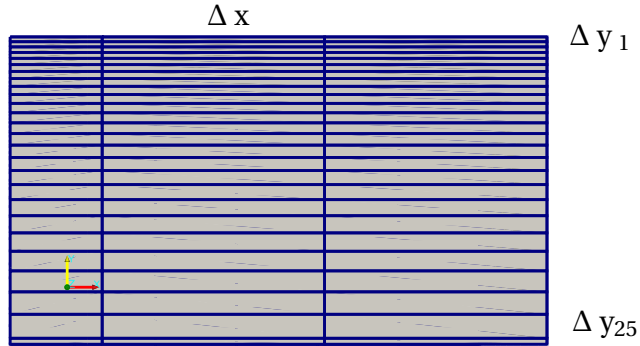


**Figure 4.2:** Detailed view of the mesh from figure 4.1 for the no-slip case.

	Position [mm]	Distance from Outlet Patch [mm]	Cell Number in x-direction
Line 1	$x = 15.075$	$\Delta x = 14.925$	100
Line 2	$x = 22.575$	$\Delta x = 7.425$	150
Line 3	$x = 28.575$	$\Delta x = 1.425$	190
Line 4	$x = 29.325$	$\Delta x = 0.675$	195
Line 5	$x = 29.925$	$\Delta x = 0.075$	200

**Table 4.1:** Overview of the probe locations in x-direction.

To see the grading at the wall more clearly, an extract from the top right corner of figure 4.1 (orange box) is shown in figure 4.2. Additionally, the cell size in y-direction for cell 25 is calculated as  $\Delta y_{25} = 1.62 \cdot 10^{-2}$  mm.

For a detailed investigation of the no-slip wall to the acoustic velocity, probe points are evaluated for every cell in y-direction over the whole geometry. To allow a comparison of the reflection coefficient in flow direction (x-axis), five planes are defined in OpenFOAM, which evaluates the cell values. As a 2D geometry is considered, the planes are called in the following lines. The line locations can be seen in table 4.1. Having a better understanding, where the probes are located, a picture from the mesh with the marked locations as defined in table 4.1 is shown in figure 4.3. Line 5 is located directly on the cell centre at the outlet patch, while Line 1 is located in the middle of the simulation domain.

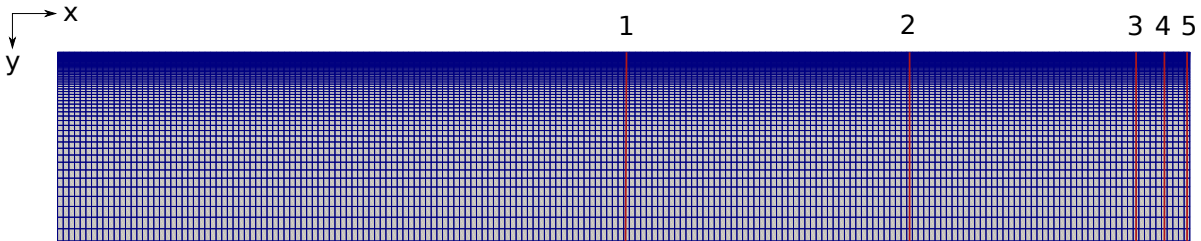


**Figure 4.3:** Line locations defined in table 4.1 displayed in the mesh.

## 4.2 Generation of Results for No-Slip Case

The procedure of calculating the reflection coefficient is shown in the diagram below (figure 4.4). From OpenFOAM, a vector of velocity and pressure is written out for every cell along

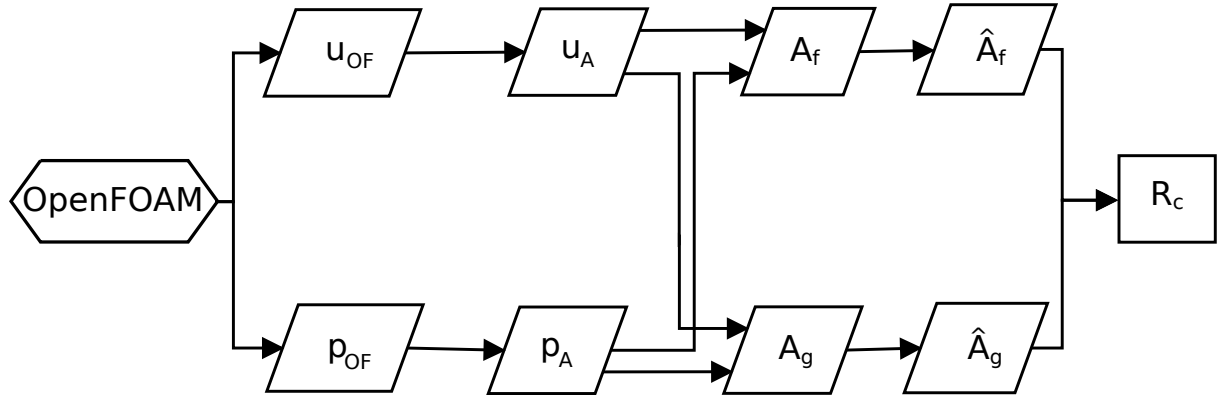


**Figure 4.4:** Diagram for calculation of  $R_c$  for the no-slip case.

the line, named here as  $u_{OF}$  and  $p_{OF}$ . The acoustic fluctuation is then separated from the mean part, resulting in vectors for the acoustic pressure  $p_A$  and for the acoustic velocity  $u_A$  (sec. 2.3). With these, the  $f$  and  $g$  wave can be calculated and are saved in the  $A_f$  and  $A_g$  matrices. For every cell along the line, the variables are calculated. This results in a matrices with a number of columns of 70. For these matrices, we want to get the maximal amplitude of our related frequency. To do so, a fast Fourier transformation is applied for each row of the matrices  $A_f$  and  $A_g$ . The coefficient of the frequencies are saved in the matrices  $\hat{A}_f$  and  $\hat{A}_g$ . The reflection coefficient is then calculated with the division of maximum amplitude of  $g$  wave over maximum amplitude of  $f$  wave for the related frequency.

This procedure is now shown for five selected cells along Line 2. To have a better understanding how the calculation was done, figures are displayed for every step. The center of the five cells are located with distances away from wall as shown in table 4.2.

Cells	y-distance from wall [mm]
Cell 5	$y = 0.012$
Cell 10	$y = 0.036$
Cell 15	$y = 0.069$
Cell 20	$y = 0.115$
Cell 50	$y = 1.155$

**Table 4.2:** Five selected cells with the corresponding distance from the no-slip wall.

The graphs of velocity and pressure for the selected cells evaluated from OpenFOAM are displayed in figure 4.5. As no mean-flow is applied, the velocity fluctuation is around  $\bar{u} = 0 \text{ m/s}$ . Cells located closer to the wall are having a lower amplitude of the velocity. Plus, a

## Simulation Results for No-Slip Boundary Condition

---

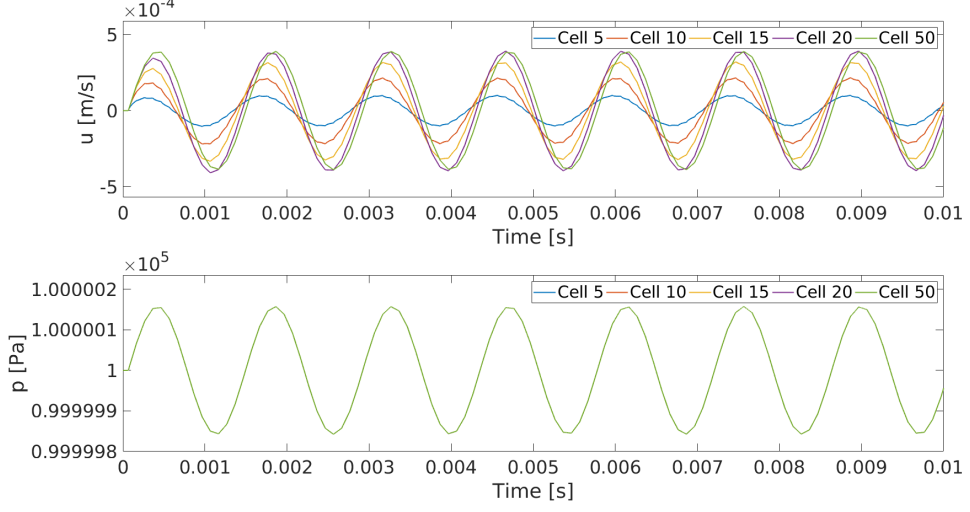


**Figure 4.5:** Velocity and pressure for selected cells along line 2.

phase displacement for the different cells in the velocity plot can be observed. The pressure fluctuation is done around  $\bar{p} = 1 \cdot 10^5$  Pa, with same values independently of the cell locations. The acoustic fluctuation of pressure and velocity is now subtracted from its mean value. Using the formula  $u_A = u - \bar{u}$  for velocity and  $p_A = p - \bar{p}$  for pressure with the mean value for the time starting at 0.05 s with a time length of three periods  $3\Delta T = 0.04286$  s, results in figure 4.6. The acoustic fluctuation of velocity  $u_A$  has no changes in comparison to figure 4.5, the

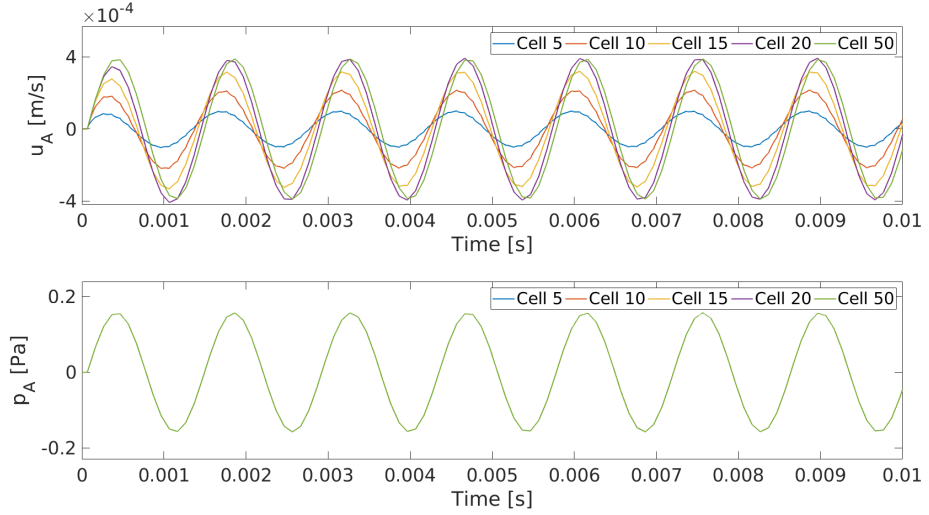


**Figure 4.6:** Acoustic velocity and pressure for selected cell along Line 2.

phase displacement stays. The amplitude range was adapted manually. The acoustic pressure fluctuation is now oscillation around a zero mean value.

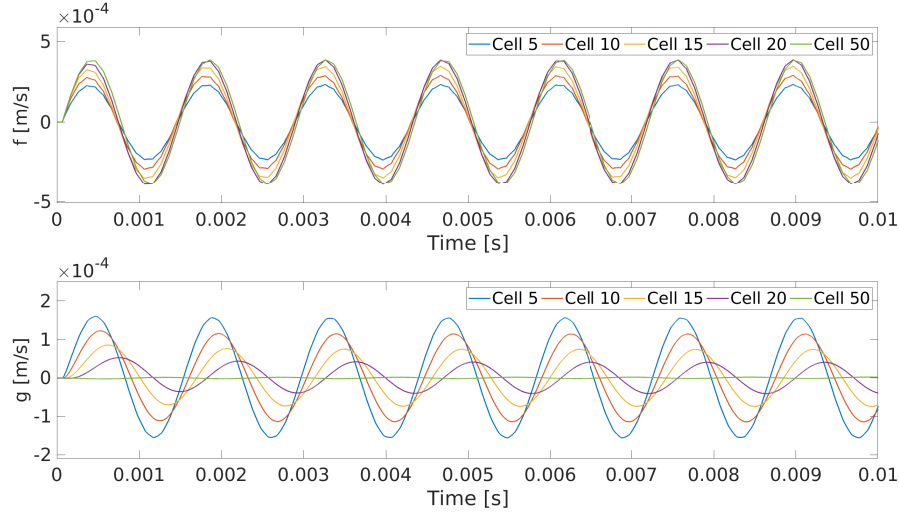


**Figure 4.7:** The  $f$  and  $g$  wave for selected cell along Line 2.

Figure 4.7 is showing the  $f$  and  $g$  wave evolution. It can be seen, that the  $f$  wave for Cell 5 has the smallest amplitude in comparison to the other cells, while it has the highest  $g$  wave amplitude. Which means, the reflection coefficient for this cell is quite high. Cell 50 has a high amplitude for  $f$  and a small amplitude for the  $g$  wave, which leads to a nearly zero reflection coefficient.

Applying a fast Fourier transformation to the  $f$  and  $g$  waves for the selected cells of figure 4.7, results in the stem plot in figure 4.8, showing the frequency amplitudes of the  $f$  and  $g$  waves. As expected, the highest peak arises for the applied frequency of  $F = 700\text{Hz}$ . The max-

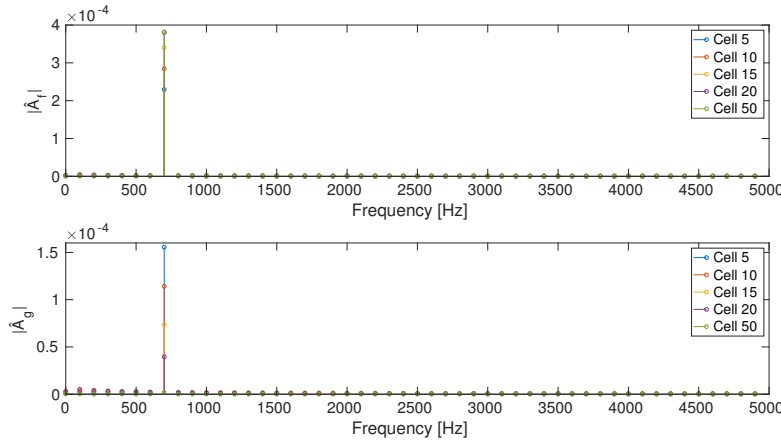


**Figure 4.8:**  $\hat{A}_f$  and  $\hat{A}_g$  for selected cell along Line 2.

imum amplitudes of the  $f$  and  $g$  waves for  $F = 700\text{Hz}$ ,  $\hat{A}_f$  and  $\hat{A}_g$ , are now used to calculate the reflection coefficient with the formula  $R_c = \hat{A}_g / \hat{A}_f$ . These three values for each cell can

## Simulation Results for No-Slip Boundary Condition

---

Cell number	$\hat{A}_f [10^{-4}]$	$\hat{A}_g [10^{-4}]$	$R_c$
Cell 5	2.300	1.555	0.677
Cell 10	2.847	1.141	0.401
Cell 15	3.400	0.7343	0.216
Cell 20	3.802	0.3959	0.104
Cell 50	3.817	0.0188	0.005

**Table 4.3:** Selected cells with the corresponding amplitudes for  $f$  and  $g$  wave and the resulting reflection coefficient.

be looked up in table 4.3. Cells located close to the wall (Cell 5 and Cell 10) are having a small amplitude of  $f$  wave, while the amplitude of the  $g$  wave is relatively high. For cells located further away from the no-slip wall, the amplitude of  $f$  is getting higher and the amplitude of  $g$  is reaching a value around zero. The resulting reflection coefficient has a decreasing behavior over the wall distance.

Rerunning the procedure for every 70 cell along the y-axis, figure 4.9 is generated, which shows the maximum amplitude of  $f$  and  $g$  wave over the distance away from wall for Line 2. The  $f$  wave shown in blue, is raising from nearly 2 close to the wall to a value of  $\hat{A}_f = 3.8 \cdot 10^{-4}$

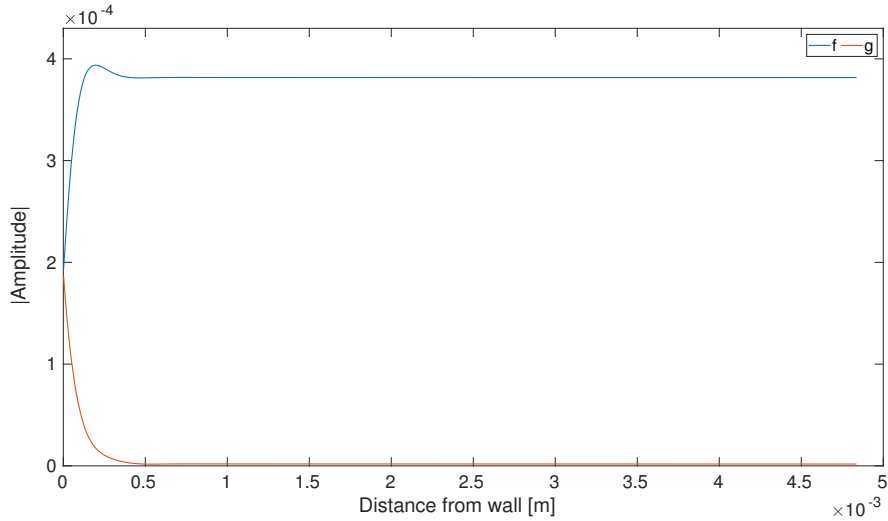


**Figure 4.9:** Maximum amplitude of  $f$  (blue) and  $g$  (red) for every cell along the wall distance.

far away from the wall. Furthermore, a little hill can be detected at the distances around  $y = 0.2\text{mm}$  with a maximum of  $\hat{A}_f = 3.9 \cdot 10^{-4}$ . Comparing both, one can already estimate the behavior of the reflection coefficient. Starting with a value of nearly 1 close to the wall, the reflection coefficient is then degrading to a smaller value around zero.

Having now a look at the reflection coefficient  $R_c$  along the wall distance, figure 4.10 is generated. The graph starts with  $R_c = 0.96$  at the closest cell near the wall, the reflection is

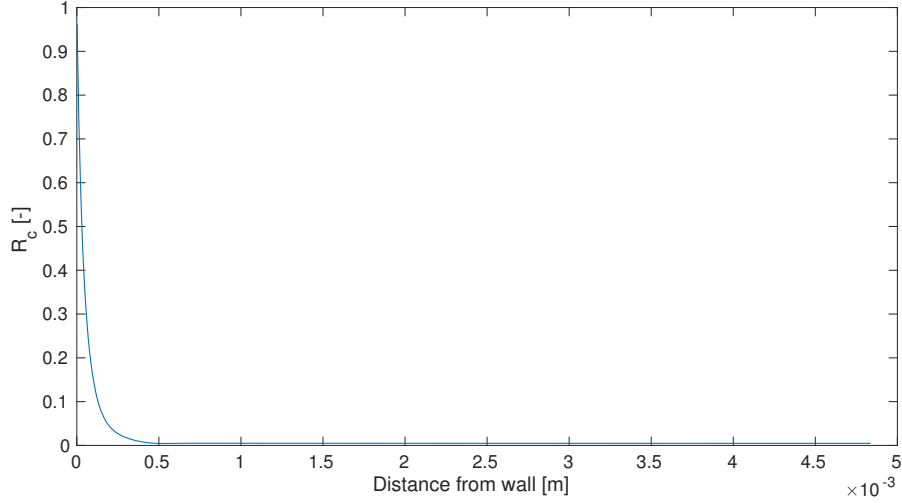


**Figure 4.10:** Reflection coefficient along the wall distance.

falling to a value of nearly zero at a distance from wall of  $y = 0.5$  mm. The most interesting part of figure 4.10 is the close wall area, therefore a new figure for a wall distance range of  $x \in [0 - 0.6]$  [mm] with a limited y-axis coordinate is shown in figure 4.11. The graph of  $R_c$  is

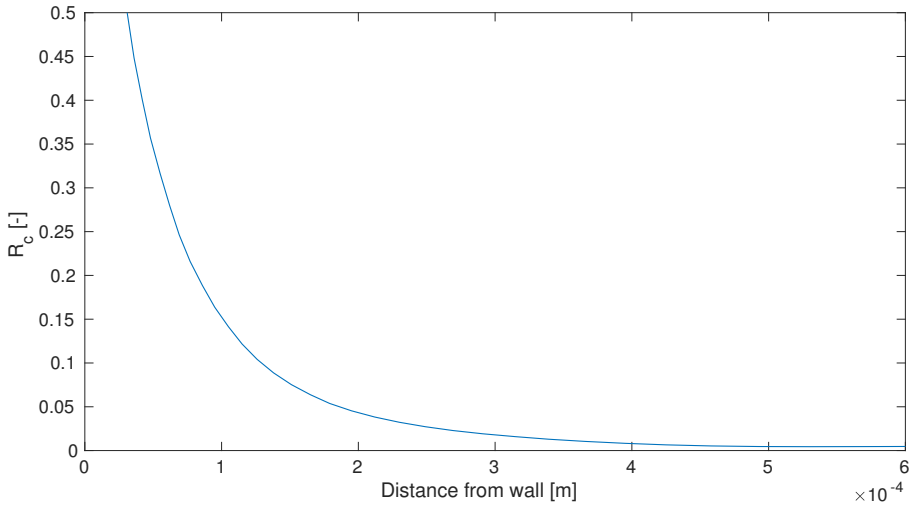


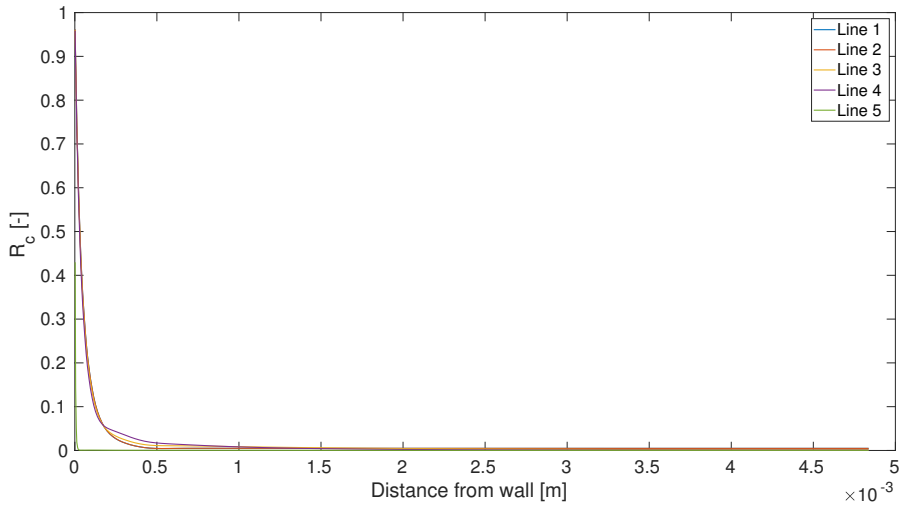
**Figure 4.11:** Reflection coefficient till 0.6 mm away from wall.

falling in an exponential behavior to a value of 0.005 till a wall distance of 0.55 mm. After this, a constant value around 0.0048 is stabilized for the reflection coefficient. No influence of the hill of the  $A_f$  course in figure 4.9 can be seen in its resulting  $R_c$  figure in 4.11.

### 4.3 Development of $R_c$ in Flow Direction

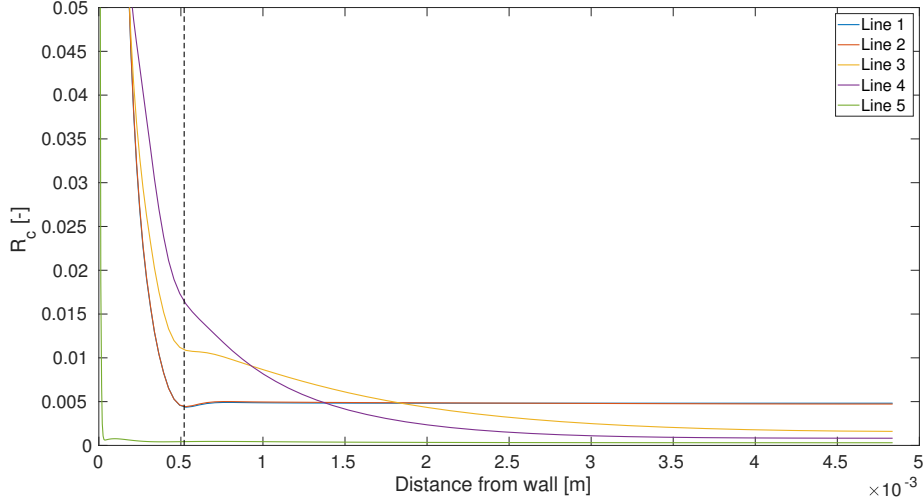
The procedure for calculating the reflection coefficient was shown in detail in the previous section (sec. 4.2). Now, only the resulting reflection coefficient graphs are investigated. This section observes the development of the reflection coefficient over the x-axis for a frequency of  $F = 700\text{Hz}$ . Reflection coefficient graphs for the five line locations, introduced in section Geometry (4.1) are calculated and set in relation in one figure.

Figure 4.12 is showing the reflection coefficient over the whole wall distance. In general, all lines are having a low reflection coefficient value of  $R_c < 0.01$  from a wall distance of  $y > 0.5\text{mm}$ . Line 5, located directly at the outlet is having the best non-reflection behavior in comparison to the other lines. At the closest wall cell, a value of only  $R_c = 0.43$  is calculated. Line 5 is then directly falling to a reflection coefficient value lower than 0.001 at a wall distance  $y = 0.031\text{mm}$ . The other lines starting with values of  $R_c \approx 0.96$ , are then decreasing with a lower gradient, and are reaching reflection coefficient values lower than 0.01 at distances  $y > 1\text{mm}$  away from the no-slip wall.



**Figure 4.12:** Development of  $R_c$  along the x-axis.

In figure 4.13, the range of the reflection coefficient is limited by the values  $R_c \in [0 - 0.05]$ , to allow a more detailed investigation of the line evolution. Firstly, a remark of the gradients at a close wall distance area lower than  $y < 0.5\text{mm}$  is made. As already indicated in figure 4.12, Line 5 is having the highest gradient of all compared lines. It is falling with a value of  $\Delta R_c = 0.43$  in a distance area of  $\Delta y = 0.031$ . Looking now at Line 4, which is located the second closest to the wall. It has the lowest descent value of all lines. Therefore, Line 4 and Line 5 are setting the limits of the gradients at a wall distance of 0.5 mm. Line 3 is having the second lowest gradient, while Line 1 and Line 2 are falling with the same gradient, the second highest in comparison to all observed. In figure 4.13, the black dotted line is showing the corresponding stokes boundary layer thickness for a frequency of  $F = 700\text{Hz}$ , which is calculated as  $\delta_{700\text{Hz}} = 0.519\text{mm}$ . A relation between the development of stokes layer and the locations



**Figure 4.13:** Development of  $R_c$  along the x-axis for a selected range.

of lines can be observed. Already for Line 4, the kink locates the end of the layer. Lines, located further away from the outlet (Line 1 to Line 3) are having a more significant change in its reflection coefficient graphs.

Now, the development of each line along the wall distance is observed in more detail. A non-reflection behavior is assumed by a value lower than  $R_c < 0.005$ , to allow a comparison between every line. Line 5 is reaching a non reflection behavior for a wall distance of  $y = 0.031$  mm with a value lower than  $R_c < 0.0001$ , which is the lowest  $R_c$  of all observed lines. Related to the whole wall distance, 99.5% of the y-axis have a behavior of non reflection. Line 2, distant  $\Delta x = 0.675$  mm away from outlet patch, is shown in the purple graph. It is falling till a wall distance around  $y = 0.5$  mm, where a kink can be detected. After, it is falling again with a lower gradient till its stabilized around  $R_c = 0.0012$  for wall distances  $y > 3$  mm. The assumed non-reflection value is reached for a distance of  $y = 1.35$  mm, which corresponds to a non-reflection behavior over the whole wall distance for 73 %. Line 3 has a higher gradient than Line 4, the kink is located at the same wall distance with a more distinct behavior. After, it is falling till it reaches values of  $R_c = 0.002$  at the end wall distances. Non-reflection is guaranteed for about 65 % over the whole wall distance. For Line 1 ( $\Delta x = 14.925$  mm) and Line 2 ( $\Delta x = 7.425$  mm), the behavior of the reflection coefficient over the wall distance are similar. The graphs are falling with the second highest gradient till its ending in a kink for a wall distance around  $y = 0.5$  mm. After the kink, the reflection coefficient is stabilized over the whole wall distance at a value of  $R_c = 0.0048$ . Non-reflection is ensured for 90 % of the whole wall distance.

In the following, the effect of Line 5 having the lowest reflection coefficient for nearly the whole wall distances is pointed out. With the help of paraView, the velocity solution fields are demonstrated. Figure 4.14 is showing the velocity field in x-direction for a time  $t = 75$  ms, while in figure 4.15, the velocity in y-direction can be detected. In both figures only the top

## Simulation Results for No-Slip Boundary Condition

---

right corner of the geometry are displayed, as the biggest changes are happening in this area.

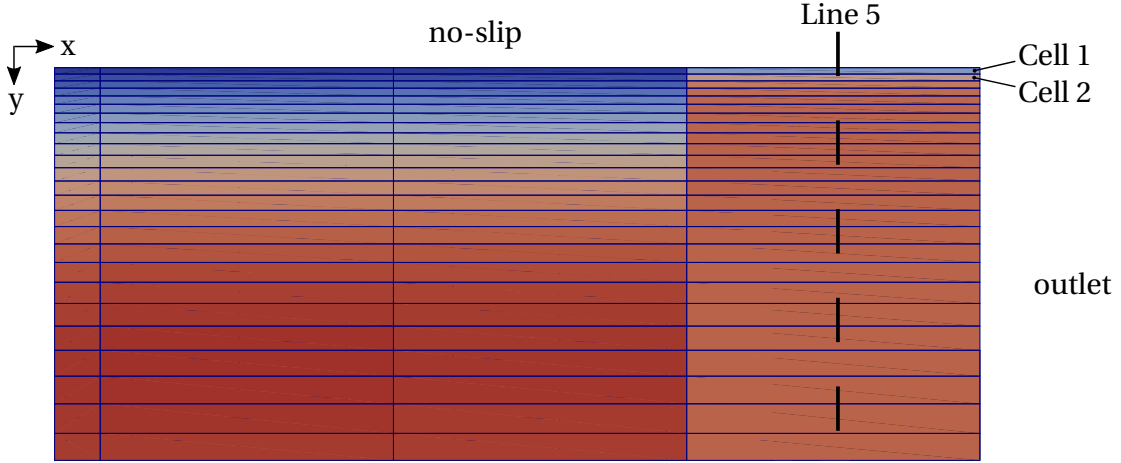


**Figure 4.14:** Velocity (x) at close wall outlet area for  $t=75$  ms; Low velocity ( $u_x \approx 0$  m/s) shown in blue and high velocity ( $u_x = 4.4 \cdot 10^{-4}$  m/s) shown in red.

Looking at the cells along Line 5, located the closest to the outlet, a homogeneous velocity field till the last two top cells can be seen. Only the two top cells are having a different velocity value. Comparing with the cells located further away from the outlet patch, a big difference is detected. Especially the influence of the no-slip wall can not be seen this clear for the cells along Line 5. It seems like the velocity are defined by the outlet boundary condition.

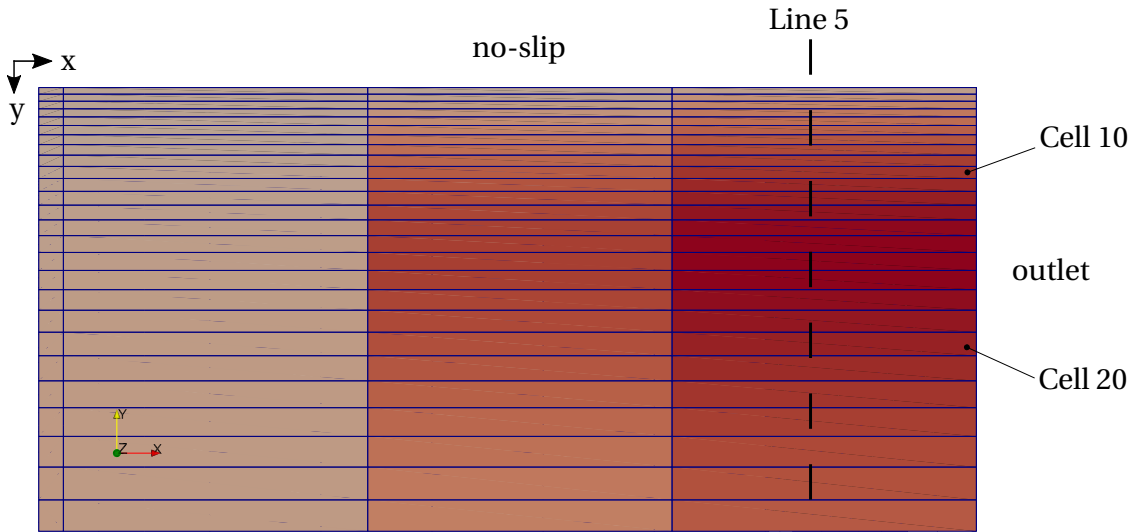


**Figure 4.15:** Velocity (y) at close wall outlet area for  $t=75$  ms; Negative velocity ( $u_y = -4.4 \cdot 10^{-5}$  m/s) shown in red and zero velocity (grey).

In figure 4.15, showing the solution field for the velocity in y-direction, velocities around a value of  $u_y = -4.4 \cdot 10^{-5}$  m/s are marked as red, while the grey color represents a velocity

of zero. Along Line 5, the cells between cell 10 and cell 20 are marked high red, which corresponds to a velocity value in negative y-direction. Cells located further away from the outlet patch are having a lower respectively no velocity component in y-direction. It seems like the y-component of velocity reduces the influence of the no-slip wall (fig. 4.14) for the cells along Line 5.

## 4.4 Comparison of $R_c$ for different Frequencies

Simulations with frequencies of 300 Hz, 500 Hz, 700 Hz, 1000 Hz and 1500 Hz are now observed. In particular, how the boundary layer is developing for every frequency. As seen in the previous chapter 4.3, the reflection coefficient for Line 1 and Line 2 are behaving almost equal. So only Line 2, Line 3, Line 4 and Line 5 are observed. Furthermore, all figures are shown out in a determined range of  $R_c \in [0 - 0.05]$ .

### Line 2

Starting with Line 2, located at the position  $x = 22.575$  mm. The resulting reflection coefficient along the wall distance is plotted in figure 4.16. Starting to observe the graph for a frequency

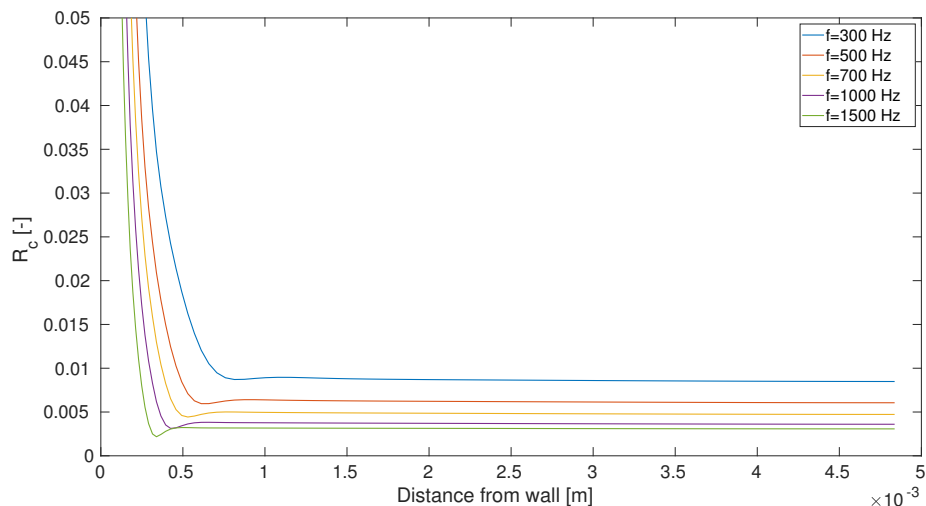


**Figure 4.16:** Reflection coefficient for different frequencies in a certain distance range along Line 2.

of  $F = 300$  Hz. It has the lowest gradient in comparison to the other one till it stabilized at a value of nearly  $R_c = 0.009$ , meaning the highest reflection coefficient value of all observed frequencies. The stabilization starts at a wall distance of  $y = 0.75$  mm, comparing with the stokes boundary layer for this frequency  $\delta_{300\text{Hz}} = 0.793$  mm, it is located in the same cell. The higher the frequency gets, the closer the stabilization around a mean value is happening. So a rela-

## Simulation Results for No-Slip Boundary Condition

---

tion between stokes boundary layer and frequency can be observed for Line 2. Furthermore, the local minimum before it stabilized is getting bigger marked, the higher the frequency gets.

### Line 3

Having now a look at the x-distance  $x = 28.575\text{ mm}$ , means closer to the outlet boundary condition, figure 4.17 is created. In comparison to Line 2, the fall before reaching the related

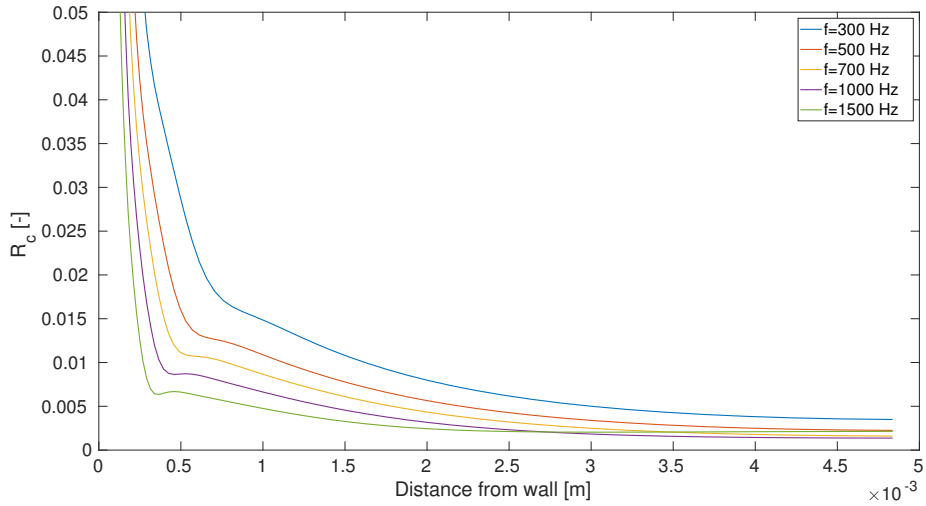


**Figure 4.17:** Reflection coefficient for different frequencies along Line 3.

stokes boundary layer is not this high. The local minimum is not this developed as for Line 2. After each graph is passing its turning point, it keeps falling with a lower gradient. No direct stable coefficient is observed. Especially for the graph for a frequency of  $F = 1500\text{ Hz}$  is to mention, as it is intersecting with the purple and yellow graph and is increasing along the wall distance.

### Line 4

Reflection coefficient evolution along the wall distance for Line 4 is showing in figure 4.18. A development of a boundary layer for a frequency of  $F = 300\text{ Hz}$  can not be observed clearly, moreover a stabilized state at a wall distance of  $y = 4.5\text{ mm}$  can not be detected. For a frequency of  $F = 700\text{ Hz}$ , a kink in its fall can be assumed, however, higher frequencies are showing a more clear difference in the graph when the boundary layer is finished. The green graph is raising after passing a wall distance of  $y = 2\text{ mm}$  and is intersecting with all other graphs, leading to the highest reflection coefficient at the symmetry patch of the simulated domain. Furthermore, the purple graph is also cutting line yellow and red.

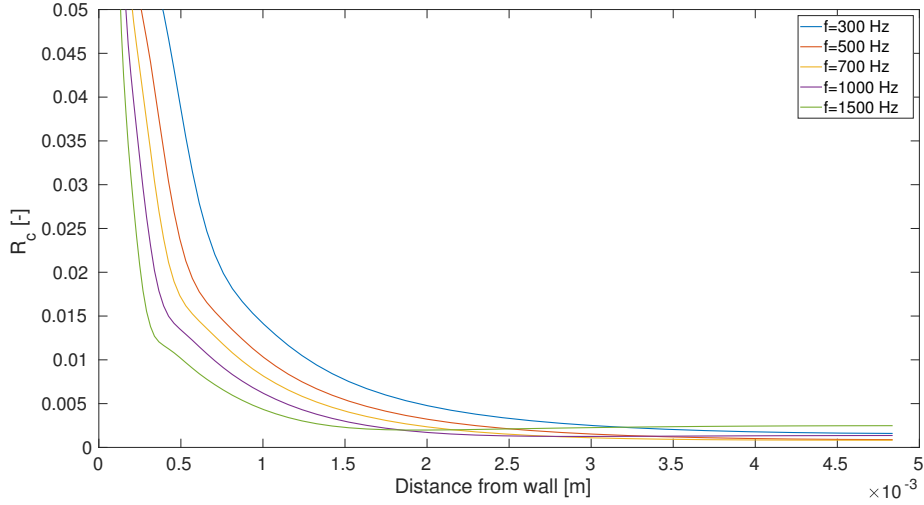


**Figure 4.18:** Reflection coefficient for different frequencies along Line 4.

## Line 5

As a last investigation, the cells, located directly at the outlet are observed. The resulting reflection coefficient plot can be seen in figure 4.19. As the effect are this small, the y range of the plot was adapted, which leads to a range of  $R_c \in [0 - 5 \cdot 10^{-3}]$ . The gradient of the observed

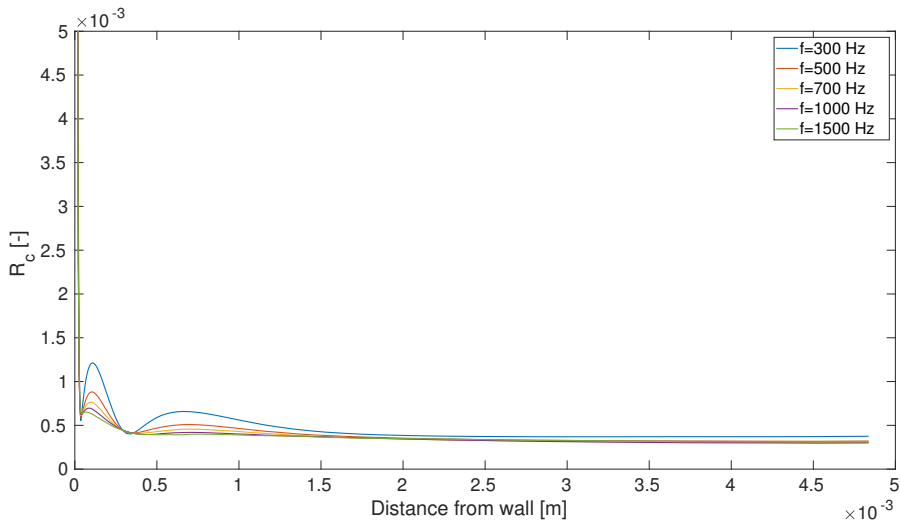


**Figure 4.19:** Reflection coefficient for different frequencies along Line 5.

frequencies are all falling in a similar behavior till a wall distance of 0.03 mm, the blue plot is even falling to the lowest value. For a frequency  $F = 300 \text{ Hz}$ , the reflection coefficient is then raising again to a value of  $R_c = 0.0012$  for a wall distance of  $y = 0.12 \text{ mm}$ . After this, it is falling again. It behaves like a damping wave. For the other frequencies, the damping of the first hill

is getting smaller, the higher the frequency is. It then stabilized after 0.5 mm at a reflection coefficient of  $R_c = 0.0005$ .

## 4.5 Discussion about $R_c$ Evolution for No Mean-Flow

Firstly the development in flow direction is discussed here. Then the influence of different frequencies are investigated more detailed.

Comparing to section 4.3, an evolution of the reflection coefficient perpendicular to the flow direction can be observed. The  $R_c$  graph needs a certain distance away from the outlet to generate a clear stokes boundary layer. Cells along Line 5, located directly at the outlet are having the lowest reflection coefficient value. It seems like the CBSBC is influencing the cells directly at the outlet (compare fig. 4.14), as the influence of the no-slip wall is reduced. For a distance away from the outlet of  $\Delta x = 0.675$  mm, a little kink can only assume a stokes boundary layer, while for Line 3 and especially for Line 1 and Line 2, a clear generation of the stokes boundary layer can be seen in the  $R_c$  plot. It would be interesting to investigate, at which exact distance away from the outlet patch a fully generated boundary layer can be detected.

For higher frequencies, a change in the graph while passing the stokes boundary layer can be clearly detected for all lines. But for a frequency of  $F = 300$  Hz, a clear generation of the stokes boundary layer can only be observed for distances higher than  $\Delta x = 7.425$  mm away from the outlet patch.

Polifke [9] added a plane wave masking to the LODI relation, as higher frequencies lead to a bad construction of the reflection coefficient. For Line 2, this can be clearly seen. However, an ascent in the  $R_c$  graphs for higher frequencies can be observed, which results in intersections of graphs with lower frequencies along the wall distance for the close outlet lines. This leads to a higher and therefore worse reflection coefficient in the middle of the domain. Especially for Line 4, a frequency of  $F = 1500$  Hz leads to the highest reflection coefficient of all observed frequencies in the middle of the domain. Table 4.4 is showing the calculated reflection coefficient to the corresponding frequencies for a wall distance of  $y = 4.5$  mm for Line 4. The relatively high  $R_c$  value for  $F = 300$  Hz can be explained, as no converged status is reached for this wall distance.

Lower frequencies leads to a higher amplitude of the damping wave along Line 5, located directly at the outlet patch. However, the range of the damping is in dimensions of  $R_c \in 0.0005 - 0.001$ .

Because of time constraints, the investigation could not be done more detailed. A modification in the CBSBC boundary file could maybe help to understand the issue more clearly.

$F$ [Hz]	300	500	700	1000	1500
$R_c$ [-]	0.016	0.0001	0.0001	0.0014	0.0025

**Table 4.4:**  $R_c$  for different frequencies for Line 4 at wall distance  $y = 4.5$  mm.

## 4.6 Applying a Mean-Flow to the No-Slip Simulation Case

Applying a mean-flow to the simulation requires also its elimination to calculate the  $f$  and  $g$  waves. Additionally, the influence of the no-slip top wall leads to different velocity evolution for every cell along the  $y$ -axis. For that reason, five cells are printed out to see the change of amplitude and mean-value for every cell. Cell 66 is added, as it is located close to the symmetry patch wall and therefore receives low influence from the no-slip wall. Furthermore, to obtain a converged state of the variables, the end time of simulation is extended to  $t_{end} = 0.1$  s. Firstly, the velocity and pressure evolution for the selected cells is shown in figure 4.20. Cell 66

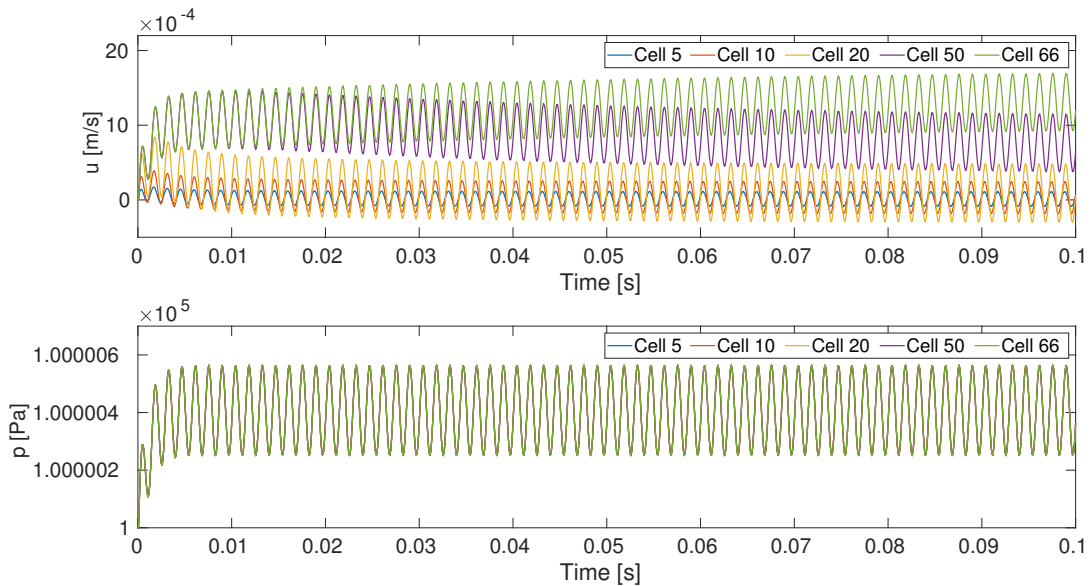


**Figure 4.20:** Velocity and pressure evolution over time for selected cells.

is having the highest mean value of velocity, as the influence of the no-slip wall is the lowest. It is growing constantly to a mean value around  $\bar{u} = 0.0012$  m/s till a time of  $t = 0.1$  s. A stabilized manner with a low gradient can be assumed for further time steps. Cell 50 is growing in the same behavior as Cell 66 up to  $t = 0.01$  s, then it is falling till it stabilized around a mean velocity of  $\bar{u} = 0.0008$  m/s. Looking at Cell 20, an incline in the first time steps is observed, afterwards the graph is stabilized around  $\bar{u} \approx 0$  m/s. The closer cells are oscillating around  $\bar{u} = 0$  m/s, while Cell 10 has a higher amplitude than Cell 5. For the pressure graphs, every cell behaves the same, the oscillations is made around  $\bar{p} = 100\,000.4$  Pa.

The mean velocity and pressure are calculated in the time interval from 0.095 s to 0.099286 s, as a stable manner for all cells can be assumed. Subtracting the mean values from the variables, seen in figure 4.20, leads to the acoustic fluctuation of pressure and velocity. With the help of these, the  $f$  and  $g$  waves can be calculated and are shown in figure 4.21. For Cell 66 and Cell 50, a similar amplitude for the  $f$  wave can be adopted. Cell 20 received a phase shift, while Cell 5 and Cell 10 are oscillating with a smaller amplitude and a phase shift in compar-

## Simulation Results for No-Slip Boundary Condition

---

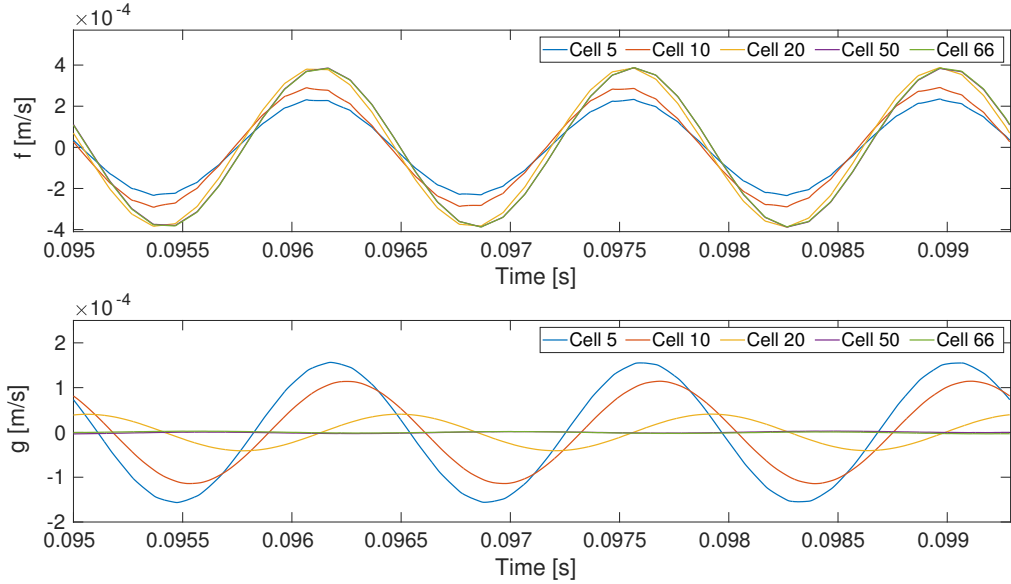


**Figure 4.21:** The f and g wave evolution over selected time.

ison to Cell 50. By observing the g waves, Cell 50 and Cell 66 are having approximately a zero amplitude. Whereas Cell 5 is having the highest amplitude and phase shift.

Cell number	Wall distance [mm]	$\hat{A}_f [10^{-4}]$	$\hat{A}_g [10^{-4}]$	$R_c [-]$
Cell 5	0.017	2.3010	1.5544	0.6756
Cell 10	0.042	2.8585	1.1419	0.3995
Cell 20	0.126	3.8192	0.4078	0.1068
Cell 50	1.238	3.8146	0.1712	0.0045
Cell 66	3.693	3.8201	0.1974	0.0052

**Table 4.5:** Selected cells with the corresponding amplitudes ( $F = 700\text{Hz}$ ) for  $f$  and  $g$  waves and the resulting reflection coefficient  $R_c$ .

Table 4.5 is showing the maximal amplitudes of  $f$  and  $g$  waves and the corresponding reflection coefficient for the selected cells. By looking at the  $R_c$  value, a tendency can be detected. The reflection coefficient is falling with a high gradient at the close wall area till Cell 50. But for Cell 60, the reflection coefficient is increasing again. So the reflection coefficient is not stable for cells located further away from the outlet. As the reflection coefficient is calculated only for five cells, the point of  $R_c$ , changing from falling to increasing can not be located this clearly. This will be investigated in more detail in the further section. Additionally, the figure of reflection coefficient over the wall distance can be looked up in figure 4.22. Starting with a value of  $R_c \approx 1$ , the graph is falling strongly till it reaches a value  $R_c < 0.01$  for wall distance of  $y > 0.5\text{ mm}$ . As a global range of  $R_c$  is shown, the growth of  $R_c$  can not be seen this clearly.

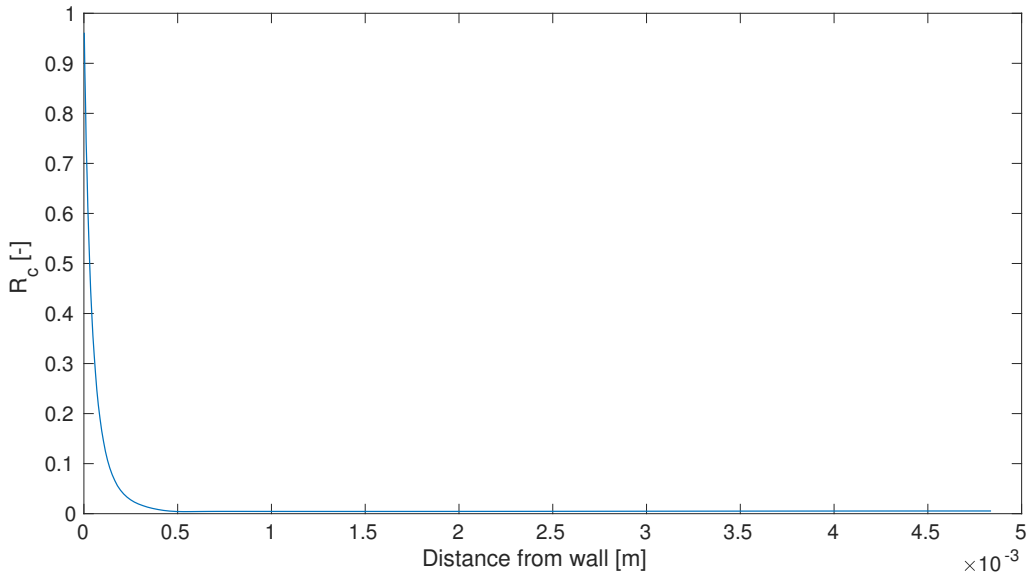


**Figure 4.22:** Reflection coefficient over wall distance

The increasing behavior of  $R_c$  can be detected more clearly for higher mean-flows. The reader is referred at this point to the next section 4.7, where a mean-flow of  $\bar{u} = 0.005 \text{ m/s}$  is investigated.

## 4.7 Development of $R_c$ in Flow Direction with Mean-Flow

As already mentioned in the last section, a growth of the reflection coefficient graph over the wall distance was detected. This will now be observed in more detail for a limited  $R_c$  range. The mean-flow is set to  $\bar{u} = 0.005 \text{ m/s}$ .

Figure 4.23 is showing the reflection coefficient for selected line locations along the x-axis. The black dotted line is marking the end of the stokes boundary layer thickness for a frequency  $F = 700 \text{ Hz}$ . Comparing figure 4.23 with the figure 4.13, displaying the reflection coefficient along the lines with no mean-flow, two big differences can be detected. Firstly, Line 1 and Line 2 are raising slowly after passing the stokes thickness to a wall distance of  $y = 2.6 \text{ mm}$ , where the graph is receiving an inflection point. A reflection coefficient value of  $R_c = 0.008$  is calculated for the close symmetry area. In comparison to the no mean-flow case, the reflection coefficient of Line 1 and Line 2 is staying stable after passing the stokes layer thickness ( $R_c = 0.0048$ ). The other big difference can be seen for the graph of line 5. It is also not staying in an converged state along the wall distance as for the no mean-flow case. It is behaving in an wave characteristic way, starting at a distance, lower than the stokes thickness. Furthermore, for a wall distance higher than  $1.6 \text{ mm}$ , a zigzag behavior for Line 5 and Line 4 can be observed.

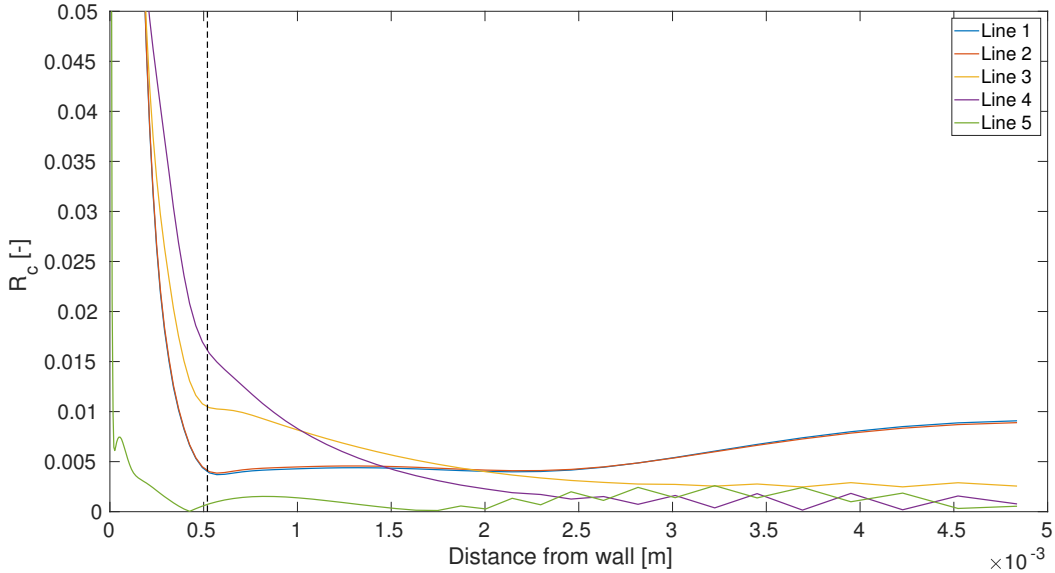


**Figure 4.23:** Reflection coefficient detailed along the x-axis for mean flow  $\bar{u} = 0.005 \text{ m/s}$ .

## 4.8 Comparison of $R_c$ for different Mean-Flows

A change in the reflection coefficient graph for a simulation setup by applying a mean-flow was observed in the previous chapter. Now, three mean-flows are set in comparison along Line 2 and Line 5. These two lines were selected, as these are showing the most interesting graph evolution. Additionally, the velocity profile for the different mean-flows are shown in the annex G.

### Line 2

For Line 2, figure 4.24 is created, showing the reflection coefficient graphs for three mean-flows over the wall distance. In the stokes boundary layer thickness area, the three observed mean-flows are behaving nearly the same. The lowest mean-flow is reaching its local minimum at the stoke thickness of  $y = 0.52 \text{ mm}$  with a value of  $R_c = 0.0041$ , while the other mean-flows keep falling and reaching their minimum at a wall distance of  $y = 0.57 \text{ mm}$ . The corresponding reflection coefficient relates to  $R_{c,\bar{u}=0.005} = 0.0039$  and to  $R_{c,\bar{u}=0.01} = 0.0053$ . After passing the stokes boundary layer, the blue line is raising slowly. The  $R_c$  value of the red graph is raising more clearly, while a mean-flow of  $\bar{u} = 0.01 \text{ m/s}$  results in wavy  $R_c$  graph over the wall distance. The calculated reflection coefficient of the mean-flows is shown for three wall distances in table 4.6. A wall distance of  $y=0.53 \text{ mm}$  was selected, as it corresponds to the stokes boundary layer thickness for a frequency of  $F = 700 \text{ Hz}$ . Furthermore, at a distance of  $2.5 \text{ mm}$ , the reflection coefficient graphs receives a wave trough, while the distance  $4.8$  relates to the closest cell at the symmetry patch.

## 4.8 Comparison of $R_c$ for different Mean-Flows

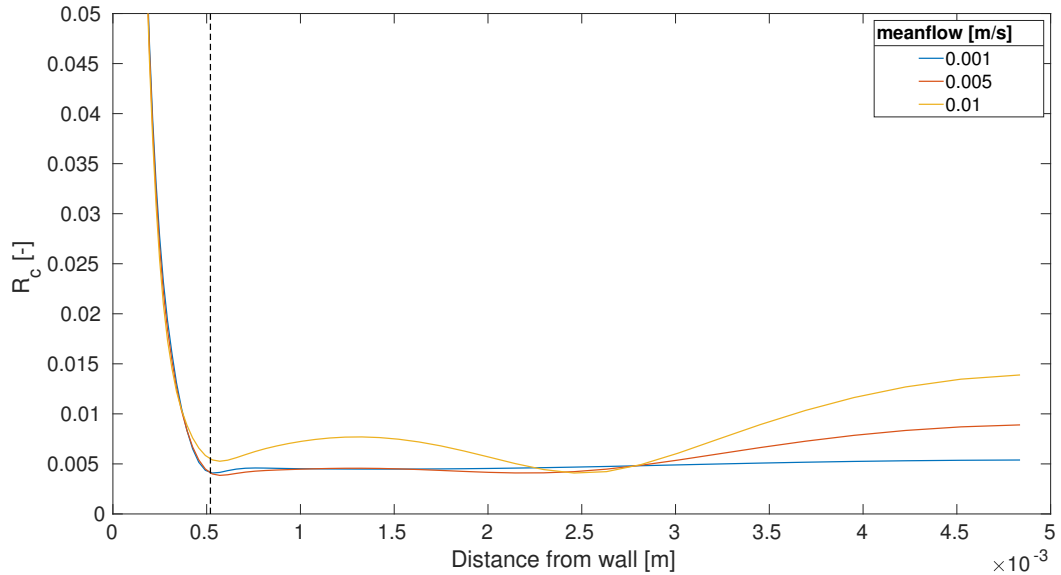


**Figure 4.24:** Reflection coefficient for different mean-flows along Line 2

Mean-Flow [m/s]	Wall Distance		
	0.53 mm	2.5 mm	4.8 mm
0.001	$R_c = 0.0041$	$R_c = 0.0047$	$R_c = 0.0054$
0.005	$R_c = 0.0040$	$R_c = 0.0042$	$R_c = 0.0089$
0.01	$R_c = 0.0054$	$R_c = 0.0041$	$R_c = 0.0139$

**Table 4.6:** Reflection coefficient for different mean-flows for selected wall distances at Line 2.

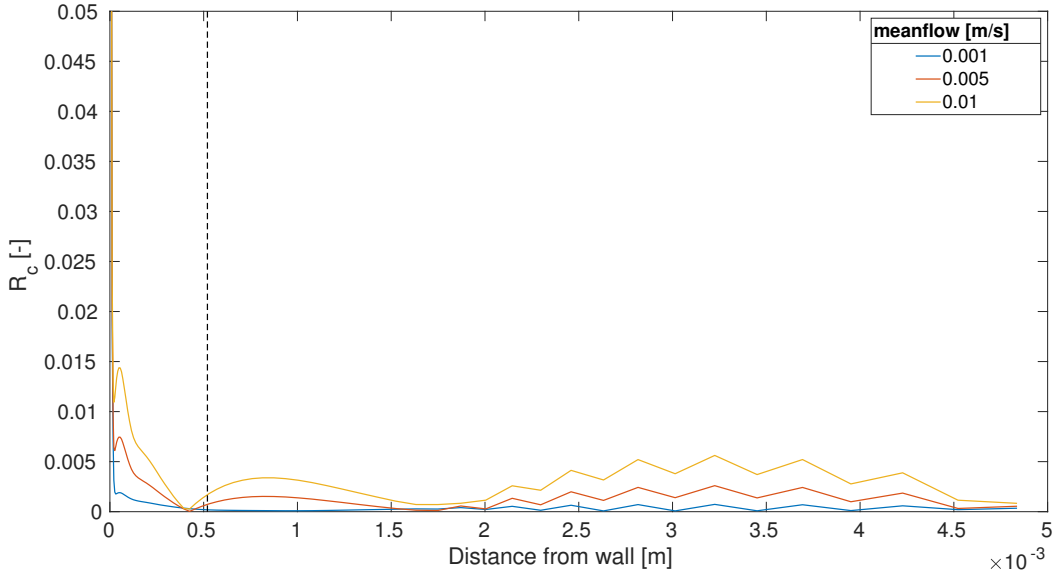


**Figure 4.25:** Reflection coefficient for different mean-flows along Line 5

Mean-Flow [m/s]	Wall Distance		
	local minimum	0.53 mm	4.8 mm
0.001	$R_c = 0.0018$	$R_c = 1.77 \cdot 10^{-4}$	$R_c = 3.47 \cdot 10^{-4}$
0.005	$R_c = 0.0061$	$R_c = 7.89 \cdot 10^{-4}$	$R_c = 5.45 \cdot 10^{-4}$
0.01	$R_c = 0.0114$	$R_c = 18.2 \cdot 10^{-4}$	$R_c = 8.34 \cdot 10^{-4}$

**Table 4.7:** Reflection coefficient  $R_c$  for the different mean-flow for selected wall distances at Line 5.

## Line 5

Another investigation is made for Line 5 at figure 4.25. The graphs are reaching a local minimum of  $R_c$  (see table 4.7) at wall distances of 0.021 mm till 0.031 mm. Higher mean-flow is reaching its minimum at a closer wall distance, while it has an higher  $R_c$  value. After a little hill, all reflection coefficient graphs are falling to reflection coefficient value lower than  $R_c < 1 \cdot 10^{-4}$  at distance around  $y = 0.4$  mm. The red and blue graph are then raising again by crossing the stokes boundary layer at  $R_c$  values see table 4.7. A local maximum is reached for the blue and red graph by a wall distance of 0.73 mm. A wavy character for graphs of mean-flow  $\bar{u} = 0.005$  m/s and  $\bar{u} = 0.01$  m/s is generated by ending for  $R_c$  values lower than 0.001.

## 4.9 Influence of Mean-Flow to $R_c$

Applying a mean-flow to the no-slip cases requires to expand the end of simulation time, as the velocity graphs for cells, located further away from the no-slip wall keeps increasing. This leads to some problems by calculating the acoustic fluctuation of pressure and velocity. As some waves have not reached their converged state, the calculation of the mean velocity is not this exact. However, setting the range to a high time reduces the impact of the non converged state. But this affect should be integrated in the discussion, as it could be possible, that it influence the calculation of the  $f$  and  $g$  wave and therefore the reflection coefficient  $R_c$ .

By looking at the resulting reflection coefficient figures for the mean-flow cases, a general low reflection coefficient is calculated. However, investigations were made in small  $R_c$  range, as differences to the cases without mean-flow could be observed.

Two areas were observed for the no-slip mean-flow case. One area, located far away from the CBSBC outlet (Line 2), and one located directly at the close outlet cell (Line 5). For both area, applying a mean-flow results in a wavy character of the reflection coefficient in the channel interior. The development of  $R_c$  in the stokes layer are almost similar, however higher mean-flows results in higher reflection coefficient values.

Furthermore, for higher mean-flows, the mesh has to be adapted. The cell size in the interior of the geometry has to be smaller to avoid the zigzag behavior as seen in figure 4.25.

Because of time constraints, no further investigations could be done. Especially the resulting reflection coefficient graph for higher mean-flows would be an interesting investigation.

## 5 Summary and Conclusion

This thesis concentrated on the validation of a new acoustic boundary condition, the CBSBC, in OpenFOAM. In the beginning, the related equations and the CBSBC approach were introduced. Furthermore, the implementation of the CBSBC in OpenFOAM is shown.

At the outset, a geometry with slip boundary condition at the wall was used. Test cases demonstrated the behavior of the new boundary condition. In general, the CBSBC is working good in a slip boundary environment. An applied reflection coefficient was proven. Applying high mean-flow leads to damping character of the  $g$  wave. This effect could not be explained in detail and should be investigated extensively in further projects.

For a no-slip boundary condition geometry, an evolution of the reflection coefficient in flow direction was observed. The stokes boundary layer was fully generated for a distance of about 7.5 mm away from the outlet CBSBC. Especially at the closest outlet cells, the no-slip area of the wall was not this distinct, which could be traced back to the CBSBC. Observing different frequencies leads to an increase of the reflection coefficient over the wall distance. For cells, located far away from the outlet, higher frequency leads to good  $R_c$  values. The closer you get to the CBSBC outlet, the higher the reflection coefficient is increasing near the symmetry patch. Applying a mean-flow to the no-slip setup leads also to an increase of  $R_c$ . The  $R_c$  evolution perpendicular to the flow direction has a damping wave character for a distance higher than 7.5 mm away from the outlet. Further investigations are proposed in particular for the mean-flow cases, as the damping character is not this clear.

By assuming a non-reflection behavior of the CBSBC for reflection coefficient value of  $R_c < 1\%$ , validations for slip boundary condition is proven. Furthermore, for the no-slip cases without mean-flow, it is also correct for a wall distance higher than the stokes boundary layer thickness. A validation of higher frequencies close to the outlet patch should be investigated in more detail. Additionally, high mean-flows applied to the no-slip boundary condition case can not be validated properly and should be examined in further projects.

The follows remark should give a short overview of some problems and difficulties, arises during writing the thesis. Generally, profound background knowledge in acoustic and in the used software tools would have been a benefit. Visiting fundamental acoustic lecture before writing the thesis would have allow to understand the subject more clearly. Furthermore, more practical experiences in OpenFOAM would have allow to set up a appropriate mesh in less time.

Because of time constraint and a limited background knowledge especially in acoustic, no detailed investigation of the concerning effects could be reached. Therefore, this thesis gives good basic informations about the CBSBC and can be used for further reseaches and discussions.

# **Appendices**

# A Inlet Pressure

## A.1 Linearization of the Inlet Pressure

$$\begin{aligned}
& \frac{\partial p}{\partial t} + \frac{1}{2} (L_5 + L_1) = 0 \\
\text{with } & L_1 = (u - c) \left[ \frac{\partial p}{\partial x} - \rho c \frac{\partial u}{\partial x} \right] \quad \text{and} \quad L_5 = \sigma_5 [u - (f_x - g_u) - u_t] + 2\rho c \frac{\partial f_x}{\partial t} \\
& \frac{\partial p}{\partial t} + \frac{1}{2} \left[ \sigma_5 (u - (f_x - g_u) - u_t) + 2\rho c \frac{\partial f_x}{\partial t} + (u - c) \left( \frac{\partial p}{\partial x} - \rho c \frac{\partial u}{\partial x} \right) \right] = 0 \\
& \frac{\partial p}{\partial t} + \frac{\sigma_5}{2} (u - u_t) - \frac{\sigma_5}{2} (f_x - g_u) + \rho c \frac{\partial f_x}{\partial t} + \frac{u - c}{2} \frac{\partial p}{\partial x} - \frac{u - c}{2} \rho c \frac{\partial u}{\partial x} = 0 \\
& \frac{\partial p}{\partial t} + \frac{u - c}{2} \frac{\partial p}{\partial x} - \frac{\sigma_5}{2} (u - u_t) - \frac{\sigma_5}{2} (f_x - g_u) - \frac{u - c}{2} \rho c \frac{\partial u}{\partial x} + \rho c \frac{\partial f_x}{\partial t} = 0 \\
& \frac{p_{face}^{n+1} - p_{face}^n}{dt} + \frac{u - c}{2} \frac{p_{face}^{n+1} - p_{centre}^{n+1}}{dx} - \frac{\sigma_5}{2} (u - u_t) - \frac{\sigma_5}{2} (f_x - g_u) - \frac{u - c}{2} \rho c \frac{\partial u}{\partial x} + \rho c \frac{\partial f_x}{\partial t} = 0 \\
& p_{face}^{n+1} \left( 1 + \frac{u - c}{2} \frac{dt}{dx} \right) = p_{face}^n + \frac{u - c}{2} \frac{dt}{dx} p_{centre}^{n+1} + \frac{\sigma_5}{2} dt (u - u_t) - \frac{\sigma_5}{2} dt (f_x - g_u) - \\
& \quad - \frac{u - c}{2} \rho c dt \frac{\partial u}{\partial x} + dt \rho c \frac{\partial f_x}{\partial t} \\
\rightarrow & p_{face}^{n+1} = \underbrace{\frac{1}{1 + \frac{u - c}{2} \frac{dt}{dx}}}_{f} \left[ p_{face}^n - \frac{\sigma_5}{2} dt [(u - u_t) + (f_x - g_u)] + dt \rho c \frac{\partial f_x}{\partial t} \right] + \\
& + \underbrace{\frac{\frac{u - c}{2} \frac{dt}{dx}}{1 + \frac{u - c}{2} \frac{dt}{dx}}}_{1-f} \left[ p_{centre}^{n+1} + \rho c \frac{\partial u}{\partial x} dx \right] \\
\Rightarrow & p_{face}^{n+1} = \underbrace{\frac{1}{1 + \frac{u - c}{2} \frac{dt}{dx}}}_{f} \underbrace{\left[ p_{face}^n - \frac{\sigma_5}{2} dt [(u - u_t) + (f_x - g_u)] + dt \rho c \frac{\partial f_x}{\partial t} \right]}_{valueExpr} + \\
& + \underbrace{\frac{\frac{u - c}{2} \frac{dt}{dx}}{1 + \frac{u - c}{2} \frac{dt}{dx}}}_{1-f} \left[ p_{centre}^{n+1} + \underbrace{\rho c \frac{\partial u}{\partial x}}_{gradExpr} dx \right]
\end{aligned}$$

## A.2 CBSBC Implementation in OpenFOAM

### A.2.1 FractionExpression

The implementation in OpenFOAM for the fractionExpression f is:

$$\begin{aligned}
valueFraction() &= 1.0 / (1.0 + dt * this->patch().deltaCoeffs() * (aP + cP) / 2.0) \\
&= \frac{1}{1 + \frac{aP + cP}{2} * this->patch().deltaCoeffs()} \\
\Rightarrow f &= \frac{1}{1 + \frac{u+c}{2} \frac{dt}{dx}}
\end{aligned}$$

### A.2.2 ValueExpression

The implementation in OpenFOAM for the valueExpression = refValue() is:

$$\begin{aligned}
refValue() &= (field.oldTime().boundaryField()[patchi] + \\
&\quad + etaAc * rhop * sqr(cP) * (1.0 - sqr(aP/cP)) / 2.0 / lInf * dt * \\
&\quad * [(this->patch().nf0 \& (Up - uInf)) + f - g] + rhop * cP * (f - f0) \\
&= P_{face}^n + etaAc(1 - \sqrt{\frac{aP}{cP}}) \frac{cP}{lInf} * \frac{cP * rhop}{2} * dt \left( \frac{\partial(Up - uInf)}{\partial x} + f - g \right) + \\
&\quad + rhop * cP * (f - f0) \\
as \quad K &= \eta_c(1 - M^2) \frac{c}{l} \quad [Poinsot] \\
&= P_{face}^n + K \frac{\rho c}{2} dt \left( \frac{\partial(Up - uInf)}{\partial x} + f - g \right) + \rho * c * (f - f0) \\
as \quad L_1 &= K(p - p_\infty) = \frac{\sigma}{\rho c} (p - p_\infty) \quad \rightarrow \quad K = \frac{\sigma}{\rho c} \\
\Rightarrow \quad refValue() &= P_{face}^n + \frac{\sigma}{2} dt \left[ \frac{\partial(Up - uInf)}{\partial x} + f - g \right] + \rho c(f - f0)
\end{aligned}$$

### A.2.3 GradExpression

The implementation in OpenFOAM for the gradientExpression = refGrad() is:

$$\begin{aligned}
refGrad() &= -1.0 * rhop * cP * (this->patch().nf0 \& Up.snGrad0) \\
\Rightarrow \quad refGrad() &= -\rho c \frac{\partial u}{\partial x}
\end{aligned}$$

# B Outlet Pressure

## B.1 Linearization of the Outlet Pressure

$$\begin{aligned}
& \frac{\partial p}{\partial t} + \frac{1}{2} (L_5 + L_1) = 0 \\
\text{with } & L_5 = \frac{1}{2} \left[ (u+c) \left( \frac{\partial p}{\partial x} + \rho c \frac{\partial u}{\partial x} \right) \right] \quad \text{and} \quad L_1 = \frac{\sigma}{\rho c} [p - \rho c(f_d + g_x) - p_\infty] + 2 \frac{\partial g_x}{\partial t} \\
& \frac{\partial p}{\partial t} + \frac{1}{2} \left[ (u+c) \left( \frac{\partial p}{\partial x} + \rho c \frac{\partial u}{\partial x} \right) + \frac{\sigma}{\rho c} (p - \rho c(f_d + g_x) - p_\infty) + 2 \frac{\partial g_x}{\partial t} \right] = 0 \\
& \frac{\partial p}{\partial t} + \frac{u+c}{2} \frac{\partial p}{\partial x} + \rho c \frac{u+c}{2} \frac{\partial u}{\partial x} + \frac{\sigma}{2\rho c} (p - p_\infty) - \frac{\sigma}{2} (f_d + g_x) + \frac{\partial g_x}{\partial t} = 0 \\
& \frac{p_{face}^{n+1} - p_{face}^n}{dt} + \frac{u+c}{2} \frac{p_{face}^{n+1} - p_{centre}^{n+1}}{dx} + \rho c \frac{u+c}{2} \frac{\partial u}{\partial x} + \frac{\sigma}{2\rho c} (p_{face}^{n+1} - p_\infty) - \frac{\sigma}{2} (f_d + g_x) + \frac{\partial g_x}{\partial t} = 0 \\
& p_{face}^{n+1} - p_{face}^n + \frac{u+c}{2} \frac{dt}{dx} (p_{face}^{n+1} - p_{centre}^{n+1}) + \rho c \frac{u+c}{2} dt \frac{\partial u}{\partial x} + \frac{\sigma}{2\rho c} dt (p_{face}^{n+1} - p_\infty) - \frac{\sigma}{2} dt (f_d + g_x) + \\
& + \frac{\partial g_x}{\partial t} dt = 0 \\
& p_{face}^{n+1} \left( 1 + \frac{u+c}{2} \frac{dt}{dx} + \frac{\sigma}{2\rho c} dt \right) = p_{face}^n + \frac{u+c}{2} \frac{dt}{dx} p_{centre}^{n+1} - \rho c \frac{u+c}{2} dt \frac{\partial u}{\partial x} + \frac{\sigma}{2} dt (f_d + g_x) + \frac{\sigma}{2\rho c} dt p_\infty - \\
& - \frac{\partial g_x}{\partial t} dt \\
& p_{face}^{n+1} = \frac{1 + \frac{\sigma dt}{2\rho c}}{1 + \frac{u+c}{2} \frac{dt}{dx} + \frac{\sigma dt}{2\rho c}} \left[ \frac{p_{face}^n + \frac{\sigma dt}{2\rho c} p_\infty + \frac{\sigma dt}{2} (f_d + g_x) - dt \frac{\partial g_x}{\partial t}}{1 + \frac{\sigma dt}{2\rho c}} \right] + \frac{\frac{u+c}{2} \frac{dt}{dx}}{1 + \frac{u+c}{2} \frac{dt}{dx} + \frac{\sigma dt}{2\rho c}} \left[ p_{centre}^{n+1} + \right. \\
& \left. + \left( -\rho c \frac{\partial u}{\partial x} dx \right) \right] \\
& p_{face}^{n+1} = \underbrace{\frac{1 + \frac{\sigma dt}{2\rho c}}{1 + \frac{u+c}{2} \frac{dt}{dx} + \frac{\sigma dt}{2\rho c}}}_{f} \left[ \frac{p_{face}^n + \frac{\sigma dt}{2\rho c} p_\infty + \frac{\sigma dt}{2} (f_d + g_x) - dt \frac{\partial g_x}{\partial t}}{1 + \frac{\sigma dt}{2\rho c}} \right] + \\
& + \underbrace{\frac{\frac{u+c}{2} \frac{dt}{dx}}{1 + \frac{u+c}{2} \frac{dt}{dx} + \frac{\sigma dt}{2\rho c}}}_{1-f} \left[ p_{centre}^{n+1} + \left( \underbrace{-\rho c \frac{\partial u}{\partial x}}_{gradExpr} dx \right) \right]
\end{aligned}$$

## B.2 CBSBC Implementation in OpenFOAM

### B.2.1 FractionExpression

The implementation in OpenFOAM for the fractionExpression f is :

$$\begin{aligned}
 f &= (1.0 + etaAc * cP * dt * (1.0 - sqr(aP/cP)) / 2.0 / lInf) / (1.0 + etaAc * cP * dt * \\
 &\quad * (1.0 - sqr(aP/cP)) / 2.0 / lInf + (aP + cP) * dt / 2.0 * this->patch().deltaCoeffs0) \\
 f &= \frac{1.0 - \text{sqr}\left(\frac{aP}{cP}\right)}{1 + etaAc * cP * dt * \frac{1.0 - \text{sqr}\left(\frac{aP}{cP}\right)}{2.0 * lInf}} = \\
 &\quad \frac{1.0 - \text{sqr}\left(\frac{aP}{cP}\right)}{1 + etaAc * cP * dt * \frac{1.0 - \text{sqr}\left(\frac{aP}{cP}\right)}{2.0 * lInf} + \frac{(aP + cP) * dt}{2.0} * this->patch().deltaCoeffs0} \\
 \text{as } K &= \sigma(1 - M^2) \frac{c}{L} \sim etaAc \left(1 - \text{sqr}\left(\frac{aP}{cP}\right)\right) \frac{cP}{lInf} \quad [\text{Pointsot}] \\
 \text{and } &this->patch().deltaCoeffs0 \sim \frac{1}{\Delta x} \\
 \rightarrow &f = \frac{1 + K \frac{dt}{2}}{1 + K \frac{dt}{2} + \frac{(aP + cP) * dt}{2} * \frac{1}{\Delta x}} = \\
 \text{as } L_1 &= K(p - p_\infty) \sim \frac{\sigma}{\rho c} (p - p_\infty) \quad [\text{Pointsot}] \\
 \rightarrow &f = \frac{1 + \frac{\sigma}{\rho c} \frac{dt}{2}}{1 + \frac{\sigma}{\rho c} \frac{dt}{2} + \frac{(aP + cP) * dt}{2} * \frac{dt}{\Delta x}} \\
 \Rightarrow &f = \frac{1 + \frac{\sigma dt}{2\rho c}}{1 + \frac{(u+c)}{2} \frac{dt}{\Delta x} + \frac{\sigma dt}{2\rho c}}
 \end{aligned}$$

### B.2.2 ValueExpression

The implementation in OpenFOAM for the valueExpression = refValue() is:

$$\begin{aligned}
 \text{refValue0} &= [field.oldTime0.boundaryField0[patchi] + etaAc * cP * dt * \\
 &\quad * (1.0 - \text{sqr}(aP/cP)) / 2.0 / lInf * (pInf + rhoP * cP * g + rhoP * cP * f) + \\
 &\quad + rhoP * cP * (g - g0)] / [1.0 + etaAc * cP * dt * (1.0 - \text{sqr}(aP/cP)) / 2.0 / lInf] = \\
 &= \frac{field.oldTime0.boundaryField0[patchi] +}{1.0 + \eta * cP * dt * \frac{1.0 - \text{sqr}\left(\frac{aP}{cP}\right)}{2.0 * lInf}} \\
 &\quad + \eta * cP * dt * \frac{1.0 - \text{sqr}\left(\frac{aP}{cP}\right)}{2.0 * lInf} * (pInf + \rho * cP * g + \rho * cP * f) + \rho * cP * (g - g0) \\
 &\quad \frac{1.0 - \text{sqr}\left(\frac{aP}{cP}\right)}{1.0 + \eta * cP * dt * \frac{1.0 - \text{sqr}\left(\frac{aP}{cP}\right)}{2.0 * lInf}} \\
 \text{as } K &= \sigma(1 - M^2) \frac{c}{L} \sim etaAc \left(1 - \text{sqr}\left(\frac{aP}{cP}\right)\right) \frac{cP}{lInf} \quad [\text{Pointsot}] \\
 \text{as } &field.oldTime0.boundaryField0[patchi] = P_{face}^n \\
 \rightarrow &\text{refValue0} = \frac{P_{face}^n + K \frac{dt}{2} * [p_\infty + \rho * cP * (g + f)] + \rho * cP * (g - g0)}{1.0 + K \frac{dt}{2}} = \\
 \text{as } L_1 &= K(p - p_\infty) \sim \frac{\sigma}{\rho c} (p - p_\infty) \quad [\text{Pointsot}] \\
 \Rightarrow &\text{refValue0} = \frac{P_{face}^n + \frac{\sigma dt}{2\rho c} p_\infty + \frac{\sigma dt}{2} (f + g) + \rho c (g - g0)}{1 + \frac{\sigma dt}{2\rho c}}
 \end{aligned}$$

### B.2.3 GradExpression

The implementation in OpenFOAM for the gradientExpression = refGrad() is:

$$\begin{aligned}refGrad() &= -rhoP * cP * this->patch().nf() \quad \& \quad Up.snGrad() \\ \Rightarrow \quad refGrad() &= -\rho c \frac{\partial u}{\partial x}\end{aligned}$$

# C Inlet Temperature

## C.1 Linearization of the Inlet Temperature

$$\begin{aligned}
& \frac{\partial T}{\partial t} + \frac{T}{\rho c^2} \left[ -L_2 + \frac{1}{2}(\gamma-1)(L_5 + L_1) \right] = 0 \\
\text{with } & L_1 = (u-c) \left[ \frac{\partial p}{\partial x} - \rho c \frac{\partial u}{\partial x} \right] \quad \text{and} \quad L_5 = -\sigma_5 [u - (fx - gu) - ut] - 2\rho c \frac{\partial fx}{\partial t} \quad \text{and} \quad L_2 = -\sigma_2 \left[ (T - T_t) - \frac{\gamma-1}{\gamma} \frac{c}{R} (f + g) \right] \\
& \frac{\partial T}{\partial t} + \frac{T}{\rho c^2} \left[ \sigma_2 \left( (T - T_t) - \frac{\gamma-1}{\gamma} \frac{c}{R} (f + g) \right) + \frac{1}{2}(\gamma-1) \left( -\sigma_5 (u - (f-g) - ut) - 2\rho c \frac{\partial f}{\partial t} + \right. \right. \\
& \left. \left. + (u-c) \left( \frac{\partial p}{\partial x} - \rho c \frac{\partial u}{\partial x} \right) \right) \right] = 0 \\
& \frac{\partial T}{\partial t} + \sigma_2 \frac{T}{\rho c^2} (T - T_t) - \sigma_2 \frac{\gamma-1}{\gamma} \frac{T}{\rho c^2} \frac{c}{R} (f + g) - \sigma_5 \frac{T}{\rho c^2} \frac{\gamma-1}{2} (u - (f-g) - ut) - \\
& - \frac{T}{\rho c^2} (\gamma-1) \rho c \frac{\partial f}{\partial t} + \frac{T}{\rho c^2} (\gamma-1) \frac{u-c}{2} \left( \frac{\partial p}{\partial x} - \rho c \frac{\partial u}{\partial x} \right) = 0 \\
\text{as } & \frac{T}{\rho c^2} = \frac{1}{\gamma \rho R} \\
& \frac{\partial T}{\partial t} + \sigma_2 \frac{1}{\gamma \rho R} (T - T_t) - \sigma_2 \frac{\gamma-1}{\gamma} \frac{1}{\gamma \rho R} \frac{c}{R} (f + g) - \sigma_5 \frac{\gamma-1}{\gamma} \frac{1}{2 \rho R} (u - (f-g) - ut) - \\
& - \frac{\gamma-1}{\gamma} \frac{c}{R} \frac{\partial f}{\partial t} + \frac{\gamma-1}{\gamma} \frac{u-c}{2 \rho R} \left( \frac{\partial p}{\partial x} - \rho c \frac{\partial u}{\partial x} \right) = 0 \\
& \frac{T_{face}^{n+1} - T_{face}^n}{dt} + \frac{\sigma_2}{\gamma \rho R} \left( T_{face}^{n+1} - T_t \right) - \sigma_2 \frac{\gamma-1}{\gamma} \frac{1}{\gamma \rho R} \frac{c}{R} (f + g) - \sigma_5 \frac{\gamma-1}{\gamma} \frac{1}{2 \rho R} (u - (f-g) - ut) - \\
& - \frac{\gamma-1}{\gamma} \frac{c}{R} \frac{\partial f}{\partial t} + \frac{\gamma-1}{\gamma} \frac{u-c}{2 \rho R} \left( \frac{\partial p}{\partial x} - \rho c \frac{\partial u}{\partial x} \right) = 0 \\
& T_{face}^{n+1} \left( 1 + \frac{\sigma_2 dt}{\gamma \rho R} \right) - T_{face}^n - \frac{\sigma_2 dt}{\gamma \rho R} T_t - \sigma_2 \frac{\gamma-1}{\gamma} \frac{dt}{\gamma \rho R} \frac{c}{R} (f + g) - \sigma_5 \frac{\gamma-1}{\gamma} \frac{dt}{2 \rho R} (u - (f-g) - ut) - \\
& - \frac{\gamma-1}{\gamma} \frac{c}{R} dt \frac{\partial f}{\partial t} + \frac{\gamma-1}{\gamma} \frac{u-c}{2 \rho R} dt \left( \frac{\partial p}{\partial x} - \rho c \frac{\partial u}{\partial x} \right) = 0 \\
\Rightarrow & T_{face}^{n+1} = \left[ T_{face}^n + \frac{\sigma_2 dt}{\gamma \rho R} T_t + \sigma_2 \frac{\gamma-1}{\gamma} \frac{dt}{\gamma \rho R} \frac{c}{R} (f + g) + \sigma_5 \frac{\gamma-1}{\gamma} \frac{dt}{2 \rho R} (u - (f-g) - ut) + \right. \\
& \left. + \frac{\gamma-1}{\gamma} \frac{c}{R} dt \frac{\partial f}{\partial t} - \frac{\gamma-1}{\gamma} \frac{u-c}{2 \rho R} dt \left( \frac{\partial p}{\partial x} - \rho c \frac{\partial u}{\partial x} \right) \right] / \left[ 1 + \frac{\sigma_2 dt}{\gamma \rho R} \right] \\
\Rightarrow & T_{face}^{n+1} = \left[ T_{face}^n + \frac{\sigma_2 dt}{\gamma \rho R} T_t + \frac{\gamma-1}{\gamma} \left[ \frac{c}{R} dt \frac{\partial f}{\partial t} - \frac{u-c}{2 \rho R} dt \left( \frac{\partial p}{\partial x} - \rho c \frac{\partial u}{\partial x} \right) \right] + \right. \\
& \left. \sigma_5 \frac{dt}{2 \rho R} (u - (f-g) - ut) + \sigma_2 \frac{dt}{\gamma \rho R} \frac{c}{R} (f + g) \right] / \left[ 1 + \frac{\sigma_2 dt}{\gamma \rho R} \right]
\end{aligned}$$

## C.2 CBSBC Implementation in OpenFOAM

### C.2.1 FractionExpression

The implementation in OpenFOAM for the fractionExpression f is:

$$\begin{aligned} & this->valueFraction() = 1.0 \\ \Rightarrow & \quad f = 1.0 \end{aligned}$$

### C.2.2 ValueExpression

The implementation in OpenFOAM for the valueExpression = refValue() is:

$$\begin{aligned} & refValue() = \\ & = [field.oldTime().boundaryField()[patchi] \\ & + etaT * cP * dt / gamma / lInf * tInf + \\ & + (gamma - 1) / gamma * (cP / R * (f - f0) - \\ & - (aP + cP) / rhoP / R / 2.0 * dt * (pp.snGrad0) + \\ & + rhop * cP * (this->patch0().nf0) & Up - snGrad0)) + \\ & + etaAc * sqr(cP) / R * (1.0 - sqr(aP / cP)) / 2.0 / lInf * \\ & * dt * (this->patch0().nf0) & (Up - uInf)) \\ & + sqr(cP) / R / lInf * dt * (etaT / gamma + etaAc * (1.0 - sqr(aP / cP)) / 2.0) * f \\ & + sqr(cP) / R / lInf * dt * etaT / gamma * g \\ & - sqr(cP) / R / lInf * dt * etaAc * (1.0 - sqr(aP / cP)) / 2.0 * g \\ & ] \\ & / (1.0 + etaT * cP * dt / gamma / lInf) \\ \\ & = \left[ T_{face}^n + \frac{etaT * cP * dt}{\gamma * lInf} * T^t + \frac{\gamma - 1}{\gamma} \left[ \frac{cP}{R} (f - f0) - \frac{aP + cP}{2\rho R} dt \left[ \frac{\partial p}{\partial x} + \rho c \frac{\partial u}{\partial x} \right] + \right. \right. \\ & + etaAc \left( 1 - \left( \frac{aP}{cP} \right)^2 \right) \frac{cP}{lInf} \frac{cP}{2R} dt (u - u_t) + \frac{cP^2}{lInf * R} dt \frac{etaT}{\gamma} (f + g) + \\ & \left. \left. + etaAc \left( 1 - \left( \frac{aP}{cP} \right)^2 \right) \frac{cP}{lInf} \frac{cP}{2R} dt (f - g) \right] \right] \\ & / \left[ 1 + \frac{etaT cP dt}{lInf \gamma} \right] \\ \\ & as \quad K = etaAc \left( 1 - \left( \frac{aP}{cP} \right)^2 \right) \frac{cP}{lInf} = \frac{\sigma_5}{\rho c} \quad and \quad \sigma_2 = \eta_t \rho R \frac{c}{l} \\ \\ & = \left[ T_{face}^n + \frac{\eta_t c dt}{\gamma l} T^t + \frac{\gamma - 1}{\gamma} \left( \frac{c}{R} (f - f0) - \frac{\gamma - 1}{\gamma} \frac{u + c}{2\rho R} dt \left( \frac{\partial p}{\partial x} + \rho c \frac{\partial u}{\partial x} \right) + \right. \right. \\ & \left. \left. + \frac{\gamma - 1}{\gamma} \frac{c dt}{2R} K (u - u_t + (f - g)) + \frac{\gamma - 1}{\gamma} \frac{c^2 dt}{lR} \frac{\eta_t}{\gamma} (f + g) \right) \right] / \left[ 1 + \frac{etaT cP dt}{lInf \gamma} \right] \\ \\ & = \left[ T_{face}^n + \frac{\eta_t c dt}{\gamma l} T^t + \frac{\gamma - 1}{\gamma} \left( \frac{c}{R} (f - f0) - \frac{u + c}{2\rho R} dt \left( \frac{\partial p}{\partial x} + \rho c \frac{\partial u}{\partial x} \right) + \right. \right. \\ & \left. \left. + \frac{c dt}{2R} K (u - u_t + (f - g)) + \frac{\gamma - 1}{\gamma} \frac{c^2 dt}{lR} \frac{\eta_t}{\gamma} (f + g) \right) \right] / \left[ 1 + \frac{etaT * cP * dt}{lInf * \gamma} \right] \\ \\ & \Rightarrow \quad refValue0 = \left[ T_{face}^n + \frac{\sigma_2 dt}{\gamma \rho R} T^t + \frac{\gamma - 1}{\gamma} \left( \frac{c}{R} (f - f0) - \frac{u + c}{2\rho R} dt \left( \frac{\partial p}{\partial x} + \rho c \frac{\partial u}{\partial x} \right) + \sigma_5 \frac{dt}{2\rho R} (u - u_t + (f - g)) + \right. \right. \\ & \left. \left. + \sigma_2 \frac{cdt}{\gamma \rho RR} (f + g) \right) \right] / \left[ 1 + \sigma_2 \frac{dt}{\gamma \rho R} \right] \end{aligned}$$

### C.2.3 GradExpression

The implementation in OpenFOAM for the gradientExpression = refGrad() is:

$$\begin{aligned} this->refGrad() &= 1.0 \\ \Rightarrow \quad refGrad() &= 1.0 \end{aligned}$$

# D Outlet Temperature

## D.1 Linearization of the Outlet Temperature

$$\frac{\partial T}{\partial t} + \frac{T}{\rho c^2} \left[ -L_2 + \frac{1}{2} (\gamma - 1) (L_5 + L_1) \right] = 0$$

with  $L_2 = u \left( c^2 \frac{\partial \rho}{\partial x} - \frac{\partial p}{\partial x} \right)$  and  $L_5 = (u + c) \left( \frac{\partial \rho}{\partial x} + \rho c \frac{\partial u}{\partial x} \right)$  and  $L_1 = \frac{\sigma}{\rho c} [p - \rho c(f_d + g_x) - p_\infty] + 2 \frac{\partial g_x}{\partial t}$

$$\frac{\partial T}{\partial t} + \frac{T}{\rho c^2} \left[ -u \left( c^2 \frac{\partial \rho}{\partial x} - \frac{\partial p}{\partial x} \right) + \frac{1}{2} (\gamma - 1) (L_5 + L_1) \right] = 0$$

$$\frac{\partial T}{\partial t} - \frac{uc^2 T}{\rho c^2} \frac{\partial \rho}{\partial x} + \frac{uT}{\rho c^2} \frac{\partial p}{\partial x} + \frac{T(\gamma - 1)}{2\rho c^2} (L_5 + L_1) = 0$$

$$\frac{\partial T}{\partial t} - \frac{uT}{\rho} \left( \frac{\rho}{p} \frac{\partial p}{\partial x} - \frac{\rho}{T} \frac{\partial T}{\partial x} \right) + \frac{uT}{\rho c^2} \frac{\partial p}{\partial x} + \frac{T(\gamma - 1)}{2\rho c^2} (L_5 + L_1) = 0$$

$$\frac{\partial T}{\partial t} - \frac{uT}{p} \frac{\partial p}{\partial x} + u \frac{\partial T}{\partial x} + \frac{uT}{\rho c^2} \frac{\partial p}{\partial x} + \frac{T(\gamma - 1)}{2\rho c^2} (L_5 + L_1) = 0$$

$$\frac{\partial T}{\partial t} + u \frac{\partial T}{\partial x} + u \left( \frac{T}{\rho c^2} - \frac{T}{p} \right) \frac{\partial p}{\partial x} + \frac{T(\gamma - 1)}{2\rho c^2} (L_5 + L_1) = 0$$

$$\frac{\partial T}{\partial t} + u \frac{\partial T}{\partial x} + u \frac{1-\gamma}{\rho R \gamma} \frac{\partial p}{\partial x} + \frac{\gamma-1}{2\rho R \gamma} (L_5 + L_1) = 0$$

$$\frac{T_{face}^{n+1} - T_{face}^n}{dt} + u \frac{T_{face}^{n+1} - T_{centre}^{n+1}}{dx} + u \frac{1-\gamma}{\rho R \gamma} \frac{\partial p}{\partial x} + \frac{\gamma-1}{2\rho R \gamma} (L_5 - L_1) = 0$$

$$T_{face}^{n+1} - T_{face}^n + \frac{u dt}{dx} \left( T_{face}^{n+1} - T_{centre}^{n+1} \right) + u dt \frac{1-\gamma}{\rho R \gamma} \frac{\partial p}{\partial x} + \frac{(\gamma-1) dt}{2\rho R \gamma} (L_5 + L_1) = 0$$

$$\rightarrow T_{face}^{n+1} \left( 1 - \frac{u dt}{dx} \right) = T_{face}^n + \frac{u dt}{dx} T_{centre}^{n+1} - u dt \frac{1-\gamma}{\rho R \gamma} \frac{\partial p}{\partial x} - \frac{(\gamma-1) dt}{2\rho R \gamma} (L_5 + L_1)$$

$$\Rightarrow T_{face}^{n+1} = \underbrace{\frac{1}{1 - \frac{u dt}{dx}}}_{f} \underbrace{\left[ T_{face}^n - \frac{(\gamma-1) dt}{2\rho R \gamma} (L_5 + L_1) \right]}_{valueExpr} + \underbrace{\frac{\frac{u dt}{dx}}{1 - \frac{u dt}{dx}}}_{1-f} \left[ T_{centre}^{n+1} + \underbrace{\frac{\gamma-1}{\rho R \gamma} \frac{\partial p}{\partial x}}_{gradExpr} dx \right]$$

## D.2 CBSBC Implementation in OpenFOAM

**L<sub>5</sub>**

$$L_5 = (aP + cP) * [pp.snGrad() + rhop * cp * (this->patch().nf() \& Up.snGrad())]$$

$$\rightarrow L_5 = (u + c) \left[ \frac{\partial p}{\partial x} + \rho c \frac{\partial u}{\partial x} \right]$$

**L<sub>1</sub>**

$$L_1 = etaAc * cP * (1.0 - sqrt(aP/cP)) / lInf * [pp - pInf - rhop * cP * g - rhop * cP * f]$$

$$- 2.0 * rhop * cP * (g - g0) / dt$$

$$= etaAc * \left( 1 - sqrt \frac{aP}{cP} \right) \frac{cP}{lInf} * [pp - pInf - rhop * cP * (g + f)] - 2 * rhop * cP * \frac{g - g0}{dt}$$

$$as \quad K = \sigma \left( 1 - M^2 \right) \frac{c}{L} \sim etaAc \left( 1 - sqrt \frac{aP}{cP} \right) \frac{cP}{lInf} \quad [Poisson]$$

$$\rightarrow L_1 = K [pp - pInf - \rho c(g + f)] - 2\rho c \frac{g - g0}{dt}$$

$$as \quad L_1 = K(p - p_\infty) \sim \frac{\sigma}{\rho c} (p - p_\infty) \quad [Poisson]$$

$$\rightarrow L_1 = \frac{\sigma}{\rho c} [pp - pInf - \rho c(g + f)] - 2\rho c \frac{g - g0}{dt}$$

$$\Rightarrow L_1 = \frac{\sigma}{\rho c} [pp - p_\infty - \rho c(g + f)] - 2\rho c \frac{g - g0}{dt}$$

### D.2.1 FractionExpression

Implementation in OpenFOAM for the fractionExpression f is:

$$f = 1.0 / [1.0 + aP * dt * this->patch().deltaCoeffs()]$$

$$\rightarrow f = \frac{1.0}{1.0 + aP * dt * this->patch().deltaCoeffs()}$$

$$\Rightarrow f = \frac{1}{1 + \frac{udt}{\Delta x}}$$

### D.2.2 ValueExpression

Implementation in OpenFOAM for the valueExpression = refValue() is:

$$refValue() = field.oldTime().boundaryField()[patchi] - dt * (gamma - 1.0) / gamma * 0.5 * (L_5 + L_1) / rhop / R$$

$$\rightarrow = field.oldTime().boundaryField()[patchi] - dt \frac{\gamma - 1}{2\gamma} \frac{L_5 + L_1}{\rho R}$$

$$\Rightarrow refValue() = T_{face}^n - \frac{(\gamma - 1)dt}{2\gamma\rho R} (L_5 + L_1)$$

### D.2.3 GradExpression

The implementation in OpenFOAM for the gradExpr = refGrad() is:

$$refGrad() = (\gamma - 1) / \gamma * pp.snGrad() / rho / R$$

$$\rightarrow = \frac{\gamma - 1}{\gamma} \frac{\partial p}{\partial x} \frac{1}{\rho R}$$

$$\Rightarrow refGrad() = \frac{\gamma - 1}{\gamma \rho R} \frac{\partial p}{\partial x}$$

# E Extract of Velocity Boundary Condition File

An extract of the velocity boundary condition file is shown here.

```

boundaryField
{
    INLET
    {
        type            CBSBCInletVelocity;
        psi             thermo:psi;
        gamma          1.4;           // Ratio of specific heats
        velocity
        {
            targetValue uniform (0 0 0); // Stationary target value
            eta            0.58;         // Optional relaxation parameter, default value 0.58
            excitation     tableFile;   // Acoustic excitation (f wave)
            tableFileCoeffs
            {
                fileName      "$FOAM_CASE/inletf_700.txt"; // Path to excitation signal file
                // outOfBounds clamp;                      // Optional, default value "warn"
            }
        }
        ssFileName      "statespace.dat";
        ssPatch         -1;           // Patch number of CBSBC
        ssDT            5e-7;         // maximum time step for state space
        l1Inf          0.1;           // Characteristic acoustic length scale
        method          converged;    // Optional, default value "lowpass" (lowpass|adaptive|converged|off)
        value          uniform (0 0 0); // Optional, initial value
    }

    OUTLET
    {
        type            CBSBCOutletVelocity;
        psi             thermo:psi; // Optional, default value "psi"
        gamma          1.4;           // ratio of specific heats
        pressure
        {
            targetValue uniform 100000; // Stationary target value
            eta            0.58;         // Optional relaxation parameter, default value 0.58
            excitation     tableFile;   // Acoustic excitation (f wave)
            tableFileCoeffs
            {
                fileName      "$FOAM_CASE/outletg.txt"; // Path to excitation signal file
            }
        }
        ssFileName      "statespace.dat";
        ssPatch         -2;           // Patch number of CBSBC
        ssDT            5e-7;         // maximum time step for state space
        l1Inf          0.1;           // Characteristic acoustic length scale
        method          converged;    // Optional, default value "lowpass" (lowpass|adaptive|converged|off)
        value          uniform (0 0 0);
    }
}

```

## F Matlab Code

The matlab code for calculating the  $f$  and  $g$  waves and the corresponding  $R_c$  value for the no-slip mean-flow case:

---

```

%Time-steps written into the acoustic part of velocity/pressure in the first column
for i = 2:71
    UA(:,1) = UWall(:,1);
    UA(:,i) = UWall(:,(2+(i-2)*3)) - mean(UWall(meanValue:(meanValue+L),(2+(i-2)*3)));
    pA(:,1) = pWall(:,1);
    pA(:,i) = pWall(:,i) - mean(pWall(meanValue:(meanValue+L),i));
end

for i = 2:71
    %Calculating the f and g wave for every cell
    A_f(:,i) = 0.5* ((pWall(:,i) - mean(pWall(meanValue:(meanValue+L),i))) / rhoc + \\
        (UWall(:,(2+(i-2)*3)) - mean(UWall(meanValue:(meanValue+L),(2+(i-2)*3)))) );
    A_g(:,i) = 0.5* ((pWall(:,i) - mean(pWall(meanValue:(meanValue+L),i))) / rhoc - \\
        (UWall(:,(2+(i-2)*3)) - mean(UWall(meanValue:(meanValue+L),(2+(i-2)*3)))) );

    %Taking only the last time steps; nearly converged state
    A_ff(:,i) = A_f(95000:99286,i);
    A_gg(:,i) = A_g(95000:99286,i);

    %Fast Fourier Transformation of f and g wave
    Y_f(:,1) = fft(A_ff(:,1));
    P2f(:,i) = abs(Y_f(:,i)/l);
    P1f(:,i) = P2f(1:(L/2)+1,i);
    P1f(2:end-1,i) = 2 * P1f(2:end-1,i);
    Y_g(:,1) = fft(A_gg(:,1));
    P2g(:,i) = abs(Y_g(:,i)/l);
    P1g(:,i) = P2g(1:(L/2)+1,i);
    P1g(2:end-1,i) = 2 * P1g(2:end-1,i);

    %Calculating the wall distance for every cell
    distance(i,2) = distance(1,1) - distance(i,1);

    %Identifie the max amplitude value for the frequency F=700 Hz
    max_temp_f = max(P1f(4,:));
    max_A(i,1) = max_temp_f; %max f
    max_temp_g = max(P1g(4,:));
    max_A(i,2) = max_temp_g; %max g
    max_A(i,3) = max_temp_g / max_temp_f; %Rc
end

%Safe the maximum amplitudes of f and g wave and the referred Rc
R = [distance(:,2),max_A];

```

## G $U_x$ for selected Mean-Flows

Following figure G.1 is showing the velocity in x-direction along the wall distance for different mean-flows.

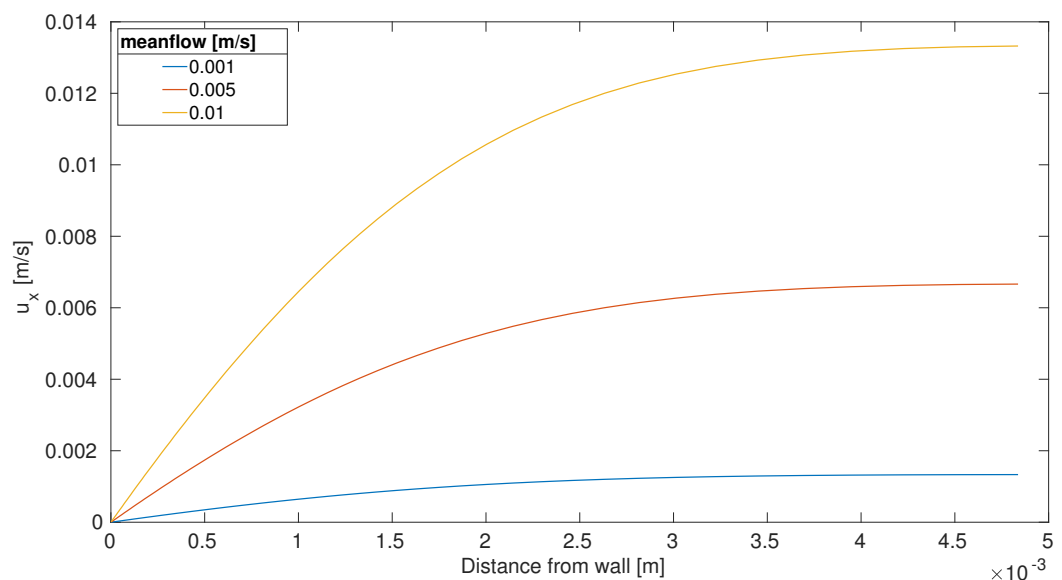


**Figure G.1:** Velocity in x-direction for different mean-flows for  $t = 85$  ms

# Bibliography

- [1] Franz Durst. *Grundlagen der Strömungsmechanik: eine Einführung in die Theorie der Strömung von Fluiden*. Springer-Verlag, 2007.
- [2] Klaus Ehrenfried. *Strömungskustik: Skript zur Vorlesung*. Mensch-und-Buch-Verlag, 2004.
- [3] Kilian Heinrich Förner. *Nonlinear Aeroacoustic Characterization of Resonators*. PhD thesis, Technische Universität München, 2017.
- [4] B. Gschaider. Swak4foam [online: <http://openfoamwiki.net/index.php/contrib/swak4foam>].
- [5] Robert L Higdon. Absorbing boundary conditions for difference approximations to the multidimensional wave equation. *Mathematics of computation*, 47(176):437–459, 1986.
- [6] Stefan Jaensch, Carlo Sovardi, and Wolfgang Polifke. On the robust, flexible and consistent implementation of time domain impedance boundary conditions for compressible flow simulations. *Journal of Computational Physics*, 314:145–159, 2016.
- [7] Heinz-Otto Kreiss. Initial boundary value problems for hyperbolic systems. *Communications on Pure and Applied Mathematics*, 23(3):277–298, 1970.
- [8] T.J. Poinsot and S.K. Lele. Boundary conditions for direct simulations of compressible viscous flows. *Journal of computational physics*, 101(1):104–129, 1992.
- [9] Wolfgang Polifke, Clifton Wall, and Parviz Moin. Partially reflecting and non-reflecting boundary conditions for simulation of compressible viscous flow. *Journal of Computational Physics*, 213(1):437–449, 2006.
- [10] Kevin W. Thompson. Time dependent boundary conditions for hyperbolic systems. *Journal of computational physics*, 68(1):1–24, 1987.
- [11] R Vilums. Implementation of transient robin boundary conditions in openfoam. In *Workshop Multiphysical Modelling in OpenFOAM, Riga, Latvia*, pages 39–40, 2011.
- [12] FA Williams. Combustion theory 2nd, 1985.